Alma Mater Studiorum - Università di Bologna

DOTTORATO DI RICERCA IN

SCIENZE BIOMEDICHE E NEUROMOTORIE

Ciclo 36

Settore Concorsuale: 05/D1 - FISIOLOGIA

Settore Scientifico Disciplinare: BIO/09 - FISIOLOGIA

CARDIAC FUNCTIONAL AND STRUCTURAL ABNORMALITIES IN A MOUSE MODEL OF CDKL5 DEFICIENCY DISORDER

Presentata da: Manuela Loi

Coordinatore Dottorato

Matilde Yung Follo

Supervisore

Elisabetta Ciani

Co-supervisore

Stefania Trazzi

Esame finale anno 2024

SUMMARY

ABSTRACT

CDKL5 (cyclin-dependent kinase-like 5) deficiency disorder (CDD) is a rare and severe neurodevelopmental disease that mostly affects girls who are heterozygous for mutations in the X-linked CDKL5 gene. The lack of CDKL5 protein expression or function leads to the appearance of numerous clinical features, including early-onset seizures, marked hypotonia, autistic features, and severe neurodevelopmental impairment. Mouse models of CDD, *Cdkl5* KO mice, exhibit several behavioral phenotypes that mimic CDD features, such as impaired learning and memory, social interaction, and motor coordination. CDD symptomatology, along with the high CDKL5 expression levels in the brain, underscores the critical role that CDKL5 plays in proper brain development and function. Nevertheless, the improvement of the clinical overview of CDD in the past few years has defined a more detailed phenotypic spectrum; this includes very common alterations in peripheral organ and tissue function, such as gastrointestinal problems, irregular breathing, hypotonia, and scoliosis, suggesting that CDKL5 deficiency compromises not only CNS function but also that of other organs/tissues. Here we report, for the first time, that a mouse model of CDD, the heterozygous *Cdkl5* KO (*Cdkl5* +/-) female mouse, exhibits cardiac functional and structural abnormalities. The mice also showed QTc prolongation and increased heart rate. These changes correlate with a marked decrease in parasympathetic activity to the heart and in the expression of the Scn5a and Hcn4 voltage-gated channels. Moreover, the *Cdkl5* +/- heart shows typical signs of heart aging, including increased fibrosis, mitochondrial dysfunctions, and increased ROS production. Overall, our study not only contributes to the understanding of the role of CDKL5 in heart structure/function but also documents a novel preclinical phenotype for future therapeutic investigation.

1. INTRODUCTION

1.1 CDKL5 Deficiency Disorder (CDD)

CDKL5 deficiency disorder (CDD, OMIM *300203) is a rare X-linked neurodevelopmental disorder caused by dominant loss of function mutations in the cyclin-dependent kinase-like 5 (*CDKL5*) gene, which is located on the short arm of the X chromosome (Tao *et al.*, 2004; Weaving *et al.*, 2004; Hector *et al.*, 2016). *CDKL5* encodes for the CDKL5 protein kinase (CDKL5/STK9) (Montini *et al.*, 1998; Kalscheuer *et al.*, 2003; Weaving *et al.*, 2004). CDD is characterized by a wide range of clinical symptoms such as early-onset intractable seizures, severe intellectual disability, and Rett's syndrome-like features such as hand stereotypies and decreased social interaction, appearing in the first few weeks or months of life.

Despite being rare, the incidence rate varies from 1:40,000 to 1:60,000 live births, making it one of the most common genetic epilepsy disorders in children (Hector *et al.*, 2017; Lindy *et al.*, 2018). Due to the fact that *CDKL5* is located in the X chromosome, the prevalence of CDD among women is four times higher than in men (Fehr *et al.*, 2015) with an incidence of 1:42.000 live birth (Symonds *et al.*, 2019), probably due to the more severe consequences of dominant X-linked mutations in male patients (Olson *et al.*, 2019).

1.1.1 CDD clinical history

The history of CDD started very recently in 2003, when Vera Kalscheuer and colleagues showed that a balanced translocation causing a truncation of the X-linked cyclin-dependent kinase–like 5 (*CDKL5/STK9*) gene was responsible for the infantile spams and profound developmental delay exhibited by two unrelated girls (Kalscheuer *et al.*, 2003). The disease associated with CDKL5 deficiency was initially diagnosed as an early-onset seizure variant of Rett syndrome, also known as "Hanefeld variant".

Rett Syndrome [RTT, OMIM 312750] is a severe childhood progressive neurological disorder, that was firstly described in 1966 by an Austrian pediatrician, Andreas Rett. RTT has an incidence of 1:10000-15000 live births (Hagberg *et al.*, 1983) and it is most often caused by mutations in the X-linked gene of the methyl-CpG-binding protein 2 (*MeCP2*), a transcriptional repressor, that is located on the X chromosome (Amir *et al.*, 1999; Cheadle *et al.*, 2000), but several atypical variants of RTT have been described. After achieving the main developmental milestones in the first 6-18 months of life, affected children show a subsequent arrest and regression of their development (Weaving *et al.*, 2005). RTT

phenotype is variable but the most common clinical features include impairment of motor and cognitive functions, spinal problems (scoliosis), epilepsy, loss of communication ability, and characteristic stereotypic hand movements.

Together with the typical RTT syndrome, several atypical variants were then described; the preserved speech variant (PSV), the congenital variant, and the early seizure variant (ESV) (also called "Hanefeld variant") (Scala *et al.*, 2005). Patients with these variants display several typical RTT symptoms but show considerable variations in type and age of onset, severity of impairment, and clinical course. Mutations in *MeCP2* gene are found in 95-97% of individuals diagnosed with the classic variant of RTT (Neul *et al.*, 2008) while only 50-70% of patients with atypical variants of RTT show mutations in *MeCP2* gene. Together with MECP2, the primary genetic drivers of the condition were thought to be mutation in *CDKL5* gene (Ariani *et al.*, 2008) and forkhead box protein G1 (*FOXG1*) (Evans *et al.*, 2005; Philippe *et al.*, 2010).

Due to many overlapping clinical features, such as neurodevelopmental delay, stereotypic hand movements, hypotonia, seizures and intellectual disability (Archer *et al.*, 2006; Bahi-Buisson *et al.*, 2008b; Artuso *et al.*, 2010; Fehr *et al.*, 2013), patients with these clinical features were studied and found to be positive for *CDKL5* mutations (Tao *et al.*, 2004; Weaving *et al.*, 2004). However, the variation in type and age of epilepsy onset, the severity of impairment, and clinical course associated with CDKL5 deficiency disorder and its genetic cause are different from those of Rett syndrome. Only in 2013, using a large international data collection (InterRett database), Fehr and colleagues recognized CDKL5 as a distinct condition from RTT syndrome especially for its unique features such as the early drug-resistant epilepsy starting within the first 6 months of life and the lack of regression after a period of normal development (Fehr *et al.*, 2013; Katayama *et al.*, 2020) (Table 1).

So, even though encephalopathies related to mutations in *MeCP2* and *CDKL5* genes share molecular pathways and present common symptomatology, they are now worldwide considered as independent diseases.

	Rett syndrome	MECP2 duplication syndrome	CDKL5 mutations/ deletions
Development	Regression at 1–3 years	Severe early delay	Severe early delay
Social interaction	Poor	Poor	Poor
Muscle tone	Initially normal, evolving to hypotonia	Early hypotonia, evolving to spasticity	Hypotonia
Speech-language	Absent	Mostly absent	Absent
Walking	Impaired (dyspraxic) or absent	Possible (70%), impaired	Absent or impaired
Abnormal movements	Hand stereotypies, myoclonus, mouthing	Choreiform movements, hand stereotypies	Hand stereotypies, bruxism (40%)
Autonomic dysfunction	+++	++	+
Breathing abnormalities	Hyperventilation during wakefulness	Absent or minimal	Absent or minimal
Autistic behavior	Often present	Often present	Poor eye contact, reduced social interaction
Sleep disturbances	Poor sleep pattern	Poor sleep pattern	Poor sleep pattern
Microcephaly	Acquired microcephaly	Absent	Mostly borderline (30%)
Facial dysmorphisms	Mostly absent	Mild, always present	Mostly absent
Epilepsy	Partial complex and GTC seizures	Multiple seizure types	Early onset epileptic encephalopathy with spasms, myoclonus and prolonged GTC

+, least severe; ++, severe; +++, most severe; GTC, generalized tonic–clonic.

Table 1. Clinical features of *MECP2*- and *CDKL5*-gene-related encephalopathies (Guerrini and Parrini, 2012)

1.1.2 CDD clinical features

The clinical profile of CDD patients is characterized by a very early onset symptomatology and is highly variable, it extends from milder forms, with controlled epilepsy and independent ambulation, to severe ones, with absolute microcephaly, no motor milestones and drug-resistant seizures.

Notwithstanding this clinical heterogeneity, the major feature of CDD is the appearance of drug-resistant epileptic seizures in the first few months of life, which manifest as epileptic encephalopathy with infantile spasms between the first few days and fourth month of life; patients also exhibit a distinct seizure pattern characterized by generalized tonic-clonic episodes, which subsequently transition into repetitive distal myoclonic jerks in a gradual manner (Guerrini and Parrini, 2012).

Bahi-Buisson and colleagues, tried to define the clinical profile of 20 patients with *CDKL5* mutations screened among 183 females with early seizure encephalopathy. They proposed

a three-stage evolution trend in epilepsy based on age. Stage I characterizes younger patients (1-10 weeks old) with early-onset epilepsy and frequent prolonged tonic-clonic seizures occurring 2-5 times a day; Stage II (from 6 months to 3 years of age) is identified by the presence of epileptic encephalopathy with infantile spasms and hypsarrhythmia; finally, in Stage III, about 71% of patients show refractory epilepsy with tonic seizures and myoclonic jerks (Bahi-Buisson *et al.*, 2008a)

CDD patients also show nonspecific abnormalities. Brain MRI demonstrates that most of them exhibit cortical atrophy combined with hyperintensities in the white matter of the temporal lobe (Bahi-Buisson *et al.*, 2008a; Artuso *et al.*, 2010). The EEG typically shows epileptiform discharges or hypsarrhythmia in the temporal or tempo-occipital head regions. Neuroimaging may show delayed myelination in the temporal lobes, hyperintensities in the posterior white matter, cerebral atrophy and dentate nuclei or may be normal (Morrison-Levy *et al.*, 2021) (Figure 1).
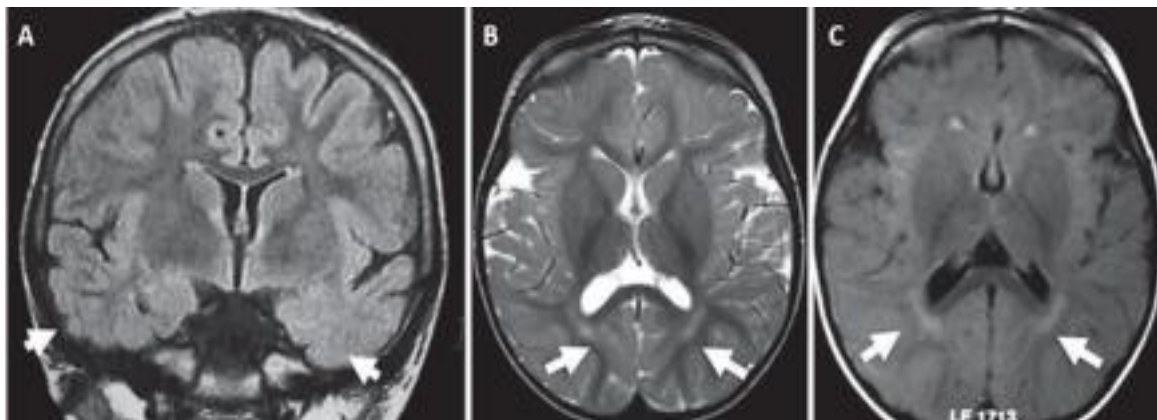
Figure 1: Brain MRI results reveal specific findings in patients with CDKL5 point mutations. Figure A displays nonspecific hyperintensities in both temporal lobes (T2 FLAIR coronal section) of a 12-year-old patient with a *CDKL5* mutation. In Figure B, a 3-year-old *CDKL5* mutation patient exhibits nonspecific periventricular hyperintensities (T2 axial section). Similarly, Figure C shows nonspecific periventricular hyperintensities (T2 FLAIR axial section) in a 9-month-old *CDKL5* mutation patient. The arrows indicate the precise locations of the primary abnormalities in each corresponding figure (Bahi-Buisson and Bienvenu, 2012b).

In addition to epileptic encephalopathy, CDD patients experience significant developmental delays, manifesting as a persistent inability to acquire proper motor skills, often accompanied by severe hypotonia. Approximately 85% of cases also exhibit autistic-like characteristics, including reduced social interaction and impaired eye fixation. However, it

is important to note that while these autistic features can contribute to poor eye contact, other factors such as visual impairment or the presence of epileptic encephalopathy can also contribute to this behavior. Moreover, individuals with CDD commonly display two types of repetitive movements: hand stereotypies, such as hand mouthing and hand clapping, and bruxism.

The CDD phenotypic spectrum encompasses various additional traits, both commonly observed and less frequently reported. These include cortical visual impairments, disruptions in sleep patterns and respiratory functions, absence of language skills, cardiorespiratory dysrhythmias, difficulties with feeding, constipation, dysautonomia (dysfunction of the autonomic nervous system), and scoliosis (Bahi-Buisson *et al.*, 2008b; Artuso *et al.*, 2010; Pini *et al.*, 2012; Fehr *et al.*, 2013; Demarest *et al.*, 2019; Kadam *et al.*, 2019) (Figure 2).
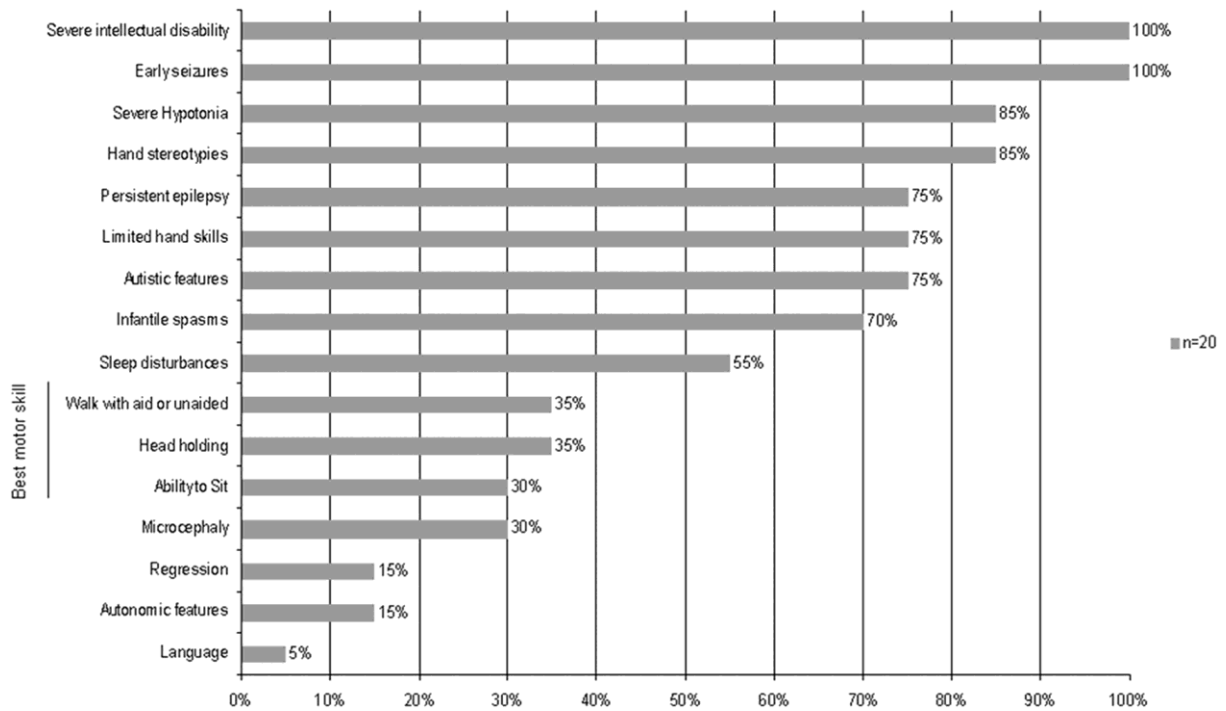
Figure 2. Prevalence of 18 clinical features in 20 CDD patients. Early seizures were observed in all CDD patients (Bahi-Buisson *et al.*, 2008b).

1.2 Cyclin-dependent kinase-like 5 (CDKL5)

1.2.1 *CDKL5* gene

The human *CDKL5* gene was initially identified through a positional cloning study to identify disease-genes mapping on the Xp22, a critical region for several pathologies on the X- chromosome (Montini *et al.*, 1998). The gene was named *STK9* (Serine Threonine Kinase 9) for the sequence homologies with the serine-threonine protein family (Montini *et al.*, 1998), given the strong similarity to some cell division protein kinases, it was subsequently renamed Cyclin-Dependent Kinase-Like 5 (*CDKL5*).

The human gene *CDKL5* is located on the short arm of the X- chromosome in position 22 (Xp22), spanning approximately 240kb. It comprises 27 exons that rearrange in five major transcript isoforms containing distinct coding regions (Hector *et al.*, 2016). Although all the isoforms appear to have the same ATG start codon from exon 2, the first 6 untranslated exons (exons 1, 1a, 1b, 1c, 1d, and 1e) contain transcriptional start sites (TSS), suggesting their role of promoters and reflecting the differences in the 5'UTR of the different transcribed mRNAs. Exons 1, 1a, and 1b act as promoters of the adult brain's isoforms, whereas exons 1c and 1d are used by isoforms that are notably expressed in the adult testis (Hector *et al.*, 2016). On the contrary, the last exons (19-22) codify for a very large 3'UTR (>6,6kb), implying their importance in the potential additional regulation of *CDKL5* transcripts, while the coding sequence is contained within the remaining exons 2-22 (Figure 3) (Hector *et al.*, 2016)

Figure 3. Human *CDKL5* gene (modified from (Balestra *et al.*, 2019). Schematic representation of the *CDKL5* gene with introns and exons represented respectively by lines and boxes. The catalytic domain is shown in green while the C-terminus domain is depicted in red.

1.2.2 CDKL5 protein structure and protein isoforms

In 1998, *CDKL5* was first reported as a gene encoding a novel protein kinase situated on the X chromosome, and coding for a protein of 1030 amino acids (Mari *et al.*, 2005; Katayama *et al.*, 2020).

CDKL5 protein has a kinase activity and it belongs to the CMGC family of serine/threonine kinases (Bertani *et al.*, 2006), which includes cyclin- dependent kinases (CDKs), mitogen-activated protein kinases (MAP kinases), glycogen synthase kinases (GSK) and CDK-like

(CDKL) kinases (Montini *et al.*, 1998; Canning *et al.*, 2018). Human CDKL5 protein is characterized by an N-terminal catalytic domain (aa 13-297), which is homologous to the one of the other CDKL-family members, but mostly by its uniquely long C- terminal tail (over 600 aa), with no obvious similarities to other protein domains but with a high degree of conservation between the different CDKL5 orthologs that differ only for the extreme C-terminus (Figure 4).

The N-terminal region includes the ATP-binding region (aa 13-43), the serine- threonine kinase active site (aa 131-143), and the typical TEY motif (Thr-Asp-Tyr, aa 169-171) of the MAPK proteins, whose dual phosphorylation usually induces protein kinase activation. Interestingly as other CMGC protein kinases, CDKL5 itself, is capable of autophosphorylate this motif (Lin *et al.*, 2005; Bertani *et al.*, 2006).

Instead, the large C-terminal region presents a unique sequence that includes two nuclear localization signals (NLSs) and one nuclear export sequence (NES), that are involved in protein import/export from the nucleus, regulating protein subcellular localization (Lin *et al.*, 2005; Rusconi *et al.*, 2008).

The kinase function of the protein is attributed to the N-terminal catalytic domain, which carries out the enzymatic activity. On the other hand, the C-terminal domain appears to play a regulatory role in controlling the catalytic action of the protein as well as its intracellular distribution (Russo *et al.*, 2009; Stalpers *et al.*, 2012; Bahi-Buisson *et al.*, 2012a) .
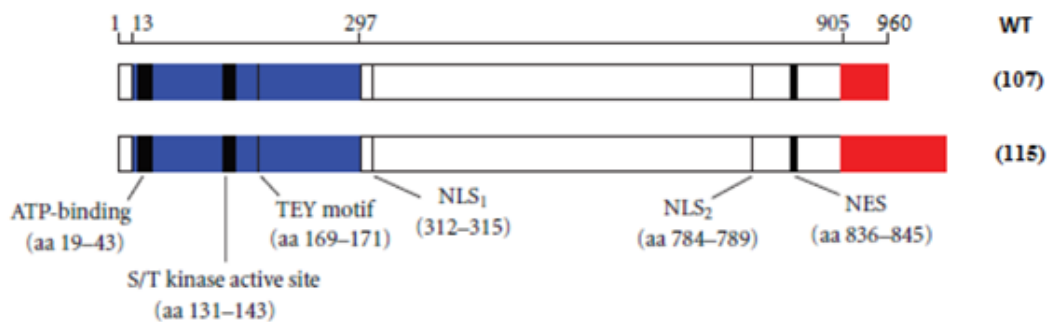
Figure 4: Schematic representation of the protein isoforms hCDKL5_1 (CDKL5$_{107}$) and hCDKL5_5 (CDKL5$_{115}$) with the functional domains and signatures indicated. *NLS:* nuclear localization signal; *NES:* nuclear export signal. (modified from Kilstrup-Nielsen *et al.*, 2012).

The human *CDKL5* gene undergoes alternative splicing events leading to the production of at least five distinct proteins in humans: hCDKL5_1 to hCDKL5_5 (Katayama *et al.*, 2020) (Figure 5). The transcripts hCDKL5_1 and hCDKL5_5 encode for the two main CDKL5 protein isoforms, namely CDKL5$_{107}$ and CDKL5$_{115}$, respectively. Initially, CDKL5$_{115}$ was the first isoform to be discovered and studied (Kalscheuer *et al.*, 2003; Tao *et al.*, 2004).

However, later research revealed that CDKL5$_{107}$ is the predominant isoform expressed in the central nervous system of humans and mice (Williamson *et al.*, 2012). This suggests that CDKL5$_{107}$ likely plays a primary pathogenic role in the development of CDKL5 disorder. The variations in weight between the two isoforms (107kDa and 115kDa) are attributed to differences in their C-terminal regions, which are believed to be involved in regulating activity, determining localization, and facilitating protein interactions (Lin *et al.*, 2005; Rusconi *et al.*, 2008). Significantly, one of these transcripts (CDKL5_1) is prevalent in several species, such as mice, which makes *Cdkl5* mouse models highly pertinent for investigating the functions of CDKL5 (Kilstrup-Nielsen *et al.*, 2012).

Additionally, three others human CDKL5 transcripts have been identified: hCDKL5_2, hCDKL5_3, and hCDKL5_4. These transcripts are highly similar to hCDKL5_1 but exhibit variations such as the inclusion of exon 17, truncation of exon 11 due to alternative splicing, or a combination of both. Exon 17 does not contain known functional elements, while truncation of exon 11 results in the potential loss of a nuclear localization signal. The specific characteristics and functions of the proteins encoded by these transcripts have not been characterized yet, likely due to their lower abundance compared to the other isoforms (Hector *et al.*, 2016).
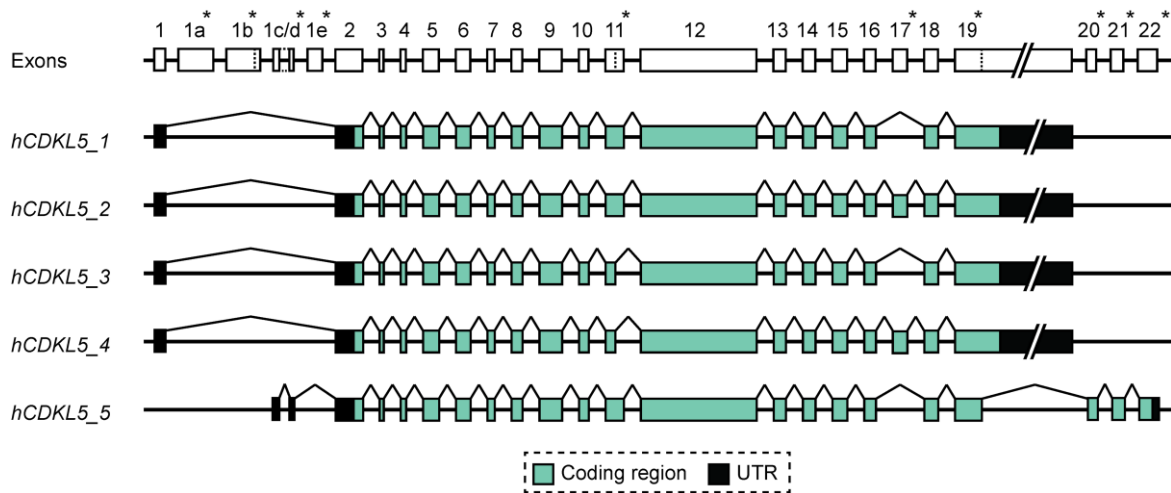
Figure 5. Human *CDKL5* gene and transcript isoforms. Splicing events are represented as angled lines connecting exons, dotted lines are used to denote alternative splice sites, suggesting the presence of multiple possible arrangements. Asterisks placed next to exon numbers highlight the locations where differences occur among various transcript isoforms (Hector *et al.*, 2016).

For this research, to provide a comprehensive overview of CDKL5 protein isoforms, it is essential to include the isoforms found in mice as well. The majority of the CDKL5 coding region is similar and well-preserved between humans and mice (as shown in Figure 6).

While mice have a total of 23 exons compared to humans (27), both species produce five major transcript isoforms with distinct coding regions. The murine isoforms mCDKL5_1-2 correspond to their human counterparts in an orthologous manner. However, the remaining three mouse isoforms, namely mCDKL5_6, mCDKL5_7, and mCDKL5_8, exhibit a higher level of dissimilarity (Hector *et al.*, 2016).
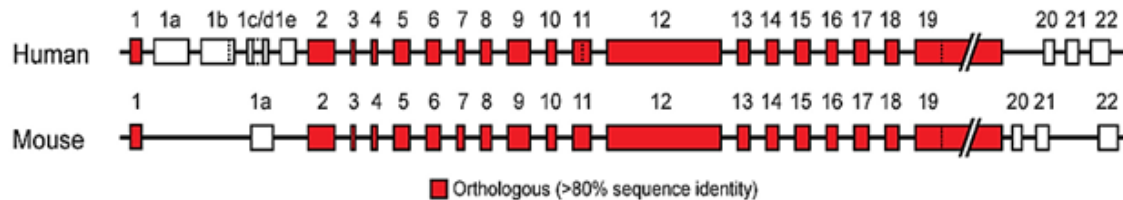
Figure 6. Correlation between human and mouse *CDKL5* gene structures (Hector *et al.*, 2016).

1.2.3 CDKL5 pathological mutations

Since the discovery of the first disease-causing mutation in the *CDKL5* gene in 2003, researchers have been investigating how disruptions in the CDKL5 protein lead to specific phenotypes. The majority cases of CDD arise from *de novo* mutations. However, there have been reported instances of *CDKL5* mutations in individuals with a family history of the disorder. These cases likely arise from germline mosaicism in one of the parents. Germline mosaicism refers to the presence of a mutation in some but not all germ cells (sperm or eggs) of an individual. In these situations, the offspring may inherit the mutated *CDKL5* gene, leading to the manifestation of CDD (Jakimiec *et al.*, 2020).

A wide range of pathogenic mutations, including missense and nonsense mutations, small and large deletions, frameshifts, and aberrant splicing, have been identified (as depicted in Figure 7) (Tao *et al.*, 2004; Kilstrup-Nielsen *et al.*, 2012; Hector *et al.*, 2017). The most common mutation (62%) was a transition at CpG dinucleotides (Bahi-Buisson *et al.*, 2012a). This mutational heterogeneity may contribute to the clinical variability observed in CDD.

Although the number of documented cases is limited, it has been noted that the *de novo* mutations identified encompass various regions of the CDKL5 protein. While large-scale mutations such as chromosomal rearrangements involve significant alterations within the *CDKL5* gene region, small-scale mutations are evenly distributed across the entire coding sequence.

Figure 7. Graphical map of *hCDKL5* genomic locus and the reported *CDKL5* mutations. (Kilstrup-Nielsen *et al.*, 2012). In color exons codifying for kinase domain (blue) and extreme C-terminal tail (red). Above: deletions, frameshift mutations and splice variants; Below: Missense and nonsense mutations (fuchsia and black).

It is interesting to note that missense mutations primarily occur in the catalytic domain of the protein. These mutations involve single amino acid substitutions that can significantly impact the structural folding required for the proper formation of the kinase pocket. This observation underscores the critical role of CDKL5 catalytic activity in ensuring correct brain function and development. On the other hand, various types of mutations such as nonsense mutations, frameshifts, and aberrant splicing can lead to premature stop codon formation and truncation of the protein. These mutations can occur in both the N-terminal and C-terminal regions, suggesting the relevance of the long tail for protein activity. While missense mutations do not typically affect protein expression levels, there are no reports of truncated proteins in human cells, indicating that these types of mutations may trigger the process of nonsense-mediated mRNA decay (Bahi-Buisson *et al.*, 2008b). To explore the molecular consequences of these mutations and the most commonly observed modifications in patients, researchers have conducted experiments involving the overexpression of mutated variants in non-neuronal cell culture lines (Lin *et al.*, 2005; Bertani *et al.*, 2006; Rusconi *et al.*, 2008). These studies have shed light on the molecular effects of the mutations. Notably, they have revealed that the C-terminal region of the protein plays multiple regulatory roles. It acts as a negative regulator of the protein's phosphorylating activity and is involved in determining its subcellular localization. Mislocalization of the protein due to mutations in this region could potentially contribute to the pathogenic phenotype associated with the disorder, particularly considering the significance of proper kinase localization-related functions.

Loss-of-function mutations, which result in impaired catalytic activity, are often associated with a more severe form of the pathology. This observation suggests a correlation between the extent of functional impairment and the severity of the resulting phenotype. Conversely, gain-of-function alterations, which typically retain kinase function but affect its control and regulation, have been proposed to have a lesser impact on the overall phenotypic outcome (Rusconi *et al.*, 2008; Fehr *et al.*, 2016).

In the context of CDKL5, two well-known derivatives associated with Rett syndrome (RTT), namely R781X and L879X, are suggested to cause neurological phenotypes. These derivatives lead to kinase mislocalization into the nucleus and exhibit increased autocatalytic activity in vitro (Bertani *et al.*, 2006). However, further investigation is needed to determine the precise in vivo expression and functional consequences of these mutations. In addition, large duplication events involving the *CDKL5* gene have also been identified in various studies (Szafranski *et al.*, 2015). However, these duplications often encompass a broad region (ranging from 8 to 21 megabases) and include multiple genes, making it challenging to interpret the specific effects of gene overexpression in such cases (Hector *et al.*, 2017). While more evidence is needed to establish a well-defined CDKL5 duplication syndrome, similar to what is observed in closely related genes such as *MeCP2* and *FOXG1*, the potential influence of gene dosage effects should be considered.

Continued investigation of cases that examine both genotypic and phenotypic expressions, as well as the diagnosis of copy number variations involving CDKL5, may contribute to a better understanding of the pathological aspects associated with *CDKL5* mutations.

1.2.4 Genotype-phenotype correlation

Genotype-phenotype characterization is useful both for the understanding of CDKL5 function and for prognostic family counseling.

The majority of reported CDD patients are girls; however, boys with CDD have been identified, with a female/male ratio of 4:1 (Olson *et al.*, 2019). Male patients, hemizygous for *CDKL5* mutations (YX-), with just one mutated copy of *CDKL5,* seemed to show a more severe phenotype compared to heterozygous females (XX-), who usually have a wild-type copy of the gene that was thought to be responsible for the milder form of the pathology (Fehr *et al.*, 2015; Liang *et al.*, 2019). Nevertheless, in a recent clinical study conducted by the International Foundation for CDKL5 Research Centres of Excellence (COEs), it was indicated that males may exhibit a less severe manifestation, and there were no notable distinctions found between genders (Olson *et al.*, 2019). However, female cells, can express

either the normal or the mutated copy, due to the process of dosage compensation of the X chromosome expression through random X-inactivation. Because of this, the different phenotypic outcomes of the disorder may arise from the resulting variable mosaic pattern among different tissues in the body (Zhou *et al.*, 2017), but the influence of somatic CDKL5 mosaicism on clinical phenotype is still unknown (Olson *et al.*, 2019). Furthermore, this big clinical heterogeneity can also be explained by the wide *CDKL5* mutational spectrum identified in patients, accounting for the severe to profound alterations in CDKL5 protein function (Bahi-Buisson *et al.*, 2008a; Bahi-Buisson *et al.*, 2008b; Fehr *et al.*, 2016). Therefore, the clinical picture of patients extends from a milder form of the disorder with independent ambulation and controlled epilepsy to severe forms that include no motor milestones, absolute microcephaly, and intractable refractory seizures. Recently, Aznar-Laìn and colleagues reported a rare and less severe phenotype of CDD that does not involve epilepsy. These findings suggest that epilepsy may not be a mandatory characteristic in CDKL5 deficiency disorder. They specifically highlight a distinct phenotype of CDD that does not manifest epilepsy and document the first male individual with this phenotype. The nature of the *CDKL5* mutation and the pattern of X-chromosome inactivation may contribute to the development of this milder form of CDD (Aznar-Laín *et al.*, 2023).

Moreover, the reported case of two twin CDD patients, showing a significant discordant phenotype, strengthened the idea that *CDKL5* mutational variability is strictly correlated to the heterogeneous clinical presentation (Weaving *et al.*, 2004). Since both girls were characterized by random X-inactivation, this observation emphasizes the idea that epigenetic or environmental factors may also play a role in influencing the phenotypic outcome of the pathology (Kilstrup-Nielsen *et al.*, 2012).

After almost a decade of data collection, in 2021, Mackay and colleagues conducted a study in which they collected data on individuals with CDD. The information gathered from these individuals and their families was submitted to the International CDKL5 Disorder database (https://www.cdkl5.com/cdkl5-international-registry-database). The data was collected through online or paper-based questionnaires that were completed by the families of individuals with CDD (Mackay *et al.*, 2021). The study spanned almost a decade, providing valuable insights into the condition, and contributing to the growing body of knowledge on CDKL5-related disorders.

During the analysis of the collected data, the CDKL5 variants were categorized into five groups based on their predicted functional consequences. These groups were as follows: (1)

variants leading to the absence of functional protein, (2) missense or in frame variants within the catalytic domain, (3) truncations occurring between amino acid 172 and amino acid 781, (4) truncations occurring after amino acid 781 (Bertani *et al.*, 2006; Fehr *et al.*, 2015). However, it remains unclear whether these categorizations are optimal and comprehensive. To enhance the accuracy and efficiency of data collection, a questionnaire was developed. This questionnaire included inquiries about developmental milestones, gross and fine motor skills, seizures, feeding and gastrointestinal health, respiratory illnesses, behavior, communication, sleep, vision, and scoliosis. To group individuals with similar expected developmental abilities together, they were assigned to specific age categories. This approach facilitated the analysis and comparison of data among individuals within the same developmental stage.

In their study utilizing a comprehensive international dataset, Mackay and colleagues found significant variations in the severity of phenotypes associated with specific recurrent variants in the *CDKL5* gene. Notably, individuals carrying missense variants such as p.Arg178Trp and p.Arg178Gln, as well as the nonsense variant p.Arg559*, exhibited the most severe phenotypes. These variants were associated with high severity scores, indicating a limited attainment of developmental milestones.

Conversely, individuals with variants like p.Arg134* and p.Arg550* demonstrated milder phenotypes with lower severity scores, suggesting a relatively better achievement of developmental milestones.

The extensive and robust data collected through the International CDKL5 Disorder Database have the potential to provide valuable prognostic information during genetic counseling. While initial research findings have demonstrated the feasibility of utilizing this data for prognostic purposes, it is important to note that only a small number of variants have been identified with sufficient recurrence, accounting for approximately 22% (62 out of 285) of the individuals in the database (Mackay *et al.*, 2021).

Currently, despite the observed relative homogeneity of certain clinical phenotypes among patients carrying the same mutation, we are still far from achieving a clear and definitive understanding of the genotype-phenotype correlation in CDKL5-related disorders. This highlights the complexity and heterogeneity of the disorder, indicating that further research and data collection are necessary to unravel its intricacies and fully comprehend its clinical manifestations.

1.2.5 CDKL5 expression profile

1.2.5.1 Tissue-dependent expression

The levels of CDKL5 proteins and their specificity in different tissues have been examined in humans and mice. Studies have revealed that CDKL5 mRNA levels are highest in the brains of both species, which aligns with the disease's pathological characteristics (Williamson *et al.*, 2012). However, CDKL5 can also be found in other organs such as the testis, prostate, spleen, lung, uterus, and placenta, albeit at lower levels. It is also detectable, albeit less prominently, in the heart, kidney, liver, and skeletal muscle (Figure 8). This broad expression suggests that CDKL5 may have functions not only in the nervous system but also in various organs.
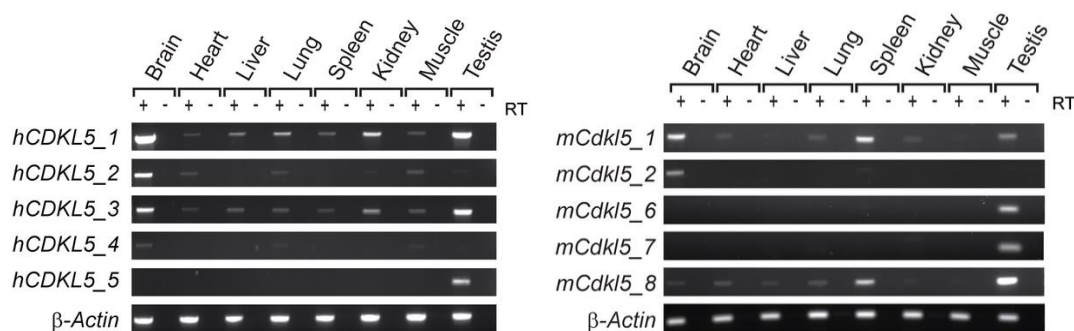
Figure 8. CDKL5 isoform expression in human tissues (left) and in mouse tissues (right). RT-PCR analysis of CDKL5 isoforms in a panel of adult tissues. β-Actin was used as a loading control (Hector *et al.*, 2016).

Research involving RT-PCR analysis of CDKL5 isoforms in adult tissues has been conducted, using β-Actin as a reference for comparison (Hector *et al.*, 2016). It is important to note that CDKL5 expression in the developing mouse brain follows a temporal and spatial pattern (Rusconi *et al.*, 2008). During embryonic stages, CDKL5 expression levels are relatively low. However, they undergo a significant induction during the first two weeks after birth, reaching a plateau at P14 in mice. Following this initial increase, CDKL5 expression gradually declines.

Considering the striking resemblance between CDD and RTT and considering the developmental expression pattern of MeCP2, a potential link between neuronal maturation and CDKL5 expression has been contemplated. In fact, although CDKL5 is diminished during embryonic stages, its expression emerges during the perinatal period and exhibits a significant increase in the early days after birth, demonstrating a well-regulated modulation

of CDKL5 expression throughout prenatal and postnatal development (Rusconi *et al.*, 2008).

Furthermore, in situ hybridization studies conducted on rat and mouse brain has revealed varying levels of CDKL5 in different brain regions (Weaving *et al.*, 2004; Mari *et al.*, 2005; Chen *et al.*, 2010). Forebrain structures like the hippocampus and cortex exhibit higher expression levels compared to other regions. The thalamus and striatum also show detectable, albeit lower, levels of CDKL5, while the cerebellum and hypothalamus display minimal presence (Rusconi *et al.*, 2008). In the hippocampus, high CDKL5 levels are found in all CA fields except the dentate gyrus (DG), where neuronal maturation and neurogenesis primarily occur in adulthood (Kilstrup-Nielsen *et al.*, 2012). As for cortical areas, superficial layers such as the motor, cingulate, pyriform, and entorhinal cortices, which play roles in higher cognitive functions such as language and information processing, exhibit higher levels of CDKL5 expression compared to other cortical areas, suggesting the physiological importance of this kinase for these brain districts (Kilstrup-Nielsen *et al.*, 2012) (Figure 9).
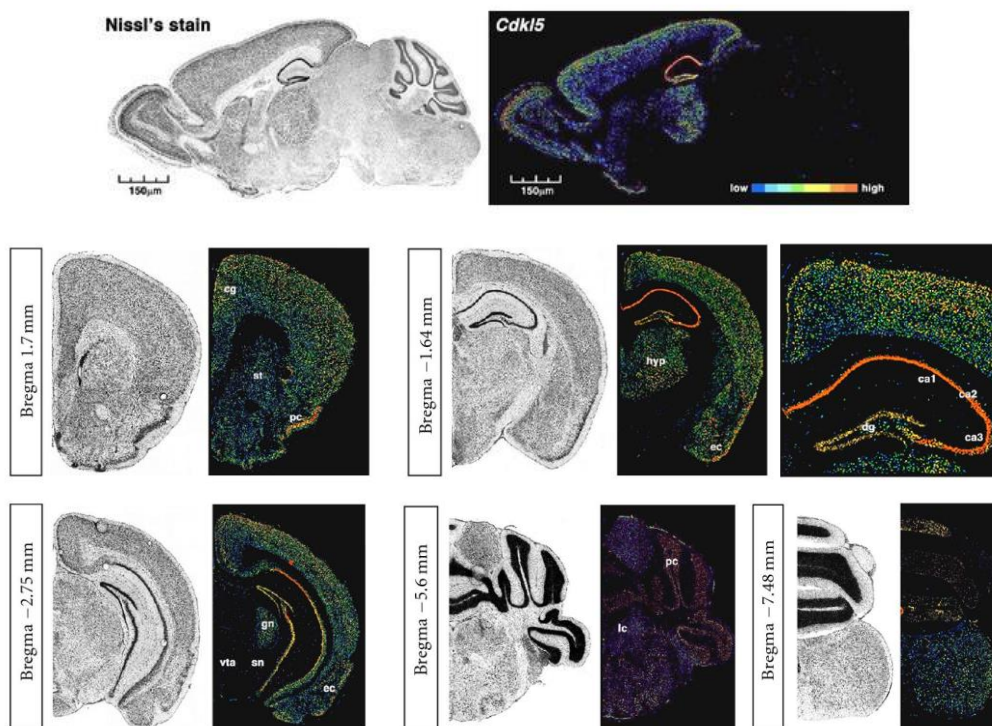
Figure 9. CDKL5 expression profile in the mouse brain (Kilstrup-Nielsen *et al.*, 2012)

1.2.5.2 Cell-type-dependent expression

At the cellular level, CDKL5 is readily detectable in most neurons but expressed at very low levels in glial cells (Rusconi *et al.*, 2008; Rusconi *et al.*, 2011), suggesting a potential

essential role in neuronal development and function. Based on its expression pattern, it has been hypothesized that CDKL5 is primarily expressed in glutamatergic and GABAergic neurons, with limited expression in dopaminergic and noradrenergic regions.

However, CDKL5 transcript levels not only differ among brain areas and cell types but also exhibit distinct spatial and temporal expression profiles within various cellular compartments (Hector *et al.*, 2016). Neuronal CDKL5 protein is found in both the nucleus and cytoplasm, with the ratio varying depending on brain regions and developmental stages (Rusconi *et al.*, 2008). During embryonic and early postnatal stages, CDKL5 is predominantly cytoplasmic (Figure 10). However, the nuclear fraction increases during postnatal stages, starting from P14 (post-natal day fourteen), until adulthood. This differential localization is particularly observed in the hippocampus, cortex, and thalamus, where approximately 40% of total CDKL5 is detected in the nucleus, compared to around 20% in the striatum and cerebellum (Rusconi *et al.*, 2008).
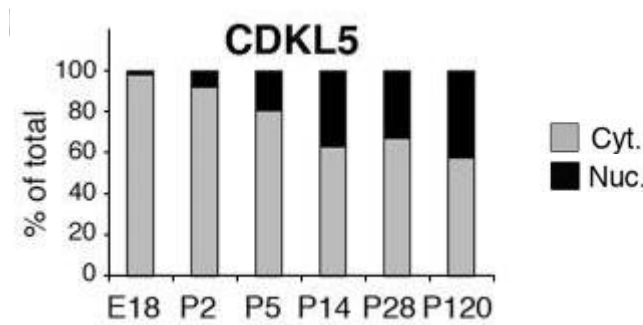
Figure 10. The cytoplasmic and nuclear levels of CDKL5 in early postnatal stages of the developing mouse brain. Grey bars indicate cytoplasmic localization, the black bars indicate nuclear levels (Rusconi *et al.*, 2008).

Additionally, CDKL5 has been discovered to be present in excitatory postsynaptic structures, playing a crucial role in regulating dendritic spine maturation, growth, and controlling excitatory synaptic function (Ricciardi *et al.*, 2012; Pizzo *et al.*, 2020). The synaptic localization of CDKL5 is facilitated by its interaction with the palmitoylated form of postsynaptic density protein 95 (PSD-95) (Zhu *et al.*, 2013; Zhang *et al.*, 2014).

Studies conducted in non-neuronal cell cultures have revealed that the translocation of CDKL5 is regulated by an active export mechanism. This process is mediated by the receptor CRM1/Exportin 1, which recognizes nuclear export signals present in the C-terminal domain of the CDKL5 protein (Rusconi *et al.*, 2008). The C-terminal domain also contains a nuclear localization signal (NLS) that is essential for the nuclear import of CDKL5. Phosphorylation of CDKL5 near its NLS by the dual specificity tyrosine-

phosphorylation-regulated kinase 1A (DYRK1A) localizes the kinase in the cytosolic compartment of cultured neuronal cells (Oi *et al.*, 2017).

Further studies have confirmed the crucial role of the C-terminal region in determining the subcellular localization of CDKL5 protein isoforms when exogenously expressed (Lin *et al.*, 2005; Bertani *et al.*, 2006; Williamson *et al.*, 2012). Interestingly, in primary murine hippocampal neurons, CDKL5 is found in both the nucleus and the cytoplasm. However, it does not undergo constitutive shuttling between these compartments as observed in proliferating cells. In contrast, glutamate stimulation resulted in the translocation and accumulation of the kinase in the perinuclear cytoplasm (Rusconi *et al.*, 2011). Additionally, prolonged exposure to glutamate stimulation led to the degradation of CDKL5 through the proteasome. These events were mediated by the specific activation of N-methyl-D-aspartate receptors (NMDARs) located in the extrasynaptic region. Furthermore, the degradation through the proteasome pathway was also triggered by the withdrawal of neurotrophic factors and the hydrogen peroxide treatment, which are two distinct methods of inducing cell death. These results indicate that the expression and positioning of CDKL5 are influenced by the activity of extrasynaptic NMDARs.

1.2.6 CDKL5 target proteins and downstream signaling pathways

Supporting the concept of a nuclear role for CDKL5, potential binding partners and targets within the nucleus have been proposed, primarily identified through in vitro kinase assays or investigations in heterologous cell lines.

 These interactions include DNA methyltransferase 1 (DNMT1) and suggest that CDKL5 may participate in regulating mRNA splicing activity by associating with the nuclear speckle component SC35 (Kameshita *et al.*, 2008; Ricciardi *et al.*, 2009).

In recent investigations, multiple laboratories have reported a growing body of evidence supporting the functional association between CDKL5 microtubules and actin (Ricciardi *et al.*, 2012; Amendola *et al.*, 2014; Barbiero *et al.*, 2017a; Barbiero *et al.*, 2017b; Muñoz *et al.*, 2018; Baltussen *et al.*, 2018b). Microtubules, along with actin and intermediate filaments, form a dynamic structural framework within neurons which plays a vital role in intracellular transportation of cargo and facilitates neuronal adaptations, crucial for synaptic plasticity (Kapitein and Hoogenraad, 2015).

A chemical-genetic approach was employed to identify direct targets of CDKL5 kinase activity, this approach utilized an ATP analog-specific mutant of CDKL5 in mouse brain tissue lysates, combined with thiophosphopeptide-targeted mass spectrometry. The study

revealed that CDKL5 directly phosphorylates peptides at the RPXS* motif, which are associated with proteins involved in the microtubule network of neurons (Baltussen *et al.*, 2018b). Notable targets included the microtubule-associated protein RP/EB family member 2 (MAPRE2/EB2), microtubule-associated protein 1S (MAP1S), and Rho guanine nucleotide exchange factor 2 (ARHGEF2). These findings were corroborated by an independent group that conducted a global phosphoproteomic screen using TMT-based labeling to identify CDKL5 substrates. This study confirmed the enrichment of CDKL5-phosphorylated proteins associated with the actin cytoskeleton and microtubule-related proteins, including MAP1S, DLG5 (discs large MAGUK scaffold protein 5) and ARHGEF2 (Rho-Rac guanine nucleotide exchange factor 2) (Muñoz *et al.*, 2018).

Furthermore, Munoz and colleagues found the interaction between CDKL5 and the centrosomal protein CEP131 (Muñoz *et al.*, 2018), this protein is implicated in the formation and function of primary cilia (Graser *et al.*, 2007). Depletion of CEP131 can cause reduced proliferation rate, centriole amplification, chromosomal instability, and DNA damage (Staples *et al.*, 2012; Villumsen *et al.*, 2013; Tollenaere *et al.*, 2015). These findings align with observations of increased cell death and DNA damage-associated biomarkers in mouse hippocampal cultures and human neuroblastoma (SH-SY5Y) cell lines following CDKL5 deletion (Barbiero *et al.*, 2017a; Fuchs *et al.*, 2019; Loi *et al.*, 2020).

Intriguing connections between CDKL5 and primary cilia have been reported, Canning et al. in 2018 showed that human CDKL5 localizes to cilia and impairs ciliogenesis when overexpressed (Canning *et al.*, 2018). Furthermore, Di Nardo et al., in 2022 reported elongated and slender cilia in rat and mouse *Cdkl5* KO brain (Di Nardo *et al.*, 2022).

Collectively, these discoveries shed light on a novel, activity-dependent molecular pathway involved in the regulation of dendritic microtubules, which may be relevant to the pathology of CDKL5-related disorders.

Several hypotheses have been proposed regarding the synaptic role of CDKL5 within neurons. In rat primary neuron cultures, it was observed that knockdown of CDKL5 disrupted neuronal morphogenesis and neurite outgrowth during BDNF-induced actin remodeling, indicating its association with Rac1 (Chen *et al.*, 2010). Similarly, two independent studies highlighted the involvement of CDKL5 in dendritic spine morphology in cultured hippocampal neurons. CDKL5 was found to interact with phosphorylating netrin-G1 ligand (NGL-1) and co-localize with palmitoylated postsynaptic density protein 95 (PSD-95), both of which are components of the postsynaptic compartment (Ricciardi *et*

al., 2012; Zhu *et al.*, 2013). In an in vitro system, CDKL5 was also linked to the phosphorylation of amphiphysin 1 at the presynaptic terminal (Sekiguchi *et al.*, 2013; Katayama *et al.*, 2015). Furthermore, a yeast two-hybrid screen identified an interaction between CDKL5 and shootin1, a regulator of neuronal polarization during axon development (Nawaz *et al.*, 2016). Notably, a mind bomb 1 (Mib1) interactome screen revealed that CDKL5 is ubiquitinated by Mib1 and targeted for degradation by the proteasome (Mertz *et al.*, 2015). However, the direct relevance of these synaptic and axonal targets in vivo is yet to be validated, largely due to limitations in visualizing and tagging endogenous CDKL5.

The protein interaction network and downstream signaling pathways involving CDKL5 are still not fully understood. However, the development of *Cdkl5* KO mice has provided initial insights into some intriguing signaling changes. A kinome profiling study conducted by Wang et al. revealed disruptions in several signaling transduction pathways associated with neuronal and synaptic plasticity in the forebrain of male *Cdkl5* KO mice (Wang *et al.*, 2012). These changes included alterations in the phosphorylation profiles of AMPK, AKT, PKC, and MAPK substrates. Importantly, these pathways converge downstream of PTEN signaling, which has been implicated in the etiology of various neurodevelopmental disorders such as autism, Rett syndrome (RTT), Fragile X syndrome (FXS), and Tuberous Sclerosis (Rademacher and Eickholt, 2019).

Similarly, Amendola et al. reported a decrease in the phosphorylation of AKT at Ser473 and rpS6 at Ser240/244 in multiple brain structures (cortex and hippocampus) of male hemizygous and female heterozygous and homozygous *Cdkl5* KO mice (Amendola *et al.*, 2014).

The AKT-GSK3β signaling pathway holds particular interest among the signaling pathways affected by the absence of CDKL5. This pathway is crucial for brain development and function (Salcedo-Tello *et al.*, 2011). Elevated GSK-3β activity contributes to various neurodevelopmental abnormalities observed in *CDKL5*-deficient brains. Notably, the inhibition of GSK-3β through pharmacological means rescues dendritic morphogenesis and synapse development in mice lacking *Cdkl5* (Fuchs *et al.*, 2015; Fuchs *et al.*, 2018b). Similarly, the AKT activator IGF-1 demonstrates beneficial effects on the impaired number and dynamics of dendritic spines in *Cdkl5* KO mice (Della Sala *et al.*, 2016). However, it is important to note that while GSK-3β inhibition proves advantageous in juvenile *Cdkl5* KO mice, it may not be as effective in adults (Fuchs *et al.*, 2018a).

This suggests that interventions targeting only the dysregulated GSK-3β activity might not suffice to fully restore the complex defects associated with CDD.

1.3 *Cdkl5* KO mouse models

Animal models enable the investigation of the underlying pathological and physiological mechanisms of diseases. Specifically, mice have emerged as the primary model organism in human disease research. Mice colonies are advantageous due to their lower maintenance costs and easier breeding in captivity compared to other mammals. The key factors contributing to the prominence of mice include their genetic similarity to humans, sharing approximately 99% of genes, and the ability to manipulate their genomes to create models of human pathologies. Thus, mice serve as a valuable tool for preliminary biomedical experimentation before testing in humans. Experimental techniques can "humanize" the mouse physiology, allowing the study of human diseases that mice do not typically develop, mimicking clinical manifestations. This approach facilitates the investigation of disease mechanisms and serves as a starting point for therapeutic interventions in patients (Rosenthal and Brown, 2007).

As mentioned earlier, both human and mouse CDKL5_1 isoforms are highly abundant in the brain, exhibiting similar expression profiles and a substantial degree of sequence similarity at the nucleotide and amino acid level (Hector *et al.*, 2016). This significant homology has enabled the development of animal models that are highly relevant for studying CDD. Although these animal models do not fully replicate the disorder, they are indispensable for in-depth investigations into the development and progression of the disease and provide a valuable foundation for therapeutic interventions.

Over the years, several KO mouse models targeting *Cdkl5* have been created and extensively characterized. Specifically, constitutive KO mouse models have been generated to examine how CDKL5 dysfunction leads to neurological defects in CDD.
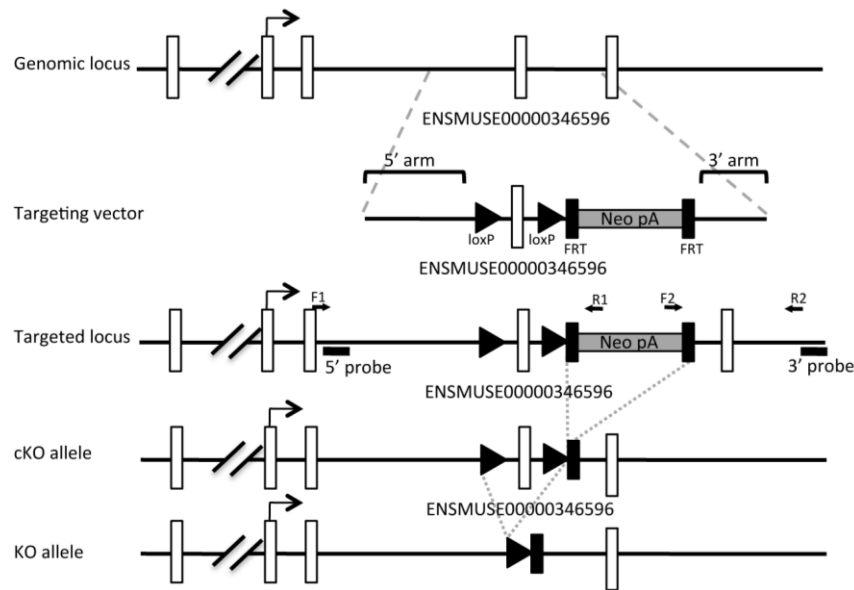
Figure 11. Generation of *Cdkl5* knockout mice (Amendola *et al.*, 2014)**.**

Utilizing the site-specific Cre-Lox recombinase technology, researchers have targeted exons 6 (Wang *et al.*, 2012; Jhang *et al.*, 2017), exon 4 (Amendola *et al.*, 2014), and exon 2 (Okuda *et al.*, 2017) in constitutive KO mouse models, resulting in a premature stop codon within the N-terminal kinase domain, effectively mimicking a loss of function mutation (Figure 11).

In addition to constitutive models, several conditional KO mouse models for *Cdkl5* have been generated to investigate the specific cell types responsible for CDKL5 deficiency-related symptoms (Amendola *et al.*, 2014; Tang *et al.*, 2017; Schroeder *et al.*, 2019; Wang *et al.*, 2021; Terzic *et al.*, 2021b). Amendola et al. crossed mice carrying a Cre-conditional knockout (cKO) allele of *Cdkl5* with the Dlx5/6::Cre transgene (targeting CDKL5 expression specifically in cortical GABAergic neurons such as cortical interneurons and striatal medium spiny neurons) or the Emx1::Cre transgene (targeting CDKL5 expression specifically in cortical glutamatergic neurons, including cortical and hippocampal pyramidal neurons) (Amendola *et al.*, 2014). Similarly, Tang et al. have developed an additional mouse model for conditional knockout of *Cdkl5*, specifically targeting the deletion of *Cdkl5* in exon 6 of excitatory forebrain neurons. This was achieved using the Nex-Cre mouse line (Tang *et al.*, 2017).

Moreover, to examine the impact of *Cdkl5* loss-of-function specifically in CaMKIIα-positive excitatory neurons and GAD65-positive inhibitory neurons, Schroeder et al developed a new conditional KO mouse model (Schroeder *et al.*, 2019). The research

conducted on this model revealed that the absence of *Cdkl5* in these specific neuronal populations disrupts various components of the mTOR signaling pathway (Schroeder *et al.*, 2019) that plays a crucial role in governing gene expression, protein synthesis, and neuronal growth (Saxton and Sabatini, 2017).

In 2021, Terzic and colleagues temporally manipulated endogenous *Cdkl5* expression in male mice and found that post developmental loss of *Cdkl5* disrupts numerous behavioral domains, hippocampal circuit communication, and dendritic spine morphology (Terzic *et al.*, 2021b). Wang and colleagues conducted a study where they created a specific conditional KO model to investigate the effects of *Cdkl5* absence in glutamatergic neurons of the forebrain, excluding GABAergic neurons. Their findings revealed that the absence of *Cdkl5* in these specific neurons lead to recurrent spontaneous epileptic seizures between 2 and 7 months of age (Wang *et al.*, 2021). This innovative model not only provides valuable insights into the underlying mechanisms of epilepsy in CDD but also serves as an experimental platform for the development of therapies targeting CDD-related seizures (Wang *et al.*, 2021).

1.3.1 Behavioral deficits in *Cdkl5* KO mice

The absence of functional Cdkl5 in KO mouse models results in various behavioral deficits that partially resemble those observed in individuals with CDD. The initial constitutive *Cdkl5* KO mice, which had exon 6 deleted, exhibited hyperactivity, reduced anxiety, motor impairments, decreased sociability, and learning and memory difficulties, mirroring features characteristics seen in CDD patients (Wang *et al.*, 2012). Amendola et al. discovered hippocampal-dependent learning and memory impairments in a CDD mouse model with exon 4 deleted, along with abnormal clasping of hind-limbs (reminiscent of hand-wringing in CDD patients) and visual impairments (Amendola *et al.*, 2014). In 2017, Jhang and colleagues characterized another mouse model with exon 6 deleted. They not only confirmed the behavioral alterations observed by Wang and colleagues but also reported additional features resembling core symptoms of attention-deficit hyperactivity disorder (ADHD) and autism, such as aggressiveness, impulsivity, disruption of dopamine synthesis, and changes in sociocommunication-associated gene expression in the corticostriatal areas (Jhang *et al.*, 2017). A recent study on a *Cdkl5* KO mouse model targeting exon 2 highlighted a significant increase in anxiety and fear-related behaviors, as well as impairment in both acquiring and retaining spatial reference memory (Okuda *et al.*, 2018).

Motor function has consistently been found to be impaired in *Cdkl5* constitutive KO mice. Studies have shown various motor deficits in these mice, including abnormal gait, reduced locomotor activity, impaired motor coordination and deficits in motor learning (Wang *et al.*, 2012; Amendola *et al.*, 2014; Jhang *et al.*, 2017). Impaired motor coordination was assessed through the accelerating Rotarod assay; however, these mice still demonstrate some ability to improve their performance over multiple trials (Wang *et al.*, 2012; Amendola *et al.*, 2014; Jhang *et al.*, 2017). In terms of locomotor activity, KO mice exhibit hyperactivity in new or unfamiliar environments during various behavioral tests (Wang et al., 2012; Jhang et al., 2017), but hypoactivity in a familiar home-cage setting with extended monitoring (Amendola *et al.*, 2014). The deficits in motor coordination and locomotor activity observed in *Cdkl5* knockout mice are also reproduced in a conditional knockout mouse model where *Cdkl5* loss is specifically limited to forebrain glutamatergic neurons (Tang *et al.*, 2017) . This suggests that CDKL5 plays a crucial role in regulating motor function within this specific population of neurons (Tang *et al.*, 2017).

Severe intellectual disability is a prominent characteristic of CDKL5 deficiency in humans (Fehr *et al.*, 2013). Similarly, mouse models of *Cdkl5* deficiency consistently exhibit impairments in various learning and memory tasks (Wang *et al.*, 2012; Fuchs *et al.*, 2014; Fuchs *et al.*, 2015; Trazzi *et al.*, 2016; Jhang *et al.*, 2017; Tang *et al.*, 2017; Ren *et al.*, 2019). These tasks include those that heavily rely on hippocampal function, such as the Barnes maze, Morris water maze, and contextual fear conditioning, as well as working memory tasks that likely involve multiple brain regions.

Recent studies demonstrated that mice lacking *Cdkl5* exhibit hyperlocomotion and impulsivity, resembling core symptoms of attention-deficit hyperactivity disorder (ADHD) (Jhang *et al.*, 2017; Jhang *et al.*, 2020; Adhikari *et al.*, 2022; Viglione *et al.*, 2022). *Cdkl5* KO mice display impulsivity, together with low levels of cognitive flexibility and perseverative behaviors (Viglione *et al.*, 2022). Pupillometry reveals in *Cdkl5* KO mice a smaller pupil size and an impaired response to unexpected stimuli associated with hyperlocomotion, demonstrating a global defect in arousal modulation (Viglione *et al.*, 2022).

In 2017, Tang and colleagues, elucidated the cellular origins of learning and memory impairments in a CDD mouse model by generating a forebrain excitatory neuron-specific *Cdkl5* knockout line (Nex-cKO). Nex-cKO mice demonstrated impaired hippocampal-dependent memory, along with context-dependent hyperactivity and hindlimb clasping. At the cellular level, altered neuronal morphology in Nex-cKO mice was accompanied by

increased spontaneous excitatory and inhibitory synaptic activity, resulting in altered spatiotemporal dynamics in the CA1 microcircuit, which is relevant to learning and memory. These findings reveal the glutamatergic origins of learning and memory impairments in CDKL5 deficiency and suggest that CDKL5 plays a role in regulating synaptic and circuit function in glutamatergic neurons (Tang *et al.*, 2017).

In 2019, researchers selectively eliminated *Cdkl5* expression in murine forebrain GABAergic neurons (Dlx-cKO). They found that these mice exhibited an autistic-like phenotype but, in contrast to Nex-cKO mice, preserved learning and memory. Additionally, Dlx-cKO mice showed enhanced excitatory synaptic transmission and circuit-level hyperexcitability, along with elevated levels of NMDA receptors. Reducing NMDAR activity using an antagonist called memantine significantly alleviated the behavioral deficits observed in Dlx-cKO mice (Tang et al. 2019). To assess the translational potential of these findings, Tang and colleagues generated a novel CDD model carrying a patient mutation (CDKL5 R59X) and found that these mice, similar to Dlx-cKO mice, exhibited increased NMDA receptor levels (Tang *et al.*, 2019). Collectively, these findings support a novel mechanism in which CDKL5 loss in GABAergic neurons leads to excessive NMDAR signaling and contributes to the development of autistic-like behaviors in mouse models of CDD. Additionally, in a recent study Tassinari and colleagues demonstrated impaired neonatal reflexes in *Cdkl5* KO pups lacking exon 4, indicating the presence of early behavioral defects during postnatal development (Tassinari *et al.*, 2023).

1.3.2 Neuroanatomical defects in *Cdkl5* KO mice

The lack of *Cdkl5* function in KO mouse models also leads to the development of various neuroanatomical abnormalities, most notably a severe dendritic hypotrophy. In *Cdkl5* KO mice targeting exon 4, there is a significantly reduced total length of dendrites and a decreased number of branches compared to control mice (Amendola *et al.*, 2014; Fuchs *et al.*, 2014; Fuchs *et al.*, 2015; Tassinari *et al.*, 2023). In the *Cdkl5* KO mouse line with exon 6 deletion, the complexity of dendrites in CA1 pyramidal neurons is diminished, while the overall length remains unaffected compared to control mice (Tang *et al.*, 2017). This suggests that the presence of CDKL5 protein is necessary and sufficient to promote dendritic growth. Indeed, overexpressing CDKL5 in neuronal cultures leads to an increase in total dendritic length (Chen *et al.*, 2010). The exact mechanism of how CDKL5 functions in the signaling pathways that regulate dendritic growth is still unknown (Zhu and Xiong,

2019).

Moreover, studies conducted on *Cdkl5* KO mice have demonstrated changes in the organization and stability of dendritic spines, as well as alterations in the density of PSD-95 dendritic clusters within various brain regions, including the somatosensory and visual cortex, and hippocampus (Fuchs *et al.*, 2015; Della Sala *et al.*, 2016; Pizzo *et al.*, 2016; Trazzi *et al.*, 2016; Gurgone *et al.*, 2023; Tassinari *et al.*, 2023). These findings suggest that the deficiency of CDKL5 results in disruptions of structural synaptic plasticity within excitatory circuits. Specifically, through repeated in vivo imaging, Della Sala and colleagues have provided insights into the underlying mechanisms of dendritic spine abnormalities in male mice lacking *Cdkl5* (Della Sala *et al.*, 2016). Their research indicates that the reduced spine density observed in *Cdkl5* mutants primarily due to an imbalance in the processes of spine formation and elimination.

Cdkl5 mutant mice exhibit an increased rate of spine elimination from early postnatal stages to adulthood, suggesting that CDKL5 plays a crucial role in synaptic stabilization throughout the lifespan (Della Sala *et al.*, 2016). However, in conditional KO mice where *Cdkl5* was specifically deleted in excitatory neurons of the forebrain, there was a tendency towards higher density and volume of dendritic spines (Tang *et al.*, 2017). The reason for this discrepancy remains unclear, but it is possible that gene deletion in large clusters of cells triggers compensatory mechanisms that complicate the analysis of phenotypes resulting from loss-of-function mutations in individual cells (Zhu and Xiong, 2019).

In *Cdkl5* KO mice, alterations have been observed in long-term potentiation (LTP), a form of synaptic plasticity associated with learning and memory, as well as in the frequency of miniature excitatory postsynaptic currents, which serve as an indicator of the level of excitatory synaptic transmission (Della Sala *et al.*, 2016; Ren *et al.*, 2019). Recent immunohistochemical studies have also revealed changes in the density of both excitatory and inhibitory synaptic markers (Pizzo *et al.*, 2016; Sivilia *et al.*, 2016; Gennaccaro *et al.*, 2021a; Gennaccaro *et al.*, 2021b). Notably, the higher number of GABAergic terminals in the cortex of *Cdkl5* KO mice compared to wild-type mice suggests that increased inhibitory transmission might contribute to the impairment of LTP observed in these mice (Gennaccaro *et al.*, 2021b).

Interestingly, recent findings have demonstrated that CDKL5 is involved in sensory-induced plasticity of both excitatory and inhibitory synapses in the barrel cortex (Pizzo *et al.*, 2020). This indicates that CDKL5 deficiency affects both excitation and inhibition, suggesting that

the delivery of sensory inputs to the cortex may be less efficient in individuals with CDKL5 deficiency disorder (CDD).

Awad and colleagues, through resting-state functional MRI (rs-fMRI) analysis conducted on adult male and female *Cdkl5*-deficient mice, found an increase in homotopic interhemispheric connectivity and functional hyperconnectivity across higher cognitive areas (Awad *et al.*, 2023). The presence of an increased number of callosal synaptic inputs combined with a decrease in local synaptic connectivity within the cingulate cortex indicates a disruption in the development of excitatory synapses and suggests that CDKL5 plays a distinct and varying role across different subtypes of excitatory neurons (Awad *et al.*, 2023). However, the underlying molecular mechanisms still need to be explored.

In conclusion, the deficits in dendritic spine formation observed in *Cdkl5* KO mice collectively underscore the role of *Cdkl5* in the regulation of dendritic development and synapse formation. Importantly, CDKL5 deficiency also affects synaptic organization and experience-dependent plasticity, highlighting the broader impact of CDKL5 on neuronal connectivity (Zhu and Xiong, 2019).

Interestingly, recent evidence has shown that CDKL5, in addition to neuronal maturation and dendritic outgrowth, also affects neuronal survival (Fuchs *et al.*, 2014; Fuchs *et al.*, 2019; Loi *et al.*, 2020). Fuchs and colleagues showed that *Cdkl5* KO mice are characterized by an increased rate of apoptotic cell death in the hippocampal dentate gyrus that causes a reduction in the final number of granule neurons, suggesting a role of CDKL5 in maintaining the delicate balance between precursor proliferation and survival (Fuchs *et al.*, 2014). In addition, *Cdkl5* KO mice are characterized by an increased rate of apoptotic cell death in the hippocampal dentate gyrus and by increased susceptibility to neurotoxic/excitotoxic stress of pyramidal hippocampal neurons (Fuchs *et al.*, 2014; Fuchs *et al.*, 2019; Loi *et al.*, 2020), indicating that an absence of Cdkl5 increases neuronal vulnerability.

Interestingly, *Cdkl5* KO mice are characterized by accelerated neuronal senescence/death during aging (Gennaccaro *et al.*, 2021a) and by a generalized status of microglia overactivation in the brain that worsens during aging (Galvani *et al.*, 2021; Tassinari *et al.*, 2023).The finding that microglia overactivation exerts a harmful action in the *Cdkl5* KO brain (Galvani *et al.*, 2021; Tassinari *et al.*, 2023), impairing brain development and neuronal survival, suggests that a neuroinflammatory process contributes to the pathogenesis of CDD.

1.3.3 Neurophysiological features of *Cdkl5* KO mice

As mentioned previously, sleep and respiratory abnormalities are commonly observed in individuals with CDKL5 deficiency (Hagebeuk *et al.*, 2013; Mangatt *et al.*, 2016; Hagebeuk *et al.*, 2023). Similar features have been identified in *Cdkl5* KO mice, which exhibit an increased occurrence of sleep apneas during both non-rapid eye movement (NREM) and rapid eye movement (REM) sleep (Lo Martire *et al.*, 2017).

Investigations of two independent *Cdkl5*-deficient mouse lines have revealed significant abnormalities in both auditory and visual evoked responses (AER and VEP, respectively) (Wang *et al.*, 2012; Amendola *et al.*, 2014; Mazziotti *et al.*, 2017). The cortical visual response is severely impaired in both hemizygous males and heterozygous females (Mazziotti *et al.*, 2017), indicating that CDKL5 is necessary for the proper functioning of cortical circuits. Using a conditional *Cdkl5* KO model, Lupori and colleagues recently demonstrated that selective deletion of *Cdkl5* from excitatory cells in the cortex is sufficient to produce abnormalities in visual cortical responses, highlighting the dependence of normal cortical circuit functioning on CDKL5 (Lupori *et al.*, 2019).

In an interesting finding, La Montanara and colleagues discovered in 2020 that CDKL5 is required for CaMKII-dependent TRPV1 signaling and the growth of sensory neurons in both murine and human CDKL5-deficient neurons. In vivo, this translates to impaired capsaicin-dependent nociceptive signaling, altered behavioral responses, and reduced epidermal innervation in a CDD animal model (La Montanara *et al.*, 2020).

1.3.4 Epileptic features of Cdkl5 KO mice

Although early onset epileptic seizures and infantile spasms are characteristic of CDD, spontaneous seizures have not been reported in three different lines of constitutive *Cdkl5* KO mice (Wang *et al.*, 2012; Amendola *et al.*, 2014; Okuda *et al.*, 2017) or in conditional *Cdkl5* KO lines that specifically delete *Cdkl5* in forebrain glutamatergic or GABAergic neurons (Amendola *et al.*, 2014; Tang *et al.*, 2017). However, various *Cdkl5* KO models have shown abnormal electroencephalogram (EEG) responses and altered susceptibility to convulsant treatments. Amendola and colleagues observed that high-dose kainic acid induced tonic-clonic seizures and epileptiform EEG activity in both hemizygous *Cdkl5* KO and wild-type mice, with the *Cdkl5* KO mice exhibiting longer duration of high amplitude bursts but lower frequency compared to wild-type littermates (Amendola *et al.*, 2014). Another study demonstrated increased seizure susceptibility in *Cdkl5* KO mice in response

to NMDA treatment (52.5 mg/kg at 4 weeks of age; 60 mg/kg at 13-15 weeks of age), which was rescued by a GluN2B-selective NMDA receptor antagonist, ifenprodil (Okuda *et al.*, 2017). This suggest that upregulation of GluN2B in *Cdkl5* mutants might be responsible for the enhanced seizure susceptibility. It is worth mentioning that this particular study did not observe a significant difference in seizure susceptibility to kainic acid in the conditional *Cdkl5* KO mice. In addition, it was recently demonstrated that NMDA-treated heterozygous *Cdkl5* KO female mice, exhibited increased seizure persistence compared to their wild-type counterparts (Galvani *et al.*, 2021).

It's worth noting that two more recent studies have reported recurrent spontaneous seizures in *Cdkl5* KO mice (Wang *et al.*, 2021; Terzic *et al.*, 2021a). Wang and colleagues utilized conditional KO mouse lines to selectively delete *Cdkl5* in either glutamatergic or GABAergic neurons and found that Cdkl5 deficiency in glutamatergic neurons led to high-frequency spontaneous seizure activities resembling the epileptic phenotype observed in individuals with CDKL5 deficiency, eventually leading to sudden death in mice (Wang *et al.*, 2021). On the other hand, Cdkl5 deficiency in GABAergic neurons did not generate such seizures.

Furthermore, spontaneous seizure activity has been described in heterozygous female *Cdkl5* mice, both in *Cdkl5* KO mice and *Cdkl5* R59X knock-in mice (Mulcahey *et al.*, 2020; Terzic *et al.*, 2021a). However, this phenotype typically manifests with aging, with a median onset around 28 weeks of age, and is not observed in hemizygous KO males or homozygous KO females, suggesting that X-linked cellular mosaicism is a contributing factor to these seizure-like events (Terzic *et al.*, 2021a) .

All together these findings highlight the complex nature of seizure susceptibility in relation to Cdkl5 deficiency in the mouse and suggests that different factors and models may influence the manifestation of seizures.

1.4 Metabolic alterations in *Cdkl5* KO mice

Emerging evidence suggests that CDKL5 plays a role in the regulation of energy metabolism. In line with recent evidence that mitochondrial dysfunction and oxidative stress occur in CDD patients (Pecorelli *et al.*, 2011; Ricciardi *et al.*, 2012; Pecorelli *et al.*, 2015), an aberrant mitochondrial function was described in isogenic neural progenitor cells (NPCs) derived from a CDD patient (Jagtap *et al.*, 2019). Other studies showed reduced activity of mitochondrial respiratory chain complexes in the brains of *Cdkl5* KO mice (Vigli *et al.*, 2019; Carli *et al.*, 2021). This reduction in activity is associated with impaired mitochondrial

ATP production rate and decreased ATP levels in the whole brain. In particular, Vigli and colleagues reported functional defects in complexes III-IV-V, suggesting that electron transport chain (ETC) complexes may be affected in the *Cdkl5* KO mouse brains (Vigli *et al.*, 2019). In 2021 Carli and colleagues, through in vivo proton-MR spectroscopy (MRS), revealed a metabolic dysregulation indicative of mitochondrial dysfunctions in the *Cdkl5* KO mouse brain (Carli *et al.*, 2021). They showed a significant reduction in ATP levels and a significant reduction of Cox7b, which is a crucial subunit of Complex IV responsible for its assembly, functioning, and mitochondrial oxidative phosphorylation, despite these findings, the quantity of mitochondria remained relatively unaffected (Carli *et al.*, 2021). The observed decrease in the transcriptional activity of Cox7b appears in line with the previously documented reduced expression of ETC genes in Rett syndrome (Gold *et al.*, 2014), autism (Chauhan *et al.*, 2011; Tang *et al.*, 2013) and other neuropsychiatric disorders (Rezin *et al.*, 2009; Indrieri *et al.*, 2012), highlighting the importance of ETC for central nervous system physiology. This finding suggests, for the first time, a potential molecular basis for the manifestation of mitochondrial dysfunctions in CDD. However, the underlying mechanisms responsible for these mitochondrial dysfunctions and their specific role in the pathogenesis of CDD have not been fully elucidated.

Recently, Fuchs and colleagues reported for the first time in a female mouse model of CDD, increased blood levels of reactive oxidizing species and a reduction in glycemia (Fuchs *et al.*, 2022). They showed that this difference in glucose levels was particularly marked at base-line, on food-deprived animals (Fuchs *et al.*, 2022). Furthermore, authors demonstrated that a treatment with FRAX486, a brain-penetrant molecule that was reported to selectively inhibit group I p21-activated kinases (PAKs) - a serine/threonine kinases critically involved in the regulation of neuronal morphology and glucose homeostasis completely rescued the fasting-induced hypoglycemia of *Cdkl5* KO mice and normalized the levels of reactive oxidizing species (Fuchs *et al.*, 2022).

1.5 Epilepsy and cardiac disorders

There is growing clinical and experimental evidence indicating that adults with epilepsy frequently report cardiovascular disease compared to those without epilepsy. The potential importance of cardiac dysfunction related to epilepsy is underscored by findings of abnormalities in the heart during seizures (ictal), between seizures (interictal), and at the molecular level. (Ravindran *et al.*, 2016). Seizure-induced changes in the heart include

alterations in heart rate, arrhythmias, asystole, and various electrocardiogram (ECG) abnormalities such as ST segment depression, T-wave inversion, and prolonged QT interval during seizures (Dlouhy *et al.*, 2016). Interictal studies have also reported prolonged QT interval, increased sympathetic tone, decreased parasympathetic tone, and myocardial damage associated with seizure activity (Lotufo *et al.*, 2012; Kishk *et al.*, 2018; Myers *et al.*, 2018).

Recent studies in animals have further revealed changes in the expression of cardiac ion channels, which regulate cardiac electrical activity, as a result of epileptogenesis. which are accompanied by abnormal cardiac electrophysiology (Powell *et al.*, 2014; Biet *et al.*, 2015; Brewster *et al.*, 2016).

Indeed, seizures have been demonstrated to modify the levels of messenger RNA (mRNA) and protein expression of specific ion channels in the heart. These include voltage-gated sodium channels such as Nav1.1 and Nav1.5, voltage-gated potassium channels (Kv4.2, Kv4.3), sodium-calcium exchangers (NCX1), and nonspecific cation-conducting channels (HCN2, HCN4) (Li *et al.*, 2019). Seizure activity can lead to alterations in the transcription and translation of these channels, which subsequently affect their functionality in cardiac tissue. These changes in ion channel expression contribute to the electrical abnormalities observed during seizures, including variations in heart rate, QT interval prolongation, and an increased susceptibility to ventricular arrhythmias (Li *et al.*, 2019).

These acquired cardiac channelopathies, caused by epilepsy, differ in their mechanisms from inherited cardiocerebral channelopathies, although they involve the same ion channels that govern both cardiac and neuronal excitability. While the exact pathophysiology of acquired cardiac channelopathies in epilepsy remains poorly understood, autonomic dysfunction and structural cardiac abnormalities are considered potential underlying mechanisms.

The association between chronic uncontrolled epilepsy and cardiac dysregulation has garnered significant attention in recent years, primarily due to the increased awareness of Sudden Unexpected Death in Epilepsy (SUDEP). SUDEP refers to the unexpected and unexplained death of an otherwise healthy individual with epilepsy, where no specific cause of death can be identified (Dlouhy *et al.*, 2016).

To be more precise, SUDEP is defined based on specific criteria. According to these criteria, SUDEP refers to the sudden and unexpected death of an individual with epilepsy, whether witnessed or unwitnessed, that occurs without any apparent traumatic or drowning-related

cause. The definition includes cases where the person experienced a seizure prior to death, as well as cases where no seizure activity was observed. It is important to note that documented status epilepticus (prolonged seizures) is excluded from the definition. Furthermore, postmortem examination should not reveal any structural abnormalities or toxicological causes that could explain the cause of death. SUDEP is a complex phenomenon with various contributing factors, and its exact mechanisms are still not fully understood (Nashef, 1997).

The majority of SUDEP cases are unwitnessed, but evidence suggests that they often occur following generalized tonic-clonic seizures (GTCS) (Nashef *et al.*, 1998).

While factors like age, gender, and ethnicity are not likely to have a significant impact on the risk of SUDEP, certain characteristics of epilepsy do play a role. The duration of epilepsy, the age at which it started, and an increased frequency of GTCS are considered risk factors for SUDEP. This suggests that SUDEP is not solely a result of something inherent or intrinsic to epilepsy that is unrelated to seizure events. Seizures themselves induce pathophysiological changes that contribute significantly to SUDEP (Dlouhy *et al.*, 2016).

However, it's important to note that the pathophysiology of SUDEP is complex and involves multiple factors. Seizure-induced changes in cardiorespiratory function are one aspect, but other factors such as arousal, patient position, time of day, intrinsic pulmonary and cardiac dysfunctions, and genetic mutations also contribute to the occurrence of SUDEP. Therefore, the development of SUDEP involves a combination of seizure-related changes and other underlying factors, making it a multifactorial phenomenon.

SUDEP accounts for a significant proportion (17-38%) of deaths among individuals with epilepsy, making it the leading cause of epilepsy-related mortality. The risk of sudden unexpected death is 20-40 times higher in individuals with chronic epilepsy compared to the general population (Ficker *et al.*, 1998; Ficker, 2000; Mohanraj *et al.*, 2006).

1.5.1 Cardiac disease and Rett syndrome

In Rett syndrome (RTT), sudden death is a prevalent occurrence, accounting for approximately 26% of all deaths in affected individuals (Kerr *et al.*, 1997). Cardiac dysfunction is strongly suspected to contribute to these cases. Studies have shown that individuals with RTT often exhibit prolonged QT intervals (LQT) on electrocardiograms (ECGs) (Acampa and Guideri, 2006; Fu *et al.*, 2020) (Table 2), indicating an abnormality

in cardiac repolarization that can predispose them to life-threatening cardiac rhythm disturbances (Morita *et al.*, 2008).

This prolonged QT interval is considered as one potential cause of death in individuals with RTT. The severity of QTc prolongation, may be linked to a higher likelihood of experiencing potentially fatal cardiac arrhythmias. Previous studies have reported an association between QTc prolongation and sudden death in individuals with RTT (Clark *et al.*, 2020).

Genetic mutations affecting potassium channels *KVLQT1* (LQT1) and *HERG* (LQT2) and sodium channels *SCN5A* (LQT3), as well as autonomic nervous system dysfunctions, contribute to the prolonged QT phenotype observed in RTT patients (Das and Zipes, 2010). Apart from genetic factors, changes in autonomic nervous system function can affect cardiac repolarization and contribute to the development of a long QT phenotype (Goldman *et al.*, 2009). Specifically, an imbalance in sympathetic activity may lead to an increased QTc interval (Cuomo *et al.*, 1997).

 Clinical and experimental evidence has shown that individuals with RTT exhibit not only ventricular repolarization abnormalities but also abnormalities in the autonomic nervous system. These autonomic nervous system abnormalities have been implicated in the development of life-threatening ventricular arrhythmias in RTT patients. Therefore, both ventricular repolarization abnormalities and autonomic nervous system dysfunction play a role in the pathogenesis of lethal ventricular arrhythmias in individuals with RTT (Dlouhy *et al.*, 2016)

Author	QTc interval (msec)				
	Total	Stage II	Stage III	Stage IV	Pts with ↑ QTc (%)
Sekul et al.,1994 (n=34)	430±20	420±20	440±30	440±20	41%
Johnsrude (n=25)	441±32				9%
Guideri et al., 1999 (n=54)	441±20	435±20	445±20	439±20	48%
Ellaway et al., 1999 (n=34)	438±4	410±42	441±27	437±8	30%
Guideri et al., 2001(n=74)	440±20	440±20	438±20	439±20	55%

Table 2. Summary of studies investigating QTc interval prolongation in Rett syndrome (Modified from (Acampa and Guideri, 2006).

Furthermore, Hara and colleagues conducted research to investigate the role of MeCP2 in cardiac development and dysfunction. They discovered that deficiency of MeCP2 was

associated with alterations in myocardial structures. Moreover, through qRT-PCR analysis, they identified changes in the expression of genes related to voltage-gated channels, including *Hcn*, *Cacna1g*, *Kcnq1*, *Scn5a*, and *Kcnj12* genes, in the hearts of Mecp2-null mice. These findings highlight the significance of MeCP2 as a crucial regulator of the gene-expression program responsible for maintaining normal cardiac development and cardiomyocyte structure. The loss of MeCP2 in the heart is considered one of the contributing factors to cardiac dysfunction, including the occurrence of arrhythmias, observed in the Mecp2-null mouse model of RTT (Hara *et al.*, 2015).

Amin and colleagues reported that one caregiver survey reported arrhythmia in 11 out of 29 individuals with CDD who underwent an electrocardiogram (Amin *et al.*, 2017). Similar to the findings observed in individuals with RTT, mild prolongation of the corrected QT interval has been identified in a subset of patients with CDD (Stansauk *et al.*, 2023). This suggests a potential overlap in cardiac abnormalities between these two conditions. A recent study utilizing next-generation sequencing has even identified CDKL5 as a gene potentially involved in cardiac disorders associated with epilepsy (Coll *et al.*, 2017), suggesting that CDKL5 may play a role in cardiac function.

Since seizures induce a variety of cardiac changes in heart rate, arrhythmias, and various other ECG abnormalities, some potentially lethal (Dlouhy *et al.*, 2016), the knowledge whether loss of CDKL5 leads to heart defects can have an important clinical impact.

2. AIM OF THE STUDY

CDKL5 (cyclin-dependent kinase-like 5) Deficiency Disorder (CDD) is a severe X-linked neurodevelopmental disease caused by mutations in the CDKL5 gene which lead to a lack of CDKL5 protein expression or function. CDD affects mostly girls, and due to the numerous clinical features, that overlap with the more well-characterized Rett syndrome (RTT), it was initially termed as an "early seizure variant" or "Hanefeld variant" of RTT. Similarities between RTT and CDD regard the severe neurodevelopmental impairment, intellectual disability, motor impairment, and, in some cases, respiratory dysregulation. Nevertheless, the improvement of the clinical overview of CDD in the past few years has defined a more detailed phenotypic spectrum; this includes very common alterations of peripheral organ and tissue function, such as gastrointestinal problems, irregular breathing, hypotonia, cardiorespiratory dysrhythmias, and scoliosis, complications that strongly impair the quality of life of patients and their families.

Unfortunately, our present knowledge of the function of CDKL5 in other organs/tissues is still rather limited, curtailing the possibility of therapeutic intervention. The role of CDKL5 in biological processes that take place in non-neuronal tissues has recently emerged. Interestingly, a recent study using next-generation sequencing has identified CDKL5 as a gene that is potentially involved in cardiac disorders associated with epilepsy, suggesting that CDKL5 may play a role in cardiac function. Moreover, two recent studies reported arrhythmia and prolonged QTc interval in some CDD patients who underwent ECG, suggesting the presence of cardiac abnormalities in the CDKL5 deficiency condition. Similarly, it has been well established that RTT patients are more prone to display a prolonged QTc interval, possibly due to immature medullary cardio inhibition and reduced cardiac vagal tone.

Based on these premises **the overall goal of the study was to carry out the first investigation into the effect of CDKL5 loss at a cardiac level and explore its relevance for CDD,** by exploiting a mouse model of the pathology.

3. MATERIALS AND METHODS

3.1 Animal Husbandry

The mice used in this work were derived from the *Cdkl5* −/Y strain in the C57BL/6N background developed in (Amendola *et al.*, 2014) and backcrossed in C57BL/6J for three generations. Heterozygous *Cdkl5* +/− and homozygous *Cdkl5* −/− females were produced and genotyped as previously described (Amendola *et al.*, 2014), and age-matched wild-type *Cdkl5* +/+ littermate controls were used for all experiments. The day of birth was designated as postnatal day (P) zero, and animals of 24 h of age were considered as 1-day-old animals (P1). After weaning (P21-23), mice were housed three to five per cage with a 12 h light/dark cycle in a temperature- and humidity-controlled environment with food and water provided ad libitum. The animals' health and comfort were controlled by the veterinary service. Experiments were carried out on a total of 121 adult (3–4-month-old) *Cdkl5* KO mice (*Cdkl5* +/+ n = 50; *Cdkl5* +/− n = 62; *Cdkl5* −/− n = 9). The study protocols complied with EU Directive 2010/63/EU and with Italian law (DL 26, 4 March 2014) and were approved by the Italian Ministry of Health (protocol n∘ 535/2022-PR). All efforts were made to minimize animal suffering and to keep the number of animals used to a minimum.

3.1.1 Genomic DNA extraction

Genomic DNA extraction and purification were performed from tail biopsies of newborn mice, using the NucleoSpin®Tissue Kit (Macherey-Nagel, Düren, DE) extraction kit. The initial step involves the lysis of the tails, obtained by incubating the samples at 56 ° C, for 1-3 hours or overnight, with the T1 buffer (180 μl) and the proteinase K (25 μl), contained in the kit. At the end of the incubation period, to complete the lysis, 200 μl of buffer B3 (10 minutes at 70° C), also contained in the kit, were added to each sample. At the end of the lysis, 210 μl of ethanol (96-100%) are added to the lysate, which allows the DNA to precipitate and bind to the silica membrane of the column, where the cell lysate is contained (centrifuge one minute at 11,000 x g). Two washes are carried out with buffer BW (500 μl) and B5 (600 μl), which allow to eliminate the protein residues and possible contaminants that could compromise the purity of the sample (centrifuge 2 times for one minute at 11,000 x g). A further centrifuge (one minute at 11,000 x g) is performed to remove residual ethanol and the genomic DNA is eluted by means of a slightly alkaline BE buffer (100 μl) (incubate for one minute at room temperature and then centrifuge to one minute at 11,000 x g). All

buffers used in the DNA extraction protocol are supplied with the extraction kit, with the exception of ethanol. The DNA obtained is quantified using a NanoDrop ND-1000 spectrophotometer (NanoDrop Technologies, Wilmington, DE, USA) which also provides the values corresponding to the purity of the samples.

3.1.2 Genotyping

The mice were genotyped using an end-point PCR to detect the presence of the knockout allele for Cdkl5 containing the loxP region in the vicinity of exon 4 (Amendola *et al.*, 2014). The primers used in the reaction are: 108F: 5′-ACGATAGAAATAGGATCAACCC-3 ′, 109R: 5′-CCCAAGTATACCCCTTTCCA-3 ′, 125R: 5′-CTGTGACTAGGGGCTAGAGA-3 ′.

The PCR reaction was performed according to the following protocol: initial denaturation at 94 °C for 4 minutes, 33 denaturation cycles (94 °C/40s), pairing (59 °C/30s), extension (72 °C /40s), final step at 72 °C for 7 minutes. The product of the PCR reaction gives rise to a fragment of 240 bp for the wild type allele and 344 bp for the knockout allele.

3.2 Surgical Procedure, In Vivo Recording, and Data Analysis

Eight *Cdkl5* +/+, 10 *Cdkl5* +/−, and 8 *Cdkl5* −/− female mice were instrumented with electroencephalographic (EEG), electromyographic (EMG), and electrocardiographic (ECG) electrodes to characterize the electrical activity of the heart during sleep under baseline conditions. A second group of mice (*Cdkl5* +/+ n = 10, *Cdkl5* +/− n = 10) instrumented with the same surgical protocol also underwent surgery to implant an intraperitoneal (IP) catheter for the continuous infusion of autonomic blockers with the purpose of testing the autonomic modulation of heart rhythm.

All mice were deeply anesthetized with isoflurane (1.8–2.4% in O2, inhalation route) and treated with intraoperative analgesia (carprofen 4 mg/kg subcutaneously, Pfizer, Italy) and postoperative antibiotic prophylaxis (benzylpenicillin benzathine, 12,500 IU/kg, and dihydrostreptomycin sulphate, 5 mg/kg, subcutaneously). For the recording of the EEG signal, mice were implanted with two miniature stainless-steel screws (2.4 mm length, PlasticsOne, Roanoke, VA, USA) in contact with the dura mater (frontoparietal derivation); for the recording of the EMG signal, mice were implanted with two multistranded PFA-coated stainless-steel wires (KF Technology srl, Roma, Italy) inserted into the nuchal muscles. For ECG recording, two PFA-coated stainless-steel wires were inserted

subcutaneously; one was put in contact with muscles in the right-upper quadrant of the thorax, while the second touched the abdominal muscles on the left flank. All electrode wires were then collected in a socket placed over the mouse's head and fixed with dental cement (RelyX Unicem, 3M ESPE, Pioltello, (MI), Italy) and dental acrylic (Respal NF, SPD, Mulazzano (LO), Italy). The second batch of mice was also implanted with a silicone catheter (Lo Martire *et al.*, 2017; Alvente *et al.*, 2021) with the tip inserted into the abdominal cavity and the other extremity tunneled to the mouse head and fixed with the abovementioned socket. After 12 days of postoperative recovery and habituation to the recording apparatus (ambient temperature set at 25 ◦C), EEG, EMG, and ECG signals of mice included in the baseline protocol were continuously recorded for 24 h. Signals were transmitted via a cable connected to a rotating electrical commutator (SL2 + 2C/SB, Plastics One, USA) and to a balanced cable suspensor, allowing the mice to make unhindered movements (Bastianini *et al.*, 2021).

Mice included in the protocol for testing of the autonomic control of heart rhythm were allowed to recover from surgery and to habituate to the recording settings for 14 days. Each mouse underwent 3 recording sessions (7 h each starting at light on) with acquisition of EEG, EMG, and ECG signals while being continuously infused with either saline, with the muscarinic receptor antagonist atropine methyl nitrate (Vinci-Biochem, Italy, 0.5 mg/mL in saline) to block parasympathetic activity to the heart, or with the selective β1-adrenergic receptor antagonist atenolol (Sigma-Aldrich, Milano, Italy, 0.25 mg/mL in saline) to block the sympathetic activity to the heart. Each mouse first received saline infusion and was then randomly subjected to atropine and atenolol infusions. Each infusion was performed at least 48 h after the preceding infusion. The IP catheter was connected to a remote infusion pump (model 22 multiple syringe pump, Harvard Apparatus, Cambridge, MA, USA) by an external tube prefilled with saline solution or drug solution, as previously described (Lo Martire *et al.*, 2017; Alvente *et al.*, 2021). A rapid infusion was performed before the start of each recording session at a rate of 30 μL/min for 5 min to fill the IP catheter with saline or either of the drug solutions; then, the infusion rate was set at 100 μL/h for 7 h. At the end of the recording session, mice were sacrificed under deep anesthesia (isoflurane 4% in O2). The EEG signal was cut with a band pass filter between 0.3 and 100 Hz and stored at 128 Hz. The EMG signal was filtered between 100 and 1000 Hz and stored at 128 Hz, while the ECG was filtered between 10 and 1000 Hz and stored at 2048 Hz. Data acquisition was performed with LabVIEW 8.0 software (National Instruments, Austin, TX, USA).

The EEG and EMG signals were imported and analyzed to automatically score the wake–sleep states (wakefulness, rapid-eye-movement sleep (REMS) and non-rapid-eye-movement sleep (NREMS)). On the contrary, the ECG signal was imported in Labchart 8.0 (ADInstruments, Colorado Springs, CO, USA), a specific notch (50 Hz) filter was digitally applied to exclude electrical noise, and the signal was then analyzed with the ECG analysis module to automatically detect QRS complexes and their intervals. For each mouse, ECG analysis was restricted to 8 episodes of NREMS and 8 episodes of REMS (longer than 30 s) homogeneously distributed throughout the whole recording. For each session, we calculated the following ECG parameters: P-wave duration, QRS, RR, PR, JT, and QT intervals. To compensate for the elevated mouse heart rate, we corrected the QT interval (QTc) with Hodges' formula (the most effective for rodents, (Botelho *et al.*, 2019)).

The vagal (parasympathetic) contribution to cardiac modulation was examined using validated mouse indices computed in the time domain on spontaneous RR fluctuations (Silvani *et al.*, 2010): pNN8, % of RR values that differ from the following values by >8 ms (Laude *et al.*, 2008); RMSSD, root mean square of the successive RR differences (Shaffer *et al.*, 2014). To date, no index of spontaneous RR fluctuation in the time domain has been validated for the sympathetic contribution to cardiac modulation.

3.3 Heart Dissection, Measurement, and Collection

Adult *Cdkl5* −/−, *Cdkl5* +/−, and *Cdkl5* +/+ female mice aged 3–4 months were weighed and put under deep anesthesia through inhalation of 2% isoflurane in pure oxygen and sacrificed through cervical dislocation. Hearts were quickly removed, cleaned from the surrounding structures, and thoroughly washed in PBS to remove all blood, then weighed. The ratio of heart weight to body weight (HW/BW) was then calculated by dividing the weight of the heart by the weight of the whole animal. The atrioventricular distance was measured. All measurements were performed by the same person with the same precision scales. Hearts were quickly frozen in isopentane, cooled in liquid nitrogen, and stored at −80 °C until used for RT-qPCR, immunohistochemistry, and Western blot analyses.

3.4 RNA Isolation and RT-qPCR

RNA isolation and RT-qPCR were conducted on frozen hearts of *Cdkl5* −/−, *Cdkl5* +/−, and *Cdkl5* +/+ female mice and on frozen cortices of *Cdkl5* +/+ female mice. Total RNA was isolated using the TRI reagent method (Sigma-Aldrich, St. Louis, MO, USA), and cDNA

synthesis was achieved with 5 μg of total RNA using an iScriptTM advanced cDNA synthesis kit (Bio-Rad, Hercules, CA, USA) according to the manufacturer's instructions. Real-time PCR was performed using SsoAdvanced Universal SYBR Green Supermix (Bio-Rad) in a CFX real-time PCR detection system (Bio-Rad). We used primer pairs (Table 3) that provided an efficiency close to 100%. Each biological replicate was run in triplicate. The mean of the two more stable reference genes (*Actb* and *Gapdh*) were used as a normalization factor in the RT-qPCR analysis, and relative quantification was performed using the ΔΔCt method. The primers used are listed in Table 1.

3.5 Histological and Immunohistochemistry Procedures

For histological and immunohistochemistry procedures, frozen hearts were cut with a cryostat (Histo-Line Laboratories) into 7 μm thick sections. Sections were mounted on super frost slides.

3.5.1 Hematoxylin and Eosin (H&E)

Sections were stained with hematoxylin and eosin (H&E), immersed in graded alcohols followed by xylene, and mounted in mounting medium (DPX mountant, Sigma-Aldrich, St. Louis, MO, USA).

3.5.2 Masson's Trichrome Staining

Sections were stained with Masson's trichrome (MT) using Masson's Trichrome Stain Kit-Mallory's (StatLab, KTMAL); the procedure was carried out according to the protocol included with the kit.

3.5.3 Connexin 43, Actinin, and β-Catenin Staining

Immunohistochemistry was performed on 7 μm thick frozen sections fixed via immersion in 4% paraformaldehyde (100 mM phosphate buffer, pH 7.4) and permeabilized with 0.2% TritonX-100 in PBS. Furthermore, 2% BSA in PBS was used as a blocking reagent. Sections were incubated overnight with anti-β-Catenin antibody or double-stained with anti-connexin 43 and anti-actinin antibodies, washed with PBS, and subsequently incubated for 2 h at room temperature with FITC-conjugated or CY3-conjugated secondary antibodies. The primary and secondary antibodies used in this study are listed in Table 4. The sections

were mounted with DAPI (4′,6-diamidino-2-phenylindole)- Fluoromount-G (SouthernBiotech, AL).

3.6 Image Acquisition and Measurements

Fluorescence images were taken with an Eclipse TE 2000-S microscope equipped with a DS-Qi2 digital SLR camera (Nikon Instruments Inc.). A light microscope (Leica Mycrosystems) equipped with a motorized stage and focus control system and a color digital camera (Coolsnap-Pro, Media Cybernetics) were used to take brightfield images of Masson's trichrome and hematoxylin eosin-stained sections.

3.6.1 Quantification of β-Catenin Staining Intensity and Areas

Starting from 20× magnification images of β-catenin-stained ventricular slices, the area of β-catenin staining in intercalated discs was manually drawn using the Image Pro Plus measurement function and expressed in μm2. The intensity of β-catenin staining within each area was then quantified by determining the sum intensity of all positive (bright) pixels within the area. Approximately 100 intercalated discs were analyzed from each sample.

3.7 Western Blotting

For the preparation of protein extracts, ventricles were homogenized in RIPA buffer and quantified using the Bradford method as previously described (Bradford, 1976).
Equivalent amounts (50 μg) of protein were subjected to electrophoresis on Bolt^{TM} 4–12% Bis-Tris Plus gel (Life Technologies Corporation, Carls- bad, CA, USA, No. 04127) and transferred to a Hybond ECL nitrocellulose membrane (GE Healthcare Bio-Science, Piscataway, NJ, USA, No. 10600003). The primary and secondary antibodies used are listed in Supplementary Table 2. The densitometric analysis of digitized Western blot images was performed using Chemidoc XRS Imaging Systems and Image Lab^{TM} software (Bio-Rad), which automatically highlights any saturated pixels of the Western blot images in red. Images acquired with exposition times that generated protein signals outside of a linear range were not considered for quantification.

3.8 Adenine Nucleotide Measurement

For the determination of adenine nucleotides, mouse hearts were quickly removed and placed in ice-cold PBS supplemented with 10 mM EDTA. The tissue was homogenized using an Ultra-Turrax (1 cycle for 10 s); then, the resuspension was transferred to a glass potter with a Teflon pestle operated at 1600 r.p.m (10 strokes). All steps were performed at 4 ∘C. ATP and ADP were extracted and detected as previously described (Jones, 1981) using HPLC (Agilent 1100 series system) using a Kinetex C18 column (250 × 4.6 mm, 100 Å, 5 µm; Phenomenex). Nucleotide peaks were identified at $\lambda = 260$ nm by comparison and coelution with the standards. Different nucleotides were quantified through peak area measurement compared with standard curves.

3.9 Mitochondrial Oxygen Consumption

Intact mitochondria from mice hearts were isolated as previously described (Frezza *et al.*, 2007). Briefly, freshly prepared mitochondria were assayed for oxygen consumption at 30 ∘C by means of a thermostatically controlled oxygraph apparatus (Instech Mod. 203, Plymouth Meeting, PA, USA) equipped with a Clark electrode and a rapid mixing device. Mitochondria (0.2 mg protein) were incubated in the respiration medium (10 mM Tris/HCl, 5 mM MgCl2, 2 mM Pi, 20 µM EGTA and 0.25 M sucrose, pH 7.4) in a final volume of 1600 µL. Respiratory substrates (5 mM glutamate–malate or 13 mM succinate) were added after signal stabilization. State 4 respiration was recorded for 2 min, and state 3 respiration was induced by the addition of 300 µM ADP. The respiratory rates were expressed in nmol oxygen/min/mg of protein.

3.10 Enzymatic Activities of the Mitochondrial Respiratory Chain

The activity of mitochondrial complexes I and II was assessed in heart mitochondria isolated from *Cdkl*5 +/− and *Cdkl*5 +/+ mice as previously described (Spinazzi *et al.*, 2012) with minor modifications. Complex I (NADH: ubiquinone oxidoreductase) activity was measured spectrophotometrically following NADH ($\varepsilon = 6.22$ mM cm−1) oxidation at $\lambda = 340$ nm and 37 ∘C using a Jasco-v750 spectrophotometer equipped with a cuvette stirring device and thermostatic control. Briefly, the isolated mitochondria were subjected to three freeze–thaw cycles in hypotonic buffer (20 mM phosphate buffer (pH 7.5)) to avoid compartmental ization. Then, 50 µg of mitochondria was added to 700 µL of distilled water in a 1 mL quartz cuvette for 1 min. Then, 100 µL of potassium phosphate buffer (0.5 M, pH

7.5), 60 μL of fatty-acid-free BSA (50 mg ml−1), 30 μL of KCN (10 mM), and 10 μL of NADH (10 mM) were added. The volume was adjusted to 994 μL with distilled water. In parallel, a separate cuvette containing the same quantity of reagents and sample with the addition of 10 μL of 1 mM rotenone was prepared. The reaction was started by adding 6 μL of 10 mM CoQ1 (2,3-dimethoxy-5-methyl-6-(3-methyl-2-butenyl)-1,4-benzoquinone, Sigma-Aldrich), and the decrease in absorbance at 340 nm was followed for 3 min. Specific complex I activity was obtained by subtracting the rotenone-insensitive activity and normalized to mitochondrial protein content as determined by a Lowry assay (Lowry *et al.*, 1951). Complex II (succinate dehydrogenase) was measured spectrophotometrically at $\lambda =$ 600 nm following the reduction of DCPIP (2,6-dichlorophenolindophenol, Sigma-Aldrich) ($\varepsilon = 19.1$ mM cm−1) at 37 ◦C. Briefly, 60 μg of cell lysate, 50 μL of potassium phosphate buffer (0.5 M, pH 7.5), 20 μL of fatty-acid-free BSA (50 mg ml−1), 30 μL of 10mM KCN, 50 μL of 400 mM succinate, and 145 μL of DCPIP (0.015% (wt/vol) were added to a 1 mL glass cuvette, and the volume was adjusted to 996 μL with distilled water. After ten minutes of incubation inside the spectrophotometer at 37 ◦C, the reaction was started by adding 4 μL of 12.5 mM decylubiquinone (2,3-dimethoxy-5-methyl-6-decyl-1,4-benzoquinone, Sigma-Aldrich), and the absorbance decrease at $\lambda = 600$ nm was followed for 3 min. To check the specificity of complex II activity, 10 μL of 1 mM carboxine (5,6-dihydro-2-methyl-N-phenyl-1,4-oxathiin- 3-carboxamide, Carbathiine, Sigma-Aldrich) was added before starting the reaction. The specific activity of complex II was obtained by subtracting the TTFA-insensitive activity and normalized to mitochondrial protein content determined by a Lowry assay (Lowry *et al.*, 1951) .

3.11 Measurement of ROS Production

Reactive oxygen species production was assessed in cardiac mitochondria from *Cdkl*5 +/− and *Cdkl*5 +/+ female mice using a fluorogenic probe (2′,7′-dichlorodihydrofluorescein diacetate; Thermo Fisher Scientific Inc, Waltham, MA, USA) as previously described (Fato *et al.*, 2009). For ROS determination, mitochondria (0.1 mg/mL in 125 mM KCl, 10 mM TRIS, 1 mM EDTA, pH 7.5) were incubated with 2 mM KCN and 10 μM DCFDA for 10 min in the presence and absence of 2 μM antimycin A. After this time, mitochondria were energized with 15 mM succinate, and the DCF fluorescence emission (λex = 485 nm; λem = 535 nm) was recorded 10 min after energization using a plate reader (EnSpire; PerkinElmer).

3.12 Measurement of Lipid Peroxidation

Lipid peroxidation in isolated mitochondria from *Cdkl*5 +/− and *Cdkl*5 +/+ female mice was assessed by measuring the biomarker malondialdehyde (MDA) as previously described by Reilly et al. (Reilly and Aust, 2001). Briefly, quantification of MDA was performed through reaction with thiobarbituric acid (TBA), and measurement of TBA-MDA adduct was carried out at 535 nm using a Jasco V-750 spectrophotometer. 1,1,3,3-tetramethoxypropane (Sigma-Aldrich, St. Louis, MO, USA) was used as a standard.

3.13 Transmission Electron Microscopy

For ultrastructural characterization, small heart specimens were fixed in 2.5% glutaraldehyde in 0.1 M cacodylate buffer and post-fixed in osmium tetroxide 1% in the same buffer. After dehydration in graded ethanol, specimens were embedded in araldite. Thin sections were counterstained with uranyl acetate and lead citrate and observed under a Philips CM100 transmission electron microscope (Philips, Amsterdam, the Netherlands).

3.14 Statistical Analysis

Statistical analysis was performed using GraphPad Prism (version 9). Values are expressed as means ± standard error (SEM). The significance of results was obtained using a two-tailed Student's *t*-test or one-way and two-way ANOVA, followed by Fisher's LSD post hoc test, as specified in the figure legends. For the in vivo recordings under the baseline condition, data were analyzed with 2-way repeated-measure ANOVAs (considering sleep state and genotype as factors) and corrected for multiple comparisons with Sidak's test. For mice included in the pharmacological testing of autonomic cardiac contribution, we first calculated the % modification of RR and QTc values induced by the drug compared to saline infusion. Then, for each experimental group, we performed a one-sample t-test, checking for significant deviations from the reference value (100%). A probability level of $p < 0.05$ was considered to statistically significant. The confidence level was taken as 95%.

Gene		Primer sequence (5'-3')
Cdkl5	Forward	TGCAGACACAAGGAAACACATGA
	Reverse	TTTCCTGCTTGAGAGTGCGAA
Gapdh	Forward	CCAGTGAGCTTCCCGTTCA
	Reverse	GAACATCATCCCTGCATCCA
Actb	Forward	AAGTGGTTACAGGAAGTCC
	Reverse	ATAATTTACACAGAAGCAATGC
Kcnq1	Forward	ATCGGTGCCCGTCTGAACAG
	Reverse	TTGCTGGGTAGGAAGAGCTCA
Kcnh2	Forward	GATCGCCTTCTACCGGAAA
	Reverse	CATTCTTCACGGGTACCACA
Kcnj2	Forward	CCCCATGATCCTGTACCAG
	Reverse	ATGGATGCTTCCGAGAACC
Scn5a	Forward	GCAGAAGGTGAAGTTCGTGG
	Reverse	TGAAGACCAAGTTTCCGACC
Hcn4	Forward	CGACAGCGCATCCATGACTA
	Reverse	GCTGGAAGACCTCGAAACGC
Chrm2	Forward	CCCCAATACAGTGTGGACAA
	Reverse	GCAGGGTTGATGGTGCTATT
Adrb1	Forward	GCTCTGGACTTCGGTAGATGTG
	Reverse	CGTCAGCAAACTCTGGTAGCGA
Col1a2	Forward	CACCCCAGCGAAGAACTCAT
	Reverse	TCTCCTCATCCAGGTACGCA
Col3a1	Forward	TGACTGTCCCACGTAAGCAC
	Reverse	AGGGCCATAGCTGAACTGAA
Gja1	Forward	GAGAGCCCGAACTCTCCTTT
	Reverse	TGGGCACCTCTCTTTCACTT

Table 1. List of primers used for quantitative RT-PCR.

Antibody against	Description	Use/Diluition	Product nr and Manufacturer
Actinin	Goat polyclonal	IHC 1:100	17829, Santa Cruz Biotechnology
AKT	Rabbit polyclonal	WB 1:1000	4691, Cell signaling Technology
β-Catenin	Rabbit polyclonal	WB 1:500	05665, Millipore
		IHC 1:300	
Cx43	Rabbit monoclonal	WB 1:500	3512, Cell signaling Technology
		IHC 1:200	
ERK1/2	Rabbit polyclonal	WB 1:1000	4695, Cell signaling Technology
GAPDH	Rabbit polyclonal	WB 1:5000	G9545, Sigma-Aldrich
GSK-3β	Rabbit polyclonal	WB 1:1000	9315, Cell Signaling Technology
LC3B	Rabbit polyclonal	WB 1:1000	PA1-16930, Thermo Fisher Scientific
Nrf 2	Rabbit polyclonal	WB 1:500	365949, Santa Cruz Biotechnology
P-AKT (Ser473)	Rabbit polyclonal	WB 1:1000	4060, Cell Signaling Technology
P-ERK1/2 (Thr202/Tyr20	Rabbit polyclonal	WB 1:1000	9101, Cell signaling Technology
P-GSK-3β Ser9)	Rabbit polyclonal	WB 1:1000	5558, Cell Signaling Technology
PARP1	Rabbit polyclonal	WB 1:500	227244, Abcam
Vimentin	Mouse monoclonal	WB 1:500	V6630, Sigma-Aldrich
Secondary antibodies			
Antibody	**Conjugate**	**Use/Diluition**	**Product nr and Manufacturer**
Donkey Anti-Rabbit IgG	Cy3	IHC 1:200	711-165-152, Jackson ImmunoResearch Laboratories, Inc.
Donkey Anti-Goat IgG	Cy3	WB 1:200	705-165-147, Jackson ImmunoResearch Laboratories, Inc.
Goat Anti-Mouse IgG	Cy3	IHC 1:200	115-165-062, Jackson ImmunoResearch Laboratories, Inc.
Goat Anti-Mouse IgG	HRP	WB 1:5000	115-005-003, Jackson ImmunoResearch Laboratories, Inc.
Goat Anti-Rabbit IgG	HRP	WB 1:5000	111-035-003, Jackson ImmunoResearch Laboratories, Inc.

Table 2. WB, western blot; IHC, Immunohistochemistry

4. RESULTS

4.1 *Cdkl5* expression in the hearts of *Cdkl5* +/− and *Cdkl5* −/− female mice

We found that *Cdkl5* is expressed in the mouse heart (Fig. 1A), albeit at lower levels than in the brain. *Cdkl5* expression was reduced to $39 \pm 5.6\%$ in heterozygous *(Cdkl5 +/−)* female mice in comparison with wild-type (*Cdkl5* +/+) mice (Fig. 1B), and was absent in *Cdkl5* −/− mice (Fig. 1B).
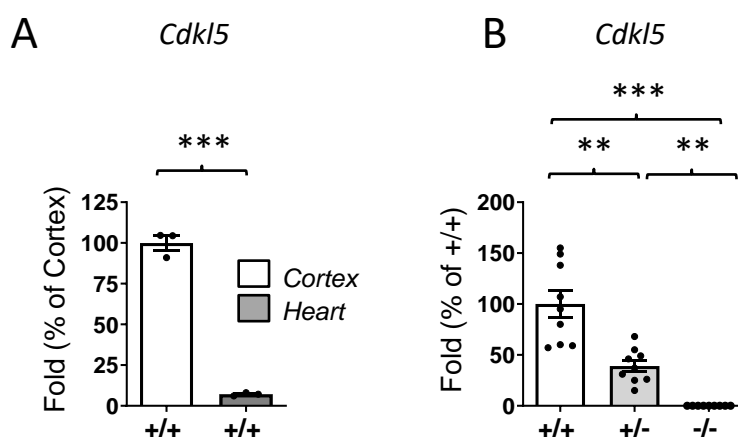
Figure 1. *Cdkl5* expression in the heart of *Cdkl5* +/- mice.
A: Real-time qPCR analysis of *Cdkl5* mRNA expression in the cortex (n=3) and heart (n=3) of 3-month-old wild-type *Cdkl5* +/+ mice. Data are given as a percentage of *Cdkl5* cortical expression. *** p<0.001 (two-tailed Student's t-test). **B:** Relative *Cdkl5* mRNA expression in the heart of 3-month-old *Cdkl5* +/+ (n=6) heterozygous *Cdkl5* +/− (n=9) and homozygous *Cdkl5* −/− (n=9) female mice. The results are expressed as percentages of *Cdkl5* cardiac expression in *Cdkl5* +/+ mice. **p<0.01; ***p<0.001 (Fisher's LSD test after one-way ANOVA).

4.2 Prolonged QTc interval and elevated heart rate in *Cdkl5* +/− mice

To determine whether CDKL5 has a physiological function in the heart, we recorded and analyzed the ECG signal during sleep in *Cdkl5* +/-, *Cdkl5* -/- and wild-type (*Cdkl5* +/+) mice. Interestingly, we found that both *Cdkl5* +/- and *Cdkl5* -/- female mice exhibited tachycardia (reduced RR interval, Fig. 2A, and Table 3 and a longer QTc interval (Fig. 2B and Table 3) in comparison with *Cdkl5* +/+ mice.

As expected, tachycardia also produced significant reductions in P wave duration, and in QRS and JT intervals in *Cdkl5* +/- mice compared to *Cdkl5* +/+ mice (Fig. 2C-F). Using validated mouse indexes computed in the time domain on spontaneous RR fluctuations (pNN8 and MRSSD), we explored the vagal (parasympathetic) contribution to cardiac

modulation (Fig. 2G,H and Table 3). Both indexes were significantly reduced in *Cdkl5 +/-* and *Cdkl5 -/-* mice compared to *Cdkl5 +/+* mice. No significant difference was found between *Cdkl5 +/-* and *Cdkl5 -/-* mice for any of these parameters.
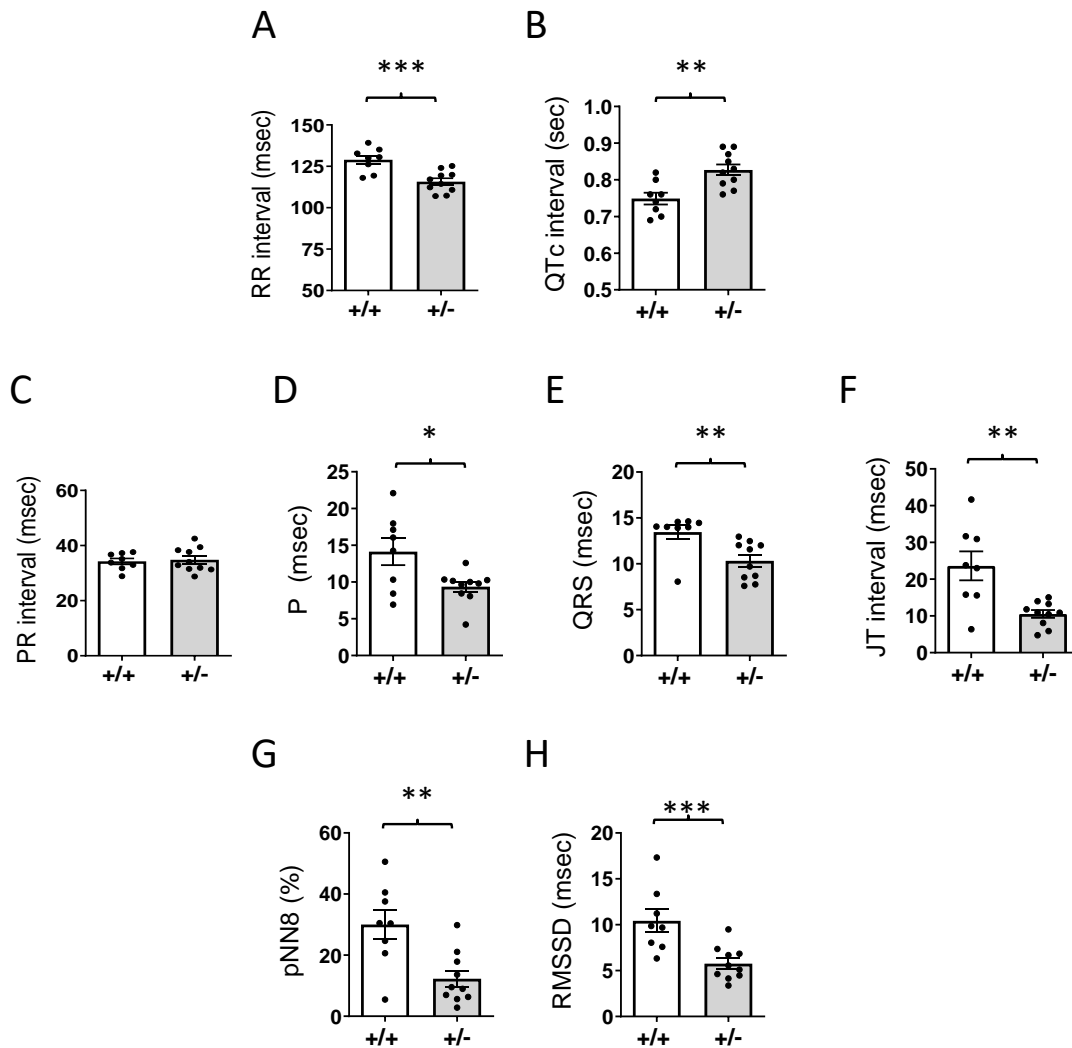
Figure 2. ECG analysis in the heart of *Cdkl5 +/-* mice.

A: Mean heart period duration (expressed as interval between 2 consecutive R waves) during non-rapid-eye-movement sleep (NREMS) in *Cdkl5 +/+* (n= 8) and *Cdkl5 +/-* (n=10) female mice. **B:** Mean duration of ventricular depolarization and repolarization (interval between Q and T waves) during NREMS. These values are reported as corrected QT interval (QTc) after applying Hodge's formula to consider potential differences in RR values between groups (*Cdkl5 +/+* (n= 8) and *Cdkl5 +/-* (n=10) female mice). **C-F:** Baseline ECG parameters calculated during non-rapid-eye-movement sleep (NREMS) in *Cdkl5 +/+* (n=8) and *Cdkl5 +/-* (n=10) female mice. **C:** Mean interval between the beginning of the P wave (onset of atrial depolarization) and the beginning of the QRS complex (onset of ventricular depolarization). **D:** Mean duration of atrial depolarization (P wave). **E:** Mean duration of the depolarization of the right and left ventricles (QRS complex). **F:** Mean duration of ventricular repolarization (JT interval). **G:** Percentage of RR values that differ from the

following ones by more than 8 ms (pNN8) during NREMS in *Cdkl5* +/+ (n= 8) and *Cdkl5* +/- (n=10) female mice. **H:** Root Mean Square of the Successive RR Differences (RMSSD) during NREMS in *Cdkl5* +/+ (n= 8) and *Cdkl5* +/- (n=10) female mice. The results are presented as means ± SEM.* p<0.05, **p<0.01, ***p<0.001 (two-tailed Student's t-test after two-way ANOVA).

	Cdkl5 +/+	*Cdkl5* +/−	*Cdkl5* −/−
RR interval (msec)	128.9 ± 2.6	115.7 ± 2.1 **	118.4 ± 3.1 *
QTc interval (sec)	0.749 ± 0.016	0.827 ± 0.015 **	0.820 ± 0.022 *
pNN8 (%)	30.3 ± 4.3	12.3 ± 2.7 ***	8.2 ± 2.8 ***
RMSSD (msec)	10.4 ± 1.3	5.8 ± 0.6 **	5.9 ± 0.9 **

Table 3. Effect of genotype on ECG parameters. Mean heart period duration (RR); mean duration of ventricular depolarization and repolarization (interval between Q and T waves) after applying Hodge's formula to consider potential differences in RR values between groups (QTc); percentage of RR values that differ from the following values by more than 8 ms (pNN8); Root Mean Square of the Successive RR Differences (RMSSD). All these values were computed during non-rapid eye movement sleep in *Cdkl5* +/+ (n= 8), *Cdkl5* +/- (n=10), and *Cdkl5* -/- (n=8) female mice. Values are represented as mean ± SE. *p<0.05 vs. *Cdkl5* +/+, **p<0.01 vs. *Cdkl5* +/+, ***p<0.001 vs. *Cdkl5* +/+ (Fisher's LSD test after one-way ANOVA).

Since CDD female patients are all heterozygous for CDKL5 deficiency, subsequent analyses were carried out in heterozygous *Cdkl5* +/− female mice. In order to investigate the influences of the autonomic nervous system on heart activity and dissect the relative contribution of each autonomic arm in *Cdkl5* +/- mice, we evaluated heart responses to selective pharmacological blockades of the parasympathetic and sympathetic systems elicited by IP injection of Atropine or Atenolol. As expected, the constant IP infusion of Atenolol in *Cdkl5* +/+ mice produced a significant increase in RR intervals, while Atropine induced a significant decrease compared to saline infusion (Fig 3A,C,D). Accordingly, in *Cdkl5* +/+ mice these drugs produced a significant increase (Atropine) or decrease (Atenolol) in QTc intervals compared to saline (Fig. 3B,C,D). Interestingly, while an effect on RR and QTc intervals was elicited in *Cdkl5* +/- mice by Atenolol infusion (Fig. 3A,B), Atropine did not produce any significant variation of RR or QTc intervals compared to saline in *Cdkl5* +/- mice (Fig. 3A,B).

To investigate whether the rate variability in *Cdkl5* +/- mice is associated with an altered vagal/sympathetic component, we analyzed the expression of muscarinic 2 (*Chrm2*) and

adrenergic beta 1 (*Adrb1*) receptors. We found that the mRNA levels of *Chrm2* were significantly lower in the hearts of *Cdkl5* +/− female mice than in those of wild-type (*Cdkl5* +/+) mice (Fig. 3E), while no difference in the expression of *Adrb1* receptor was observed between *Cdkl5* +/+ and *Cdkl5* +/− female hearts (Fig. 3F).
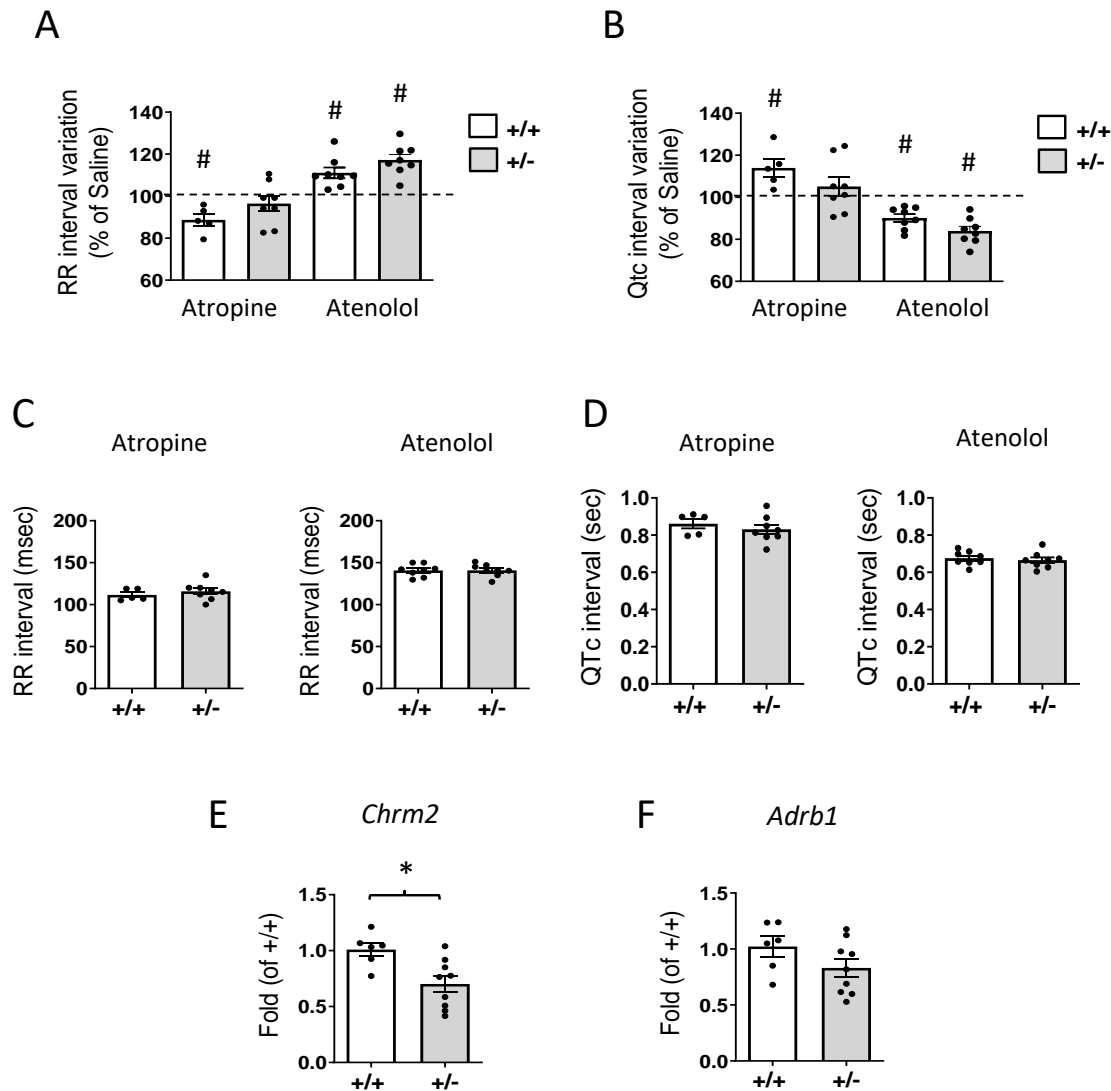
Figure 3. ECG analysis in the heart of *Cdkl5* +/- mice. A: Percentage modification of the RR interval induced by either atropine (5 *Cdkl5* +/+ and 8 *Cdkl5* +/− mice) or atenolol (8 *Cdkl5* +/+ and 8 *Cdkl5* +/− mice) infusion compared to saline infusion (horizontal dotted line). **B**: Percentage modification of the QTc interval induced by either atropine (5 *Cdkl5* +/+ and 8 *Cdkl5* +/− mice) or atenolol (8 *Cdkl5* +/+ and 8 *Cdkl5* +/− mice) infusion compared to saline infusion (horizontal dotted line). The results in (**A,B**) are presented as means ± SEM. # <0.05 vs. saline infusion reference value (dotted line, one-sample *t*-test). **C,D**: Absolute value of RR (mean heart period duration, C) and QTc (mean duration of interval between Q and T waves after applying Hodge's formula, D) intervals after either Atropine (*Cdkl5* +/+ n= 5 and *Cdkl5* +/- n= 8) or Atenolol (*Cdkl5* +/+ n= 8 and

Cdkl5 +/- n= 8) infusion. **E,F:** Real-time qPCR analysis of the muscarinic acetylcholine receptors 2 ((**E**), *Chrm2*) and the adrenoceptor beta 1 ((**F**), *Adrb1*) gene expression in the ventricle of 3-month-old *Cdkl5* +/+ (n = 6) and *Cdkl5* +/− (n = 9) mice. Data are presented as fold change in comparison with ventricular tissue from *Cdkl5* +/+ mice. *$p<0.05$ (two-tailed Student's *t*-test).

4.3 Alterations of voltage-gated channel expression in the hearts of *Cdkl5*+/− mice

To investigate the molecular alterations underlying the prolonged QTc interval and elevated heart rate in *Cdkl5* +/- mice, we analyzed the expression of different voltage-gated channels involved in action potential of cardiac myocytes. In particular, we focused our attention on the genes encoding for the voltage-gated potassium (*Kcnq1*, *Kcnh2*) and sodium (*Scn5a*) channels. Mutations in these genes are the most common causes of inherited long QT interval syndrome (LQTS), a condition characterized by a prolongation of the QT interval on the ECG, an increase in heart rate, and the risk of ventricular arrhythmias (Van Niekerk *et al.*, 2017).

From RT-qPCR analyses, no differences in the expression of *Kcnq1*, *Kcnh2*, or *Kcnj2* channels were observed between *Cdkl5* +/+ and *Cdkl5* +/− female hearts (Table 2); however, we did find that the mRNA levels of *Scn5a* were significantly lower in the hearts of *Cdkl5* +/− female mice than in those of wild-type (*Cdkl5* +/+) mice (Table 2).

To rule out any potential abnormalities in the sinoatrial node as possible contributing factors to the sinus tachycardia observed, *Hcn4* expression was examined. Interestingly, we found that *Hcn4* mRNA levels were significantly lower in *Cdkl5* +/− female mice than in wild type mice (Table 4).

Genes	*Cdkl5* +/+	*Cdkl5* +/−	*p*
Kcnq1	1.00 ± 0.119 (n = 7)	1.08 ± 0.048 (n = 9)	n.s.
Kcnh2	1.00 ± 0.055 (n = 7)	0.88 ± 0.032 (n = 9)	n.s.
Kcnj2	1.00 ± 0.069 (n = 7)	0.99 ± 0.037 (n = 9)	n.s.
Scn5a	1.00 ± 0.054 (n = 5)	0.87 ± 0.030 (n = 5)	*
Hcn4	1.00 ± 0.067 (n = 7)	0.76 ± 0.039 (n = 9)	*

Table 4. Comparative expression of ion channel cardiac genes between *Cdkl5* +/+ and *Cdkl5* +/- mice. mRNA expression levels of ion channel genes in the ventricle of 3-month-old *Cdkl5* +/+ and *Cdkl5* +/- mice. mRNA levels in tissues obtained from *Cdkl5* +/+ mice were set to 1, and relative expression levels in *Cdkl5* +/- mice are represented as mean ± SEM. Relative

quantification was performed using the DDCt method. The means of two stable reference genes (*Actin* and *Gapdh*) were used as normalization factors. *p<0.05, n.s. not significant (two-tailed Student's t-test).

4.4 Increased cardiac fibrosis in *Cdkl5* +/− mice

To determine whether the absence of *Cdkl5* could impact on heart morphological structure in *Cdkl5* KO mice, dissected hearts were weighed. Since the weight of the heart positively correlates with body weight and growth, each animal's body weight was measured before sacrifice, and heart weight to body weight ratio (HW/BW) was calculated. No significant differences in heart weight, body weight, or HW/BW were found between *Cdkl5* +/− and *Cdkl5* +/+ mice (Table 5). Similarly, atrioventricular distance (Table 3) and gross morphology of hearts (data not shown) revealed no differences in the chamber diameters of wild-type (*Cdkl5* +/+) and *Cdkl5* +/− mouse hearts.

	Cdkl5 +/+	*Cdkl5* +/−	*p*
Heart weight (mg)	110.83 ± 3.24	105.89 ± 2.27	n.s.
Body weight (g)	22.19 ± 0.27	21.74 ± 0.31	n.s.
Heart/body weight (mg/g)	4.98 ± 0.12	4.87 ± 0.07	n.s.
Atrioventricular distance (cm)	0.51 ± 0.01	0.52 ± 0.03	n.s.

Table 5. Effect of genotype on heart weight and dimension. Heart weight, body weight, heart over body weight ratio, and atrioventricular distance of 3-4-month-old *Cdkl5* +/+ (n = 18) and *Cdkl5* +/- (n = 27) mice. Values are represented as mean ± SEM, n.s. not significant (two-tailed Student's t-test).

Heart sections stained with hematoxylin and eosin showed normal architecture of cardiac myocytes (Fig. 4A). However, Masson's trichrome-stained sections showed increased collagen deposition in the hearts of *Cdkl5* +/- mice compared with wild-type (*Cdkl5* +/+) mice (Fig. 4B). The increased fibrosis was accompanied by increased expression of fibrotic genes such as α-2 chain of collagen type 1 (*Col1a2*) and α-3 chain of collagen type 2 (*Col3a1*) (Fig. 4C).

Given that cardiac fibrosis is mainly due to the proliferation and trans-differentiation of cardiac fibroblasts, we measured the content of vimentin, a marker of cardiac fibroblasts (Lajiness and Conway, 2014). Western blot analysis showed significantly higher vimentin levels in the hearts of *Cdkl5 +/−* mice in comparison with wild-type (*Cdkl5 +/+*) mice (Fig. 4D).
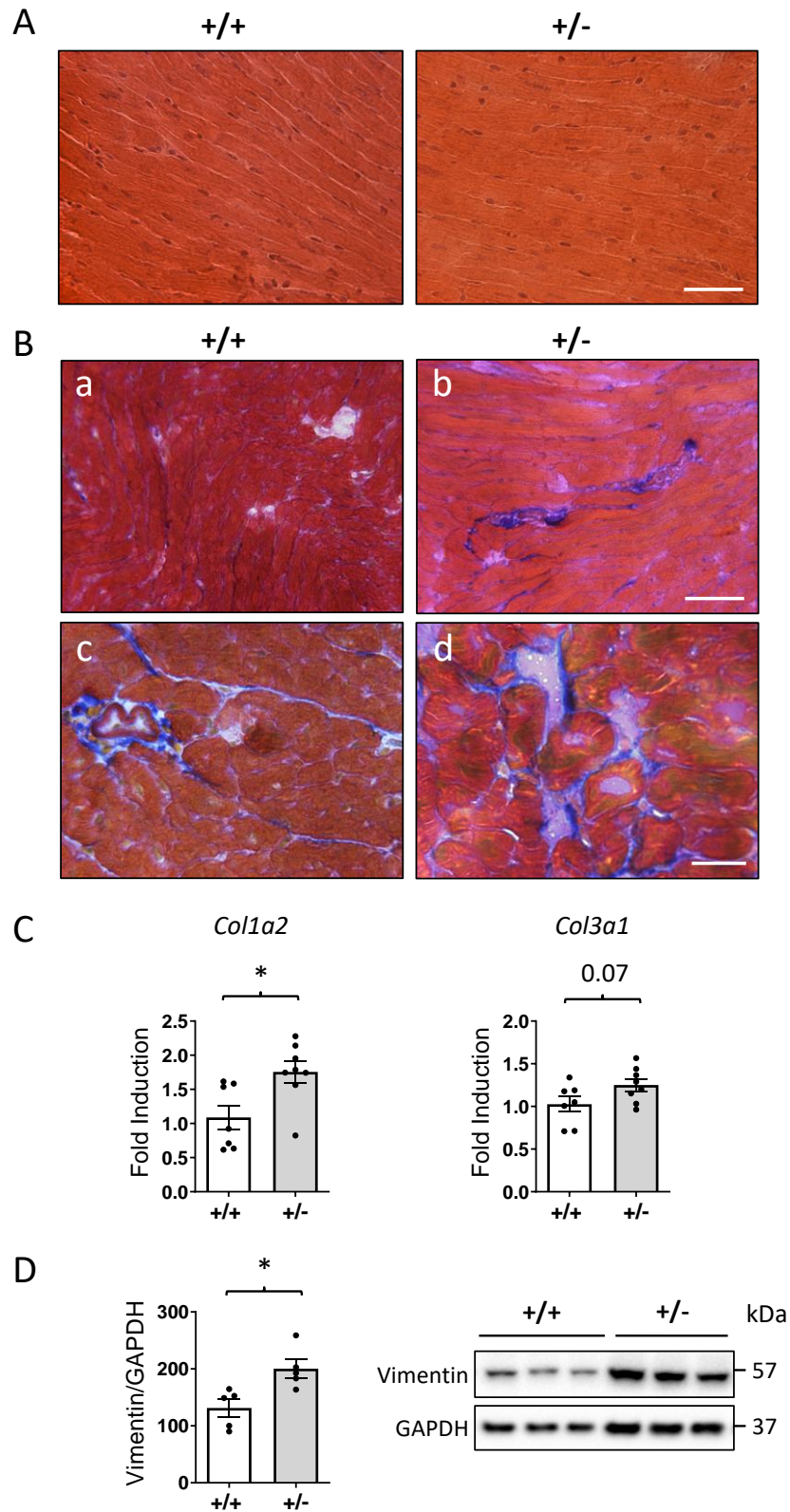
Figure 4. Myocardial fibrosis in the heart of *Cdkl5* +/- mice.

A: Representative images of hematoxylin and eosin staining of longitudinal sections of the ventricular tissue of a *Cdkl5* +/+ (left panel) and a *Cdkl5* +/- (right panel) mouse. Scale bar 50 μm. **B:** Representative images of Masson's Trichrome staining of longitudinal (a, b) and transverse (c, d) sections of the ventricular tissue of a *Cdkl5* +/+ (left panels) and a *Cdkl5* +/- (right panels) mouse showing an increase in blue-stained collagen fibers in the heart of *Cdkl5* +/- mice compared to wild-type (+/+) mice. Scale bars 50 μm. **C:** Expression of collagen Type I Alpha 2 Chain (*Col1a2*) and collagen Type III Alpha 1 Chain (*Col3a1*) in ventricular tissue isolated from the heart of 3-month-old *Cdkl5* +/+ (n=7) and *Cdkl5* +/- (n=8) mice. Data are given as fold change in comparison with cardiac tissue from *Cdkl5* +/+ mice. **D:** Histogram shows quantification of vimentin protein levels normalized to GAPDH in protein extracts of ventricular tissue from 3-month-old *Cdkl5* +/+ (n=5) and *Cdkl5* +/- (n=5) mice. Data are expressed as percentages of *Cdkl5* +/+ mice. Example of immunoblots of three animals from each experimental group on the right. Values in C and D are presented as means ± SEM; *p<0.05 (two-tailed Student's t-test).

4.5 Altered gap junction organization and connexin expression in the hearts of *Cdkl5* +/− mice

The electrical conduction in cardiac muscle relies on an efficient gap junction-mediated intercellular communication between cardiomyocytes, which involves the rapid anisotropic impulse propagation through connexin (Cx)-containing channels, namely of Cx43, the most abundant Cx in the heart.

Western blotting analysis revealed significantly diminished expression of Cx43 in *Cdkl5* +/- mice in comparison to *Cdkl5* +/+ mice (Fig. 5A,B). The mean density of the Cx43 band in western blotting was reduced by 24% in *Cdkl5* +/- mice as compared to the *Cdkl5* +/+ group (Fig. 5B). In parallel, the mRNA levels of Cx43 were not different between *Cdkl5* +/- and *Cdkl5* +/+ mice (Fig. 5C), suggesting a post-transcriptional mechanism of Cx43 downregulation. Immunofluorescence labelling showed Cx43 expression to be mainly located at the intercalated discs (Fig. 5D). As compared to *Cdkl5* +/+ mice, the Cx43 fluorescence in *Cdkl5* +/- mice was slightly less intensive (Fig. 5D). It is interesting to note that some degree of lateralization of the Cx43 expression on the cardiomyocytes of *Cdkl5* +/- mice was also present (Fig. 5D).

Interestingly, the expression of β-catenin protein, a component of the adherens junction of the intercalated disc, was increased in the myocardium of *Cdkl5* +/- mice (Fig. 5E-H). Western blot analysis revealed that *β*-catenin levels were increased by 71.9% in *Cdkl5* +/- mice in comparison with *Cdkl5* +/+ mice (Fig. 5E,F), which correlated with the much

stronger immunoreactivity for β-catenin at the intercalated discs in the hearts of *Cdkl5* +/- mice (Fig. 5G,H).
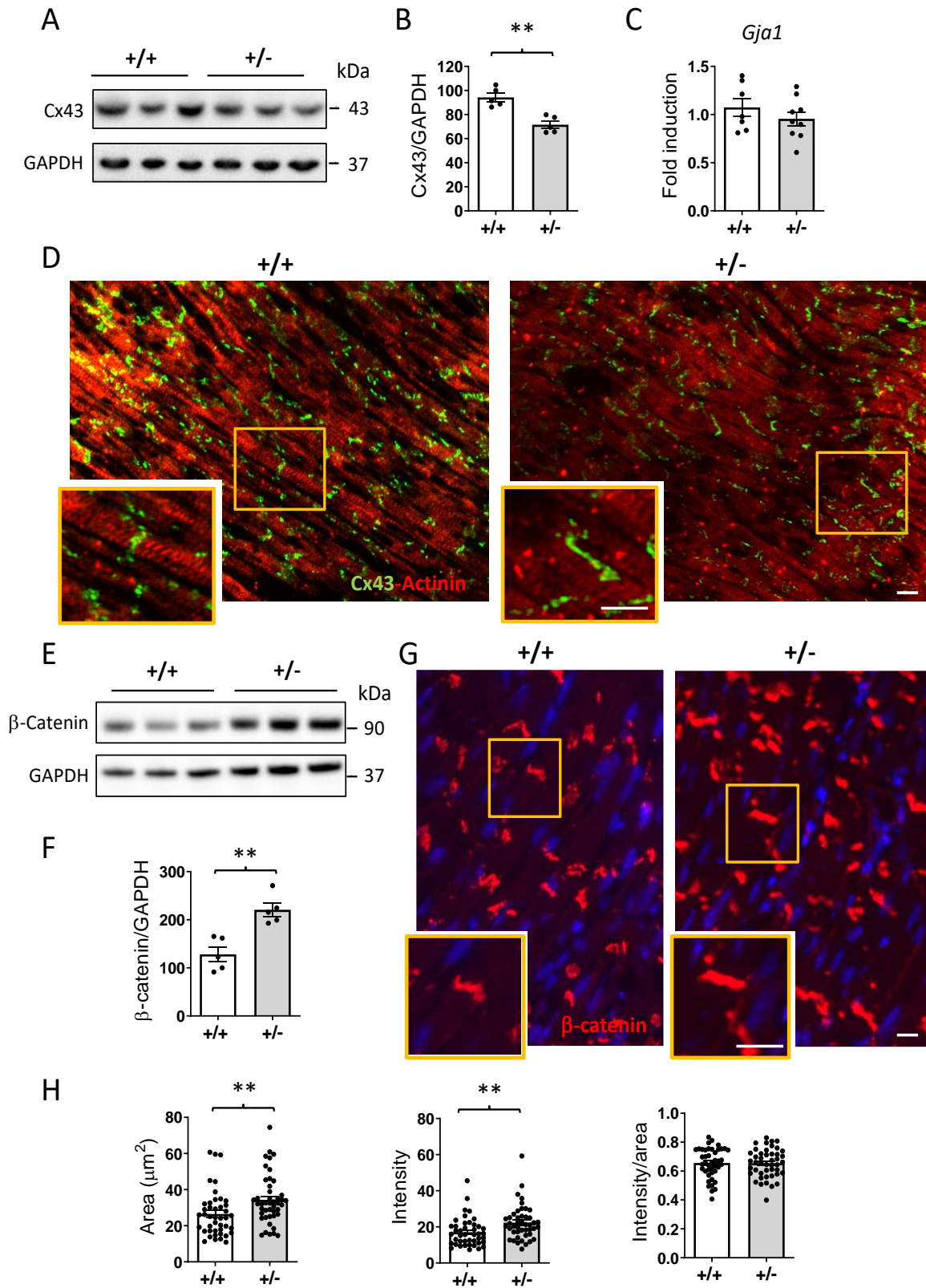
Figure 5. Connexin 43 and β-catenin expression in the heart of *Cdkl5* +/- mice.

A: Example of immunoblot showing Connexin 43 (Cx43) and GAPDH levels in extracts of ventricular heart tissue of *Cdkl5* +/+ (n=3) and *Cdkl5* +/- (n=3) mice. **B:** Histogram shows quantification of connexin 43 (Cx43) protein levels normalized to GAPDH in extracts of ventricular heart tissue from *Cdkl5* +/+ (n=5) and *Cdkl5* +/- (n=5) mice. Data are expressed as percentages of *Cdkl5* +/+ mice. **C:** Relative Gap Junction protein alpha 1 (*Gja1*) mRNA expression in ventricular tissue isolated from the heart of 3-month-old *Cdkl5* +/+ (n=6) and *Cdkl5* +/- (n=9) mice. Data are given as fold change in comparison with cardiac tissue from *Cdkl5* +/+ mice. **D:** Representative fluorescence images of ventricular tissue sections immunostained for Connexin 43 (green) and actinin (red) from a *Cdkl5* +/+ (left panel) and a *Cdkl5* +/- (right panel) mouse. The orange boxes highlight the regions shown in the high magnification panels. Scale bars = 50 μm (low and high magnifications). **E,F:** Western blot analysis of β-catenin levels normalized to GAPDH levels in protein extracts of ventricular heart tissue of *Cdkl5* +/+ (n=5) and *Cdkl5* +/- (n=5) mice. Examples of immunoblot in E and quantification in F. Data are given as a percentage of β-catenin levels in *Cdkl5* +/+ mice. **G:** Representative fluorescent images of ventricular tissue sections immunostained for β-catenin (red) from a *Cdkl5* +/+ (left panel) and a *Cdkl5* +/- (right panel) mouse. Nuclei were counterstained with DAPI. The orange boxes highlight the regions shown in the high magnification panels. Scale bars = 50 μm (low and high magnifications). **H:** Quantification of area (left histogram), intensity (middle histogram), and intensity per area (right histogram) of β-catenin immunostaining in ventricular tissue sections from *Cdkl5* +/+ and *Cdkl5* +/- mice. The results in B, C, F, and H are presented as means ± SEM. **p<0.01 (two-tailed Student's t-test).

4.6 Increased AKT activation in the hearts of *Cdkl5* +/− mice

Evidence has described a potential role of AKT in aging-associated organ deterioration including cardiac hypertrophy and fibrosis (Hua *et al.*, 2011). In particular, aging enhances AKT phosphorylation in the mouse heart, while GSK-3β phosphorylation levels are unaffected by aging or AKT overexpression (Hua *et al.*, 2011). Evaluation of the phosphorylation levels of the AKT/GSK-3β pathway showed higher phosphorylation levels of AKT in the hearts of *Cdkl5* +/- mice in comparison with *Cdkl5* +/+ mice (Fig. 6A,B), but no difference in phosphorylated GSK-3β levels between *Cdkl5* +/+ and *Cdkl5* +/- mice (Fig. 6C,D). Similarly, there was no difference in phosphorylated extracellular regulated kinases (ERK) 1 and 2 in the hearts of *Cdkl5* +/- mice in comparison with *Cdkl5* +/+ mice (Fig. 6C,D).
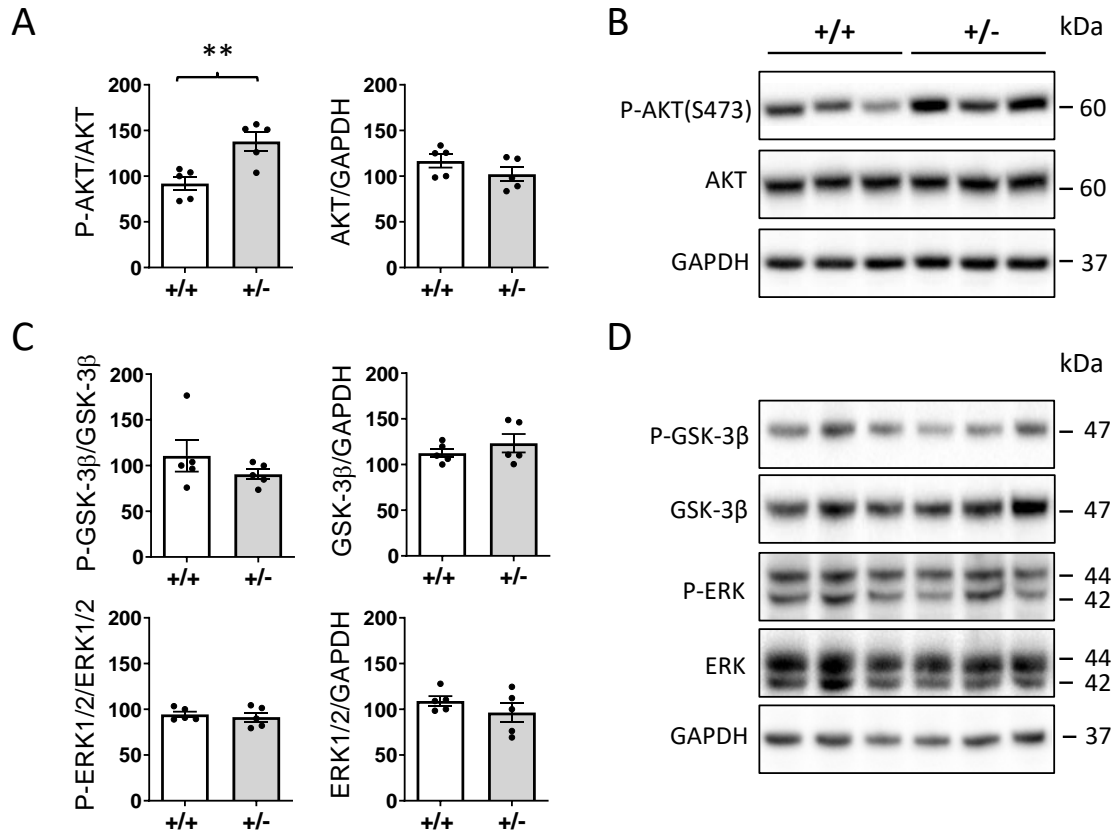
Figure 6. AKT, GSK-3β and ERK pathways in the heart of *Cdkl5* +/- mice.

A: Western blot analysis of phosphorylated AKT (P-AKT, Ser473) levels normalized to total AKT content (left histogram) and total AKT levels normalized to GAPDH levels (right histogram) in ventricular extracts from *Cdkl5* +/+ (n= 5) and *Cdkl5* +/- (n= 5) mice. **B**: Examples of immunoblot for P-AKT, AKT, and GAPDH for three mice from each experiential group. **C:** Western blot analysis of P-GSK-3β and P-ERK1/2 levels in ventricular extracts of mice as in A. Histograms on the left show P-GSK-3β (upper) and P-ERK1/2 (lower) levels normalized to corresponding total protein content. Histograms on the right show ERK1/2 and GSK-3β protein levels normalized to GAPDH levels. D: Examples of immunoblot for P-GSK-3β, GSK-3β, P-ERK1/2, ERK, and GAPDH of three animals from each experimental group. Data are expressed as a percentage of expression in *Cdkl5* +/+ mice. Values represent mean ± SEM. **p < 0.01 (two-tailed Student's t-test).

4.7 Mitochondrial dysfunction in the hearts of *Cdkl5* +/− mice

There is growing evidence that mitochondrial dysfunction contributes to the development and progression of cardiac fibrosis (Jakimiec *et al.*, 2020). To address whether the mitochondrial function is affected in the Cdkl5-deficient heart, we first measured the ATP and ADP content in *Cdkl5* +/- mice heart homogenates using HPLC. This analysis detected

a 35% decline in total ATP content in heart tissue from *Cdkl5* +/- mice compared to controls (Fig. 7A).

Moreover, in *Cdkl5* +/- mice, we found a significant decrease in the ATP/ADP ratio compared to wild-type animals (Fig. 7B), suggesting a diminished cell energy status.

Since mitochondria are the major site of ATP production within the cell, we evaluated whether there were alterations in the process of oxidative phosphorylation (OXPHOS) in *Cdkl5* +/- mice. For this purpose, we isolated intact mitochondria from mouse hearts and evaluated the oxygen consumption in the presence of glutamate-malate or succinate under non-phosphorylating conditions (state 4) and in the presence of ADP (state 3, phosphorylating condition). Glutamate-malate and succinate donate electrons to the respiratory chain at Complex I and Complex II, respectively. State 3 of respiration, in the presence of glutamate-malate or succinate, was significantly decreased in cardiac mitochondria from *Cdkl5* +/- compared to wild-type mice (Fig. 7C). In accordance with the oxygen consumption data, the spectrophotometric analysis of the single respiratory enzyme activity in isolated cardiac mitochondria provided evidence supporting reduced activity of succinate CoQ reductase (Complex II) in *Cdkl5* +/- mice in comparison with *Cdkl5* +/+ mice (Fig. 7D). The Complex I activity in *Cdkl5* +/- heart mitochondria showed a trend of reduction compared to controls, although it did not reach statistical significance (Fig. 7D).

The decrease in the activity of mitochondrial respiratory chain enzymes, prompted us to assess whether overall mitochondrial content, size, and distribution were altered in the hearts of *Cdkl5* +/- mice. We found no significant difference in the density of mitochondria in the myocytes (data not shown), nor was there any difference in the overall size of individual mitochondria (Fig. 7E). However, crystalline-like inclusions in the intracristal space were found in mitochondria of *Cdkl5* +/- mice (Fig. 7E), indicating mitochondrial morphological abnormalities in the *Cdkl5* +/- condition.
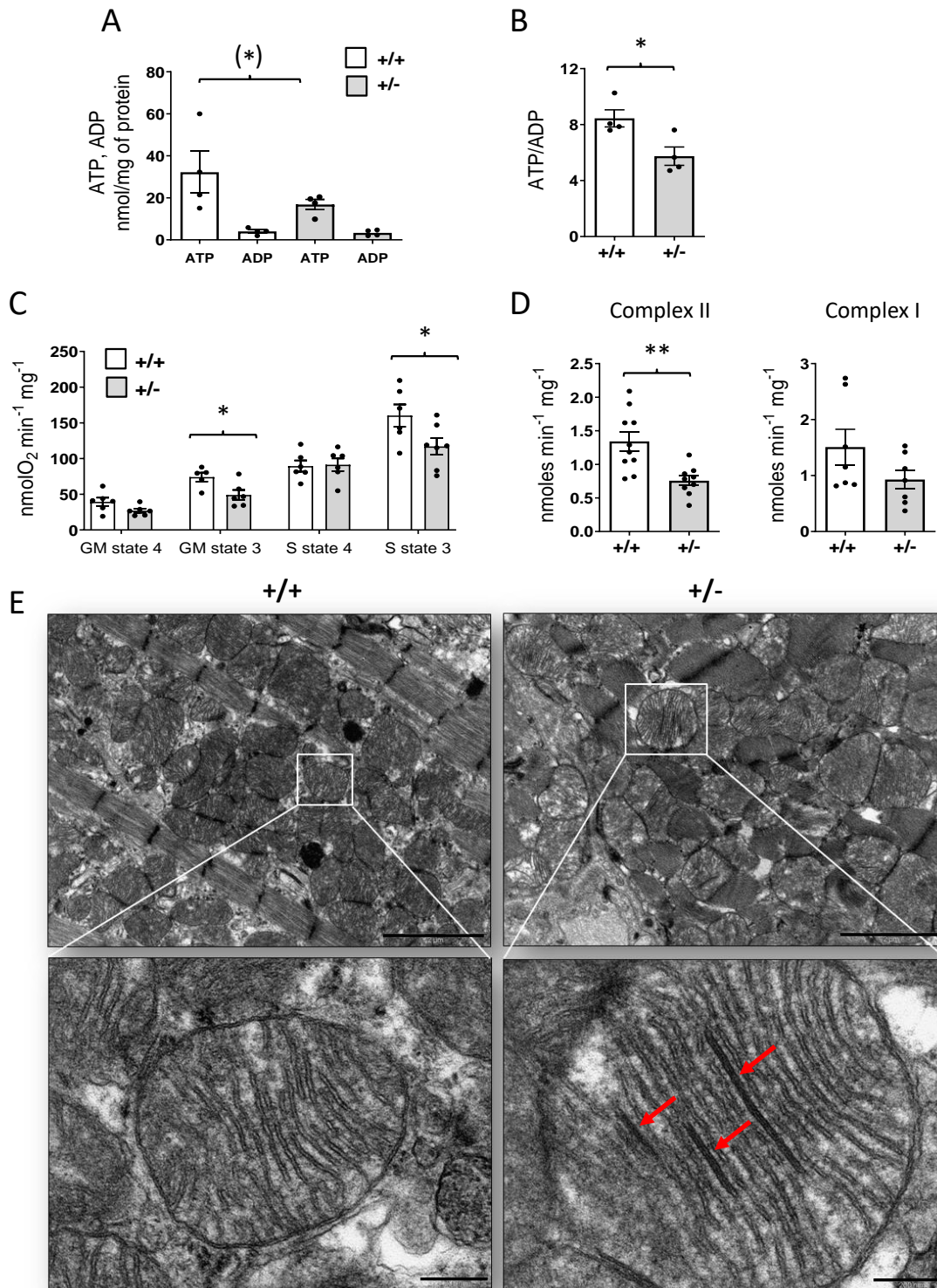
Figure 7. Mitochondrial activity in the heart of *Cdkl5* +/− mice.

A,B: ATP and ADP content (A) and ATP/ADP ratio (B) in heart homogenates from *Cdkl5* +/+ and *Cdkl5* +/- mice measured through HPLC (n=4). **C:** Oxygen consumption rate (OCR) in isolated cardiac mitochondria from *Cdkl5* +/+ and *Cdkl5* +/- mice. The mitochondria were energized with glutamate-malate (GM) or succinate (S) in the presence (state 3) and absence (state 4) of ADP (n=6).

D: Specific Complex I (NADH-CoQ$_1$) and Complex II (Succinate-DCPIP) activities in isolated cardiac mitochondria from *Cdkl5* +/+ and *Cdkl5* +/- mice (n=10). **E:** Representative electron microscopy images of ventricular tissue from a *Cdkl5* +/+ (left panel) and a *Cdkl5* +/- (right panel) mouse. In the *Cdkl5* +/- heart, linear densities are evident inside the intracristal matrix of mitochondria, while a normal cristae structure is observed in *Cdkl5* +/+ mitochondria. The white boxes highlight the regions shown in the high magnification panels. Scale bars: low magnifications = 2 μm, high magnifications = 200 nm. The results in A-D are presented as means ± SEM; in A $^{(*)}$p = 0.055 (Fisher's LSD test after two-way ANOVA); in B-D *p<0.05, **p<0.01 (two-tailed Student's t-test).

4.8 Increased ROS production in the hearts of *Cdkl5* +/− mice

Mitochondrial dysfunction is often associated with increased oxidative stress. The level of reactive oxygen species production (ROS), determined using the fluorogenic probe DFCDA, was significantly higher in *Cdkl5* +/- mitochondria energized with succinate in comparison with the *Cdkl5* +/+ condition (Fig. 8A).
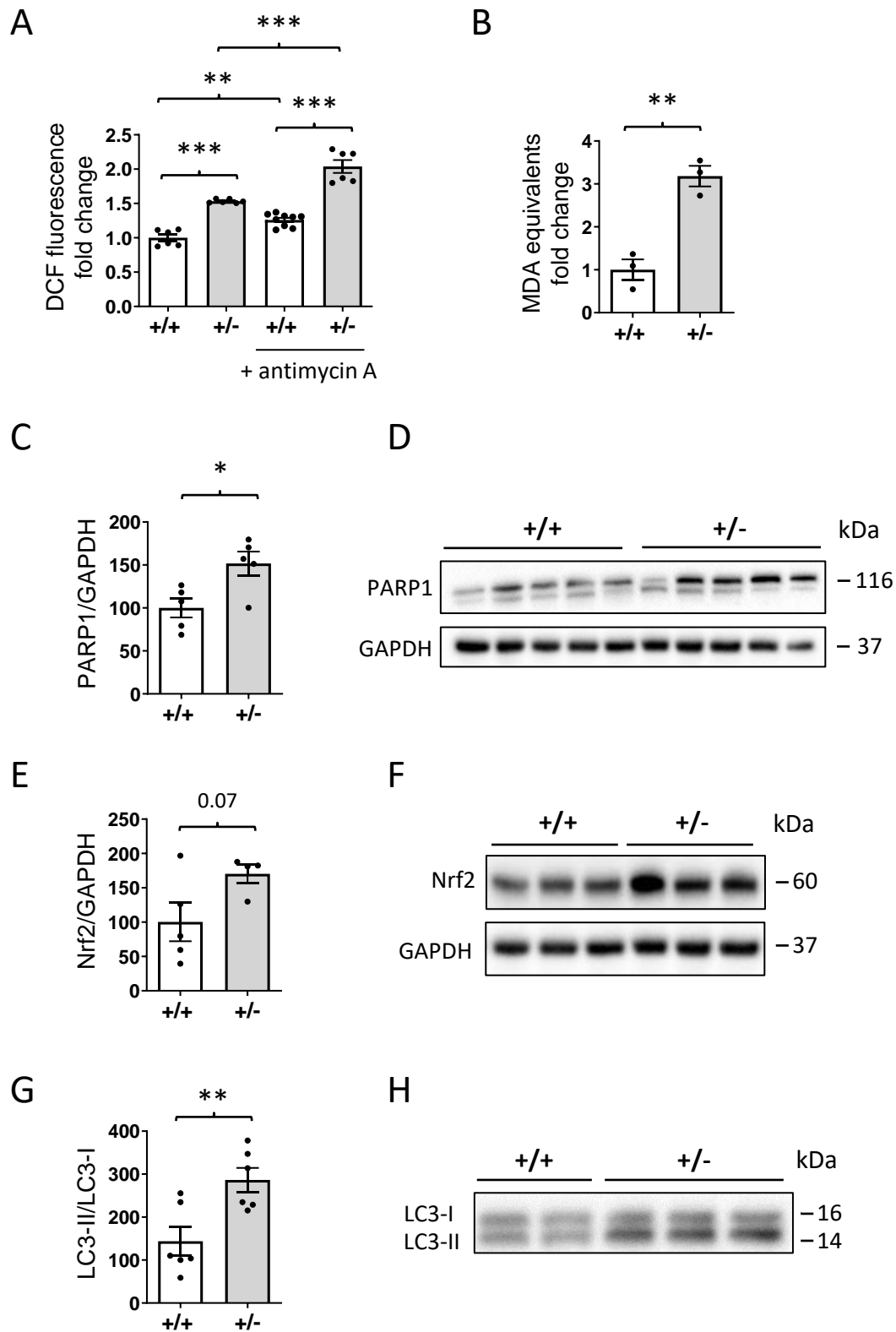
Figure 8. Oxidative stress in the heart of *Cdkl5* +/− mice.

A: Reactive oxygen species (ROS) production in isolated heart mitochondria from *Cdkl5* +/+ and *Cdkl5* +/- mice measured using the fluorescent probe DCFDA. The mitochondria were energized with succinate and the ROS production was determined by following the oxidation of H$_2$DCF to its fluorescent form DCF. The specific inhibitor antimycin A was used to promote ROS production from

mitochondrial Complex III (n=6). Data are expressed as fold change over controls and normalized on protein content; **p < 0.01; ***p < 0.001 (Fisher's LSD test after two-way ANOVA). **B:** Measurement of the lipid peroxidation biomarker malondialdehyde (MDA) levels in isolated heart mitochondria from *Cdkl5* +/+ and *Cdkl5* +/- mice (n=3). Data are expressed as fold change over controls and normalized on protein content; **p < 0.01 (two-tailed Student's t-test). **C,D:** Western blot analysis of Poly(ADP-ribose) polymerase 1 (PARP1) levels in extracts of ventricular heart tissue from *Cdkl5* +/+ (n=5) and *Cdkl5* +/- (n=5) mice. The histogram in C shows PARP1 protein levels normalized to GAPDH. Examples of immunoblot for PARP1 and GAPDH of five animals from each experimental group in D. **E,F:** Expression of nuclear factor erythroid 2-related factor 2 (Nrf2) in extracts of ventricular heart tissue from mice as in C. The histogram in E shows quantification of Nrf2 protein levels normalized to GAPDH. Example of immunoblots of three animals from each experimental group in F. **G,H:** Expression of autophagy marker Light Chain 3(LC3) in extracts of ventricular heart tissue from mice as in C. The histogram in G shows the ratio of LC3II/LC3I. Example of immunoblots for LC3 of three animals from each experimental group are shown in H. Data in C, E, and G are expressed as percentages of *Cdkl5* +/+ mice; values are presented as means ± SEM; *p<0.05; **p<0.01 (two-tailed Student's t-test).

Moreover, ROS production in *Cdkl5* +/- heart mitochondria treated with antimycin A, a specific inhibitor which induces reactive oxygen species production from Complex III, was significantly higher in comparison with the antimycin A-treated *Cdkl5* +/+ condition (Fig. 8A). The mitochondria isolated from *Cdkl5* +/- mouse hearts also showed higher levels of malondialdehyde (MDA), an end product of lipid peroxidation, consistent with a condition of oxidative stress (Fig. 8B).

Interestingly, two proteins, the Poly(ADP-ribose) polymerase 1 (PARP1) and the nuclear factor erythroid 2-related factor 2 (Nrf2), that are known to be activated due to oxidative stress, showed increased levels in the hearts of *Cdkl5* +/- mice compared to *Cdkl5* +/+ mice (Fig. 8C-F). Similarly, we found an increase in the LC3-II/LC3-I ratio (Fig. 8G,H), indicative of increased autophagosome formation*,* following oxidative stress.

5. DISCUSSION

CDD is a very severe and debilitating neurodevelopmental infantile disorder with harsh neurological symptoms such as intractable seizures, neurodevelopmental delay, and autistic-like features. Nevertheless, the improvement of the clinical overview of CDD in the past few years has defined a more detailed phenotypic spectrum; this includes very common alterations in peripheral organ and tissue function, such as gastrointestinal problems, irregular breathing, hypotonia, and scoliosis (Jakimiec *et al.*, 2020) , suggesting that CDKL5 deficiency compromises not only CNS function but also that of other organs/tissues. Here we report, for the first time, that a mouse model of CDD, the heterozygous *Cdkl5* KO (*Cdkl5* +/-) female mouse, exhibits cardiac functional and structural abnormalities. *Cdkl5* +/- mice exhibited QTc prolongation and increased heart rate that are accompanied by impaired cardiac autonomic control. Moreover, the *Cdkl5* +/- heart shows typical signs of heart aging, including increased fibrosis, mitochondrial dysfunctions and increased ROS production.

ECG measurements from *Cdkl5* +/- mice showed statistically significant increases in heart rate and in rate-corrected QTc interval, indicative of delayed ventricular depolarization and repolarization. This is in line with a recent finding showing that, in a cohort of individuals with CDD, the incidence of prolonged QTc or other abnormalities which included sinus tachycardia was higher than the prevalence seen within the general population (Stansauk *et al.*, 2023) . However, as mentioned by the authors, this first patient study has some important limitations: it is retrospective and the sample size is small (Stansauk *et al.*, 2023). Here, using an experimental approach that allows for a continuous ECG recording during sleep in a validated mouse model of CDD, we could overcome these limitations and, importantly, deeply reduce environmental confounders besides the genetic ones. We found that, similarly to heterozygous *Cdkl5* +/− mice, homozygous *Cdkl5* −/− female mice exhibited tachycardia and a longer QTc interval in comparison with *Cdkl5* +/+ mice. Interestingly, the magnitude of the cardiac defects was similar in the two *Cdkl5* deficient conditions. This is not surprising, since it has been shown that heterozygous *Cdkl5* +/− mice develop some behavioral abnormalities that are comparable to defects identified in homozygous *Cdkl5* −/− females (Fuchs *et al.*, 2018b). The putative skewing toward the mutated X chromosome found in the heart of heterozygous females (levels of Cdkl5 decreased to 39%) could explain the similar cardiac phenotypic outcome that heterozygous and homozygous *Cdkl5* KO female mice show.

It is well known that neurological dysfunction may affect the control of cardiac rate and rhythm (Bernardi *et al.*, 2020). Particularly, it has previously been described that autonomic

neuropathies prolong QTc interval in patients with CNS disease, including Rett syndrome (Miura *et al.*, 1984; Guideri *et al.*, 2001; Guideri and Acampa, 2005; Lopez-Santiago *et al.*, 2007; Koschke *et al.*, 2009). Therefore, we tested the hypothesis that cardiac autonomic control is impaired in *Cdkl5* +/- mice. By applying validated indexes of spontaneous RR variability in mice, we assessed cardiac vagal modulation during sleep under baseline conditions and following pharmacological manipulations. Our findings that in *Cdkl5* +/- mice pNN8 and RMSSD indexes were lower than in control mice indicate an impairment in the vagal modulation of the heart period in *Cdkl5* +/- mice. Compared to saline infusion, treatment with muscarinic antagonist (Atropine) did not significantly modify heart rate or QTc interval in *Cdkl5* +/- mice, confirming the reduction in parasympathetic tone in the heart. A growing body of evidence indicates that reduced cardiac parasympathetic activity is a common alteration in brain disorders; it is present in children with autism and Rett syndrome (Julu *et al.*, 2001; Ming *et al.*, 2005), as well as in neurological conditions characterized by neuronal degeneration (Aharon-Peretz *et al.*, 1992; Toledo and Junqueira, 2010; Xiong and Leung, 2019). The mechanism underlying this autonomic alteration is partly unknown (Vanoli and Schwartz, 1990; Fukuda *et al.*, 2015); however, reduced cardiac vagal tone is thought to be prodromic for lethal arrythmias and sudden death. The observed reduction of cardiac M_2 receptor expression in the heart of *Cdkl5* +/- mice may be one of the possible mechanisms underlying the parasympathetic dysfunction in the mouse model of CDD. However, since, in many situations, loss of Cdkl5 function appears to lead to impaired neuronal activity (Della Sala *et al.*, 2016; Hao *et al.*, 2021; Gennaccaro *et al.*, 2021a), we cannot exclude that an overall reduced activity in regions of the brainstem that are important for cardiorespiratory function may underlie this autonomic dysfunction. Regarding the sympathetic regulation of the heart, similarly to wild-type mice, *Cdkl5* -/+ hearts responded to atenolol infusion by increasing RR and decreasing QTc intervals, indicating the presence of a sympathetic modulation on the *Cdkl5* +/- heart. Interestingly, after atenolol infusion, RR and QTc intervals no longer differed between genotypes. Since, there are no validated indices to determine the sympathetic contribution to the heart, at the moment we cannot exclude the presence of a heart control impairment which also involves sympathetic regulation.

The discovery that two cardiac-specific genes (*Scn5a* and *Hcn4*) are altered in their expression in *Cdkl5* +/- female hearts indicates that CDKL5, directly or indirectly, regulates the expression of genes that play a role in the cardiac conduction systems at the cardiomyocyte level. Loss-of-function mutations in the *SCN5A* gene, which encodes the α-

subunit of the cardiac voltage-gated Na+ channel NaV1.5, underlie cardiac disorders, including long QT syndrome (Li *et al.*, 2018). Notably, long QT has been described in almost 20% of Rett syndrome patients, and alterations in the expression of *Scn5a* genes have been reported in the Mecp2-null mouse (Hara *et al.*, 2015). The lower expression of the cardiac pacemaker-specific channel *Hcn4* found in *Cdkl5* +/- hearts could also contribute to the altered heart rate in *Cdkl5* +/- mice. Our results suggest that Cdkl5 deficiency selectively affects the expression of voltage-gated channel genes in the heart and that abnormal cardiac gene expression may be an arrhythmogenic substrate in *Cdkl5* +/- mice.

Immunostaining for Cx43 in *Cdkl5* +/- ventricular tissues revealed a significant reduction in Cx43 levels at cell-cell junctions, confirmed by western blot analysis. Deregulation in β-catenin levels was also present in the intercalated discs of *Cdkl5* +/- cardiomyocytes. Both Cx43, as a major component of gap junctions (Severs *et al.*, 2008) and β-catenin, as a component of the gap junctions and intercalated discs contribute to regulate the transmission of electrical signals through cardiac myocytes. Therefore, the present findings strongly suggest an impairment of intercellular communication in *Cdkl5* +/- cardiomyocytes, which could further be considered as an arrhythmogenic substrate in *Cdkl5* +/- hearts. Indeed, heterogeneous reduction in Cx43 expression and altered patterns of gap junction distribution feature in human ventricular disease and correlate with electrophysiologically identified arrhythmic changes in animal models (Lerner *et al.*, 2000; Severs *et al.*, 2008). It is of note that age-related disorganization of intercalated discs, including increased β-catenin expression, which may be responsible for the slower conduction of the depolarization wave within the heart, has been recently described (Bonda *et al.*, 2016), suggesting an accelerated cardiac senescence in *Cdkl5* +/- mice.

One of the main risk factors for cardiovascular diseases is aging (Hayflick, 2007). Previously, we showed that *Cdkl5* KO mice are characterized by an increased rate of apoptotic cell death during brain aging due to accelerated neuronal senescence, a factor that causes a consequent age-related cognitive and motor decline (Gennaccaro *et al.*, 2021a). Here, we observed a similar accelerated senescence in the heart of *Cdkl5* +/- mice. We found signs of increased cardiac fibrosis and an increased extracellular matrix deposition of collagen and vimentin expression. Premature senescence develops through various external as well as internal stress signals, and these include energetic dysfunction giving rise to free radical reactive oxygen species (ROS) that cause damage to cellular macromolecules; accumulation of this damage leads to the physiological compromise seen in aging (Liguori

et al., 2018). Current evidence suggests that mitochondrial dysregulation is the cause and primary target of energetic dysfunction and free radical production (Mancuso *et al.*, 2007). Here, we found a decrease in mitochondrial oxygen consumption rate in isolated mitochondria from *Cdkl5* +/- hearts when ADP was supplied as a substrate for the ATP synthase (state 3 respiration) and a diminished specific activity of Complex I and II. These data are consistent with the decreased level of ATP and the decreased ATP/ADP ratio measured in heart tissue homogenates from *Cdkl5* +/- mice compared with wild-type animals. In addition, mitochondria isolated from the hearts of *Cdkl5* +/- mice showed increased ROS and lipid peroxidation biomarker (MDA) production compared with controls, suggesting a link between mitochondrial dysfunction and the onset of oxidative and energetic stress.

These findings are in line with recent evidence that mitochondrial dysfunction and oxidative stress occur in CDD (Pecorelli *et al.*, 2011; Pecorelli *et al.*, 2015). A cytokine dysregulation, inflammatory status, oxidative stress marker 4HNE-Pas, and redox imbalance was evidenced in plasma from CDD patients (Pecorelli *et al.*, 2011; Leoncini *et al.*, 2015; Cortelazzo *et al.*, 2017). Additionally, studies in *Cdkl5* KO mice identified brain mitochondrial functional abnormalities, including reduced activity of mitochondrial respiratory chain complexes and impairment in mitochondrial ATP production rate (Vigli *et al.*, 2019; Carli *et al.*, 2021), alterations present also in patient-derived iPSCs (Jagtap *et al.*, 2019; Van Bergen *et al.*, 2021). It is worth noting that we found here mitochondrial structural changes that were consistent in development of intramitochondrial crystalline-like inclusions in the *Cdkl5* +/- heart. The presence of mitochondrial paracrystalline inclusions in a clinically characterized group of patients with genetically defined mitochondrial disease (Stadhouders *et al.*, 1994; Vincent *et al.*, 2016) suggests that this ultrastructure alteration could contribute to mitochondrial function. Therefore, we can speculate that the crystalline inclusions found in the inner membrane may underlie the bioenergetic defects found in *Cdkl5* +/- mitochondria. However, we cannot exclude the possibility that the crystalline-like inclusions represent compensatory responses to mitochondrial stress.

Recent evidence has described a potential role of AKT and autophagy, molecular mechanisms of cellular senescence, in aging-associated organ deterioration. When cardiomyocytes incur oxidative stress, they activate the PI3K/AKT-signalling pathway (Sugden and Clerk, 2006), suggesting that oxidative stress is an upstream event related to the activation of the AKT pathway in cardiomyocytes. Our finding that AKT pathway

activation is increased in the heart of the *Cdkl5* +/- female mouse could be the consequence of an increase in the generation of ROS due to aberrant mitochondrial function. Similarly, increased LC3-II levels, associated with either enhanced autophagosome synthesis or reduced autophagosome turnover (Barth *et al.*, 2010), can be associated with increased ROS production and the resulting oxidative cell stress that occurs in many disease states (Scherz-Shouval *et al.*, 2019). We found that the ratio of LC3-II/LC3-I was enhanced in the *Cdkl5* +/- heart, suggesting an increasing number of autophagosomes.

The principal growth-promoting intracellular signaling pathways that are activated by ROS in cardiac myocytes include not only the AKT pathway, but also the mitogen-activated protein kinase cascades (ERK1/2 pathway) (Sugden and Clerk, 2006). In association with *Cdkl5* +/- cardiac myocyte dysfunctions, we found here alterations in AKT activity but not in ERK1/2 signaling. Activation of ERK1/2 is generally associated with cell growth and survival, and studies with transgenic mice have shown that selective activation of the ERK1/2 cascade in the myocardium induces an adaptive cardiac hypertrophy (Bueno *et al.*, 2000). Further evidence linking ERK1/2 with hypertrophy has been reviewed (Bueno *et al.*, 2000). Since no signs of hypertrophy are evident in the *Cdkl5* +/- heart, this might explain the lack of ERK1/2 dysregulation in these mice.

Considering the protective molecular pathways that might be triggered by oxidative stress (Nguyen *et al.*, 2009) and autophagy (Walker *et al.*, 2018), we found increased levels of Nrf2, a transcription factor known to activate multiple enzymes with antioxidant properties (Ma, 2013), and of PARP1, a DNA damage sensor that facilities base excision repair (Wang and Luo, 2019), in the *Cdkl5* +/- heart. We hypothesized that increased levels of Nrf2 are triggered by ROS production, and this increase is most likely a compensatory effort to increase antioxidant defences in the *Cdkl5* +/- context. This should correlate with a reduction in oxidative stress in *Cdkl5* +/- hearts; however, this is not the case and the issue requires further investigation. It is worth noting that PARP activation has been demonstrated to impair mitochondrial function (Bai *et al.*, 2015) and promote autophagy in cardiomyocytes (Wang *et al.*, 2018). Therefore, increased PARP1 levels could contributed to the pathologic signs observed in the *Cdkl5* +/- heart.

At present, we have no evidence of which of the observed Cdkl5-related alterations is the primary cause underlying the structural and functional abnormalities in the *Cdkl5* +/- heart. However, increasing evidence suggests that ROS production is associated with cardiac arrhythmias; in particular, elevated cellular ROS can cause alterations to the cardiac ion channels, changes in mitochondrial function, and gap junction remodeling, leading to

arrhythmic conditions (Jeong *et al.*, 2012; Adameova *et al.*, 2020; Szyller *et al.*, 2022). Therefore, oxidative stress, a common pathophysiological factor in cardiac disease (Pignatelli *et al.*, 2018; Senoner and Dichtl, 2019; Shaito *et al.*, 2022), may be the main defect underlying cardiac alterations in the *Cdkl5* deficient heart. Future studies aimed at rescuing the cardiac phenotype in *Cdkl5* KO mice, targeting one of the observed defects, could help to shed light on the primary causes that drive cardiac abnormalities in the absence of *Cdkl5*.

6.BIBLIOGRAPHY

ACAMPA, M.; GUIDERI, F. Cardiac disease and Rett syndrome. **Arch Dis Child,** v. 91, n. 5, p. 440-3, May 2006. ISSN 1468-2044. Available at: < https://www.ncbi.nlm.nih.gov/pubmed/16632674 >.

ADAMEOVA, A.; SHAH, A. K.; DHALLA, N. S. Role of Oxidative Stress in the Genesis of Ventricular Arrhythmias. **Int J Mol Sci,** v. 21, n. 12, Jun 12 2020. ISSN 1422-0067 (Electronic) 1422-0067 (Linking). Available at: < https://www.ncbi.nlm.nih.gov/pubmed/32545595 >.

ADHIKARI, A. et al. Touchscreen cognitive deficits, hyperexcitability and hyperactivity in males and females using two models of Cdkl5 deficiency. **Hum Mol Genet,** v. 31, n. 18, p. 3032-3050, Sep 10 2022. ISSN 1460-2083. Available at: < https://www.ncbi.nlm.nih.gov/pubmed/35445702 >.

AHARON-PERETZ, J. et al. Increased sympathetic and decreased parasympathetic cardiac innervation in patients with Alzheimer's disease. **Arch Neurol,** v. 49, n. 9, p. 919-22, Sep 1992. ISSN 0003-9942 (Print)
0003-9942 (Linking). Available at: < https://www.ncbi.nlm.nih.gov/pubmed/1520081 >.

ALVENTE, S. et al. Autonomic mechanisms of blood pressure alterations during sleep in orexin/hypocretin-deficient narcoleptic mice. **Sleep,** v. 44, n. 7, Jul 09 2021. ISSN 1550-9109. Available at: < https://www.ncbi.nlm.nih.gov/pubmed/33517440 >.

AMENDOLA, E. et al. Mapping pathological phenotypes in a mouse model of CDKL5 disorder. **PLoS One,** v. 9, n. 5, p. e91613, 2014. ISSN 1932-6203. Available at: < https://www.ncbi.nlm.nih.gov/pubmed/24838000 >.

AMIN, S. et al. Caregiver's perception of epilepsy treatment, quality of life and comorbidities in an international cohort of CDKL5 patients. **Hippokratia,** v. 21, n. 3, p. 130-135, 2017. ISSN 1108-4189. Available at: < https://www.ncbi.nlm.nih.gov/pubmed/30479474 >.

AMIR, R. E. et al. Rett syndrome is caused by mutations in X-linked MECP2, encoding methyl-CpG-binding protein 2. **Nat Genet,** v. 23, n. 2, p. 185-8, Oct 1999. ISSN 1061-4036. Available at: < https://www.ncbi.nlm.nih.gov/pubmed/10508514 >.

ARCHER, H. L. et al. CDKL5 mutations cause infantile spasms, early onset seizures, and severe mental retardation in female patients. **J Med Genet,** v. 43, n. 9, p. 729-34, Sep 2006. ISSN 1468-6244. Available at: < https://www.ncbi.nlm.nih.gov/pubmed/16611748 >.

ARIANI, F. et al. FOXG1 is responsible for the congenital variant of Rett syndrome. **Am J Hum Genet,** v. 83, n. 1, p. 89-93, Jul 2008. ISSN 1537-6605. Available at: < https://www.ncbi.nlm.nih.gov/pubmed/18571142 >.

ARTUSO, R. et al. Early-onset seizure variant of Rett syndrome: definition of the clinical diagnostic criteria. **Brain Dev,** v. 32, n. 1, p. 17-24, Jan 2010. ISSN 1872-7131. Available at: < https://www.ncbi.nlm.nih.gov/pubmed/19362436 >.

AWAD, P. N. et al. CDKL5 sculpts functional callosal connectivity to promote cognitive flexibility. **Mol Psychiatry**, Feb 03 2023. ISSN 1476-5578. Available at: < https://www.ncbi.nlm.nih.gov/pubmed/36737483 >.

AZNAR-LAÍN, G. et al. CDKL5 Deficiency Disorder Without Epilepsy. **Pediatr Neurol,** v. 144, p. 84-89, Apr 26 2023. ISSN 1873-5150. Available at: < https://www.ncbi.nlm.nih.gov/pubmed/37201242 >.

BAHI-BUISSON, N.; BIENVENU, T. CDKL5-Related Disorders: From Clinical Description to Molecular Genetics. **Mol Syndromol,** v. 2, n. 3-5, p. 137-152, Apr 2012b. ISSN 1661-8769. Available at: < https://www.ncbi.nlm.nih.gov/pubmed/22670135 >.

BAHI-BUISSON, N. et al. The three stages of epilepsy in patients with CDKL5 mutations. **Epilepsia,** v. 49, n. 6, p. 1027-37, Jun 2008a. ISSN 1528-1167. Available at: < https://www.ncbi.nlm.nih.gov/pubmed/18266744 >.

BAHI-BUISSON, N. et al. Key clinical features to identify girls with CDKL5 mutations. **Brain,** v. 131, n. Pt 10, p. 2647-61, Oct 2008b. ISSN 1460-2156. Available at: < https://www.ncbi.nlm.nih.gov/pubmed/18790821 >.

BAHI-BUISSON, N. et al. Recurrent mutations in the CDKL5 gene: genotype-phenotype relationships. **Am J Med Genet A,** v. 158A, n. 7, p. 1612-9, Jul 2012a. ISSN 1552-4833. Available at: < https://www.ncbi.nlm.nih.gov/pubmed/22678952 >.

BAI, P. et al. Poly(ADP-ribose) polymerases as modulators of mitochondrial activity. **Trends Endocrinol Metab,** v. 26, n. 2, p. 75-83, Feb 2015. ISSN 1879-3061 (Electronic) 1043-2760 (Linking). Available at: < https://www.ncbi.nlm.nih.gov/pubmed/25497347 >.

BALESTRA, D. et al. Splicing Mutations Impairing CDKL5 Expression and Activity Can be Efficiently Rescued by U1snRNA-Based Therapy. **Int J Mol Sci,** v. 20, n. 17, Aug 24 2019. ISSN 1422-0067. Available at: < https://www.ncbi.nlm.nih.gov/pubmed/31450582 >.

BALTUSSEN, L. L. et al. Chemical genetic identification of CDKL5 substrates reveals its role in neuronal microtubule dynamics. **EMBO J,** v. 37, n. 24, Dec 14 2018b. ISSN 1460-2075. Available at: < https://www.ncbi.nlm.nih.gov/pubmed/30266824 >.

BARBIERO, I. et al. The neurosteroid pregnenolone reverts microtubule derangement induced by the loss of a functional CDKL5-IQGAP1 complex. **Hum Mol Genet,** v. 26, n. 18, p. 3520-3530, Sep 15 2017b. ISSN 1460-2083. Available at: < https://www.ncbi.nlm.nih.gov/pubmed/28641386 >.

BARBIERO, I. et al. CDKL5 localizes at the centrosome and midbody and is required for faithful cell division. **Sci Rep,** v. 7, n. 1, p. 6228, Jul 24 2017a. ISSN 2045-2322. Available at: < https://www.ncbi.nlm.nih.gov/pubmed/28740074 >.

BARTH, S.; GLICK, D.; MACLEOD, K. F. Autophagy: assays and artifacts. **J Pathol,** v. 221, n. 2, p. 117-24, Jun 2010. ISSN 1096-9896 (Electronic) 0022-3417 (Linking). Available at: < https://www.ncbi.nlm.nih.gov/pubmed/20225337 >.

BASTIANINI, S. et al. Early-life nicotine or cotinine exposure produces long-lasting sleep alterations and downregulation of hippocampal corticosteroid receptors in adult mice. **Sci Rep,** v. 11, n. 1, p. 23897, Dec 13 2021. ISSN 2045-2322. Available at: < https://www.ncbi.nlm.nih.gov/pubmed/34903845 >.

BERNARDI, J.; AROMOLARAN, K. A.; AROMOLARAN, A. S. Neurological Disorders and Risk of Arrhythmia. **Int J Mol Sci,** v. 22, n. 1, Dec 27 2020. ISSN 1422-0067 (Electronic) 1422-0067 (Linking). Available at: < https://www.ncbi.nlm.nih.gov/pubmed/33375447 >.

BERTANI, I. et al. Functional consequences of mutations in CDKL5, an X-linked gene involved in infantile spasms and mental retardation. **J Biol Chem,** v. 281, n. 42, p. 32048-56, Oct 20 2006. ISSN 0021-9258. Available at: < https://www.ncbi.nlm.nih.gov/pubmed/16935860 >.

BIET, M. et al. Prolongation of action potential duration and QT interval during epilepsy linked to increased contribution of neuronal sodium channels to cardiac late Na+ current: potential

mechanism for sudden death in epilepsy. **Circ Arrhythm Electrophysiol,** v. 8, n. 4, p. 912-20, Aug 2015. ISSN 1941-3084. Available at: < https://www.ncbi.nlm.nih.gov/pubmed/26067667 >.

BONDA, T. A. et al. Remodeling of the intercalated disc related to aging in the mouse heart. **J Cardiol,** v. 68, n. 3, p. 261-8, Sep 2016. ISSN 1876-4738 (Electronic)
0914-5087 (Linking). Available at: < https://www.ncbi.nlm.nih.gov/pubmed/26584974 >.

BOTELHO, A. F. M. et al. **Non-invasive ECG recording and QT interval correction assessment in anesthetized rats and mice** Pesq. Vet. Bras 2019.

BRADFORD, M. M. A rapid and sensitive method for the quantitation of microgram quantities of protein utilizing the principle of protein-dye binding. **Anal Biochem,** v. 72, p. 248-54, May 07 1976. ISSN 0003-2697. Available at: < https://www.ncbi.nlm.nih.gov/pubmed/942051 >.

BREWSTER, A. L. et al. Early cardiac electrographic and molecular remodeling in a model of status epilepticus and acquired epilepsy. **Epilepsia,** v. 57, n. 11, p. 1907-1915, Nov 2016. ISSN 1528-1167. Available at: < https://www.ncbi.nlm.nih.gov/pubmed/27555091 >.

BUENO, O. F. et al. The MEK1-ERK1/2 signaling pathway promotes compensated cardiac hypertrophy in transgenic mice. **EMBO J,** v. 19, n. 23, p. 6341-50, Dec 1 2000. ISSN 0261-4189 (Print)
1460-2075 (Electronic)
0261-4189 (Linking). Available at: < https://www.ncbi.nlm.nih.gov/pubmed/11101507 >.

CANNING, P. et al. CDKL Family Kinases Have Evolved Distinct Structural Features and Ciliary Function. **Cell Rep,** v. 22, n. 4, p. 885-894, Jan 23 2018. ISSN 2211-1247. Available at: < https://www.ncbi.nlm.nih.gov/pubmed/29420175 >.

CARLI, S. et al. In vivo magnetic resonance spectroscopy in the brain of Cdkl5 null mice reveals a metabolic profile indicative of mitochondrial dysfunctions. **J Neurochem,** v. 157, n. 4, p. 1253-1269, May 2021. ISSN 1471-4159 (Electronic)
0022-3042 (Linking). Available at: < https://www.ncbi.nlm.nih.gov/pubmed/33448385 >.

CHAUHAN, A. et al. Brain region-specific deficit in mitochondrial electron transport chain complexes in children with autism. **J Neurochem,** v. 117, n. 2, p. 209-20, Apr 2011. ISSN 1471-4159. Available at: < https://www.ncbi.nlm.nih.gov/pubmed/21250997 >.

CHEADLE, J. P. et al. Long-read sequence analysis of the MECP2 gene in Rett syndrome patients: correlation of disease severity with mutation type and location. **Hum Mol Genet,** v. 9, n. 7, p. 1119-29, Apr 12 2000. ISSN 0964-6906. Available at: < https://www.ncbi.nlm.nih.gov/pubmed/10767337 >.

CHEN, Q. et al. CDKL5, a protein associated with rett syndrome, regulates neuronal morphogenesis via Rac1 signaling. **J Neurosci,** v. 30, n. 38, p. 12777-86, Sep 22 2010. ISSN 1529-2401. Available at: < https://www.ncbi.nlm.nih.gov/pubmed/20861382 >.

CLARK, B. C. et al. Serial follow-up of corrected QT interval in Rett syndrome. **Dev Med Child Neurol,** v. 62, n. 7, p. 833-836, Jul 2020. ISSN 1469-8749. Available at: < https://www.ncbi.nlm.nih.gov/pubmed/31797351 >.

COLL, M. et al. Targeted next-generation sequencing provides novel clues for associated epilepsy and cardiac conduction disorder/SUDEP. **PLoS One,** v. 12, n. 12, p. e0189618, 2017. ISSN 1932-6203. Available at: < https://www.ncbi.nlm.nih.gov/pubmed/29261713 >.

CORTELAZZO, A. et al. Inflammatory protein response in CDKL5-Rett syndrome: evidence of a subclinical smouldering inflammation. **Inflamm Res,** v. 66, n. 3, p. 269-280, Mar 2017. ISSN 1420-908X (Electronic)
1023-3830 (Linking). Available at: < http://www.ncbi.nlm.nih.gov/pubmed/27900411 >.

CUOMO, S. et al. Influence of autonomic tone on QT interval duration. **Cardiologia,** v. 42, n. 10, p. 1071-6, Oct 1997. ISSN 0393-1978. Available at: < https://www.ncbi.nlm.nih.gov/pubmed/9534283 >.

DAS, M. K.; ZIPES, D. P. Antiarrhythmic and nonantiarrhythmic drugs for sudden cardiac death prevention. **J Cardiovasc Pharmacol,** v. 55, n. 5, p. 438-49, May 2010. ISSN 1533-4023. Available at: < https://www.ncbi.nlm.nih.gov/pubmed/20509177 >.

DELLA SALA, G. et al. Dendritic Spine Instability in a Mouse Model of CDKL5 Disorder Is Rescued by Insulin-like Growth Factor 1. **Biol Psychiatry,** v. 80, n. 4, p. 302-311, Aug 15 2016. ISSN 1873-2402 (Electronic)
0006-3223 (Linking). Available at: < http://www.ncbi.nlm.nih.gov/pubmed/26452614 >.

DEMAREST, S. et al. Severity Assessment in CDKL5 Deficiency Disorder. **Pediatr Neurol,** v. 97, p. 38-42, Aug 2019. ISSN 1873-5150. Available at: < https://www.ncbi.nlm.nih.gov/pubmed/31147226 >.

DI NARDO, A. et al. Phenotypic characterization of Cdkl5-knockdown neurons establishes elongated cilia as a functional assay for CDKL5 Deficiency Disorder. **Neurosci Res,** v. 176, p. 73-78, Mar 2022. ISSN 1872-8111. Available at: < https://www.ncbi.nlm.nih.gov/pubmed/34624412 >.

DLOUHY, B. J.; GEHLBACH, B. K.; RICHERSON, G. B. Sudden unexpected death in epilepsy: basic mechanisms and clinical implications for prevention. **J Neurol Neurosurg Psychiatry,** v. 87, n. 4, p. 402-13, Apr 2016. ISSN 1468-330X. Available at: < https://www.ncbi.nlm.nih.gov/pubmed/26979537 >.

EVANS, J. C. et al. Early onset seizures and Rett-like features associated with mutations in CDKL5. **Eur J Hum Genet,** v. 13, n. 10, p. 1113-20, Oct 2005. ISSN 1018-4813. Available at: < https://www.ncbi.nlm.nih.gov/pubmed/16015284 >.

FATO, R. et al. Differential effects of mitochondrial Complex I inhibitors on production of reactive oxygen species. **Biochim Biophys Acta,** v. 1787, n. 5, p. 384-92, May 2009. ISSN 0006-3002. Available at: < https://www.ncbi.nlm.nih.gov/pubmed/19059197 >.

FEHR, S. et al. There is variability in the attainment of developmental milestones in the CDKL5 disorder. **J Neurodev Disord,** v. 7, n. 1, p. 2, 2015. ISSN 1866-1947. Available at: < https://www.ncbi.nlm.nih.gov/pubmed/25657822 >.

FEHR, S. et al. The CDKL5 disorder is an independent clinical entity associated with early-onset encephalopathy. **Eur J Hum Genet,** v. 21, n. 3, p. 266-73, Mar 2013. ISSN 1476-5438. Available at: < https://www.ncbi.nlm.nih.gov/pubmed/22872100 >.

FEHR, S. et al. Seizure variables and their relationship to genotype and functional abilities in the CDKL5 disorder. **Neurology,** v. 87, n. 21, p. 2206-2213, Nov 22 2016. ISSN 1526-632X. Available at: < https://www.ncbi.nlm.nih.gov/pubmed/27770071 >.

FICKER, D. M. Sudden unexplained death and injury in epilepsy. **Epilepsia,** v. 41 Suppl 2, p. S7-12, 2000. ISSN 0013-9580. Available at: < https://www.ncbi.nlm.nih.gov/pubmed/10885735 >.

FICKER, D. M. et al. Population-based study of the incidence of sudden unexplained death in epilepsy. **Neurology,** v. 51, n. 5, p. 1270-4, Nov 1998. ISSN 0028-3878. Available at: < https://www.ncbi.nlm.nih.gov/pubmed/9818844 >.

FREZZA, C.; CIPOLAT, S.; SCORRANO, L. Organelle isolation: functional mitochondria from mouse liver, muscle and cultured fibroblasts. **Nat Protoc,** v. 2, n. 2, p. 287-95, 2007. ISSN 1750-2799. Available at: < https://www.ncbi.nlm.nih.gov/pubmed/17406588 >.

FU, C. et al. Consensus guidelines on managing Rett syndrome across the lifespan. **BMJ Paediatr Open,** v. 4, n. 1, p. e000717, 2020. ISSN 2399-9772. Available at: < https://www.ncbi.nlm.nih.gov/pubmed/32984552 >.

FUCHS, C. et al. Treatment with FRAX486 rescues neurobehavioral and metabolic alterations in a female mouse model of CDKL5 deficiency disorder. **CNS Neurosci Ther,** v. 28, n. 11, p. 1718-1732, Nov 2022. ISSN 1755-5949. Available at: < https://www.ncbi.nlm.nih.gov/pubmed/35932179 >.

FUCHS, C. et al. Treatment with the GSK3-beta inhibitor Tideglusib improves hippocampal development and memory performance in juvenile, but not adult, Cdkl5 knockout mice. **Eur J Neurosci,** v. 47, n. 9, p. 1054-1066, May 2018a. ISSN 1460-9568. Available at: < https://www.ncbi.nlm.nih.gov/pubmed/29603837 >.

FUCHS, C. et al. Heterozygous CDKL5 Knockout Female Mice Are a Valuable Animal Model for CDKL5 Disorder. **Neural Plast,** v. 2018, p. 9726950, 2018b. ISSN 1687-5443. Available at: < https://www.ncbi.nlm.nih.gov/pubmed/29977282 >.

FUCHS, C. et al.CDKL5 deficiency predisposes neurons to cell death through the deregulation of SMAD3 signaling. **Brain Pathol,** v. 29, n. 5, p. 658-674, Sep 2019. ISSN 1750-3639. Available at: < https://www.ncbi.nlm.nih.gov/pubmed/30793413 >.

FUCHS, C. et al. Inhibition of GSK3β rescues hippocampal development and learning in a mouse model of CDKL5 disorder. **Neurobiol Dis,** v. 82, p. 298-310, Oct 2015. ISSN 1095-953X. Available at: < https://www.ncbi.nlm.nih.gov/pubmed/26143616 >.

FUCHS, C. et al. Loss of CDKL5 impairs survival and dendritic growth of newborn neurons by altering AKT/GSK-3β signaling. **Neurobiol Dis,** v. 70, n. 100, p. 53-68, Oct 2014. ISSN 1095-953X. Available at: < https://www.ncbi.nlm.nih.gov/pubmed/24952363 >.

FUKUDA, K. et al. Cardiac innervation and sudden cardiac death. **Circ Res,** v. 116, n. 12, p. 2005-19, Jun 5 2015. ISSN 1524-4571 (Electronic)
0009-7330 (Print)
0009-7330 (Linking). Available at: < https://www.ncbi.nlm.nih.gov/pubmed/26044253 >.

GALVANI, G. et al. Inhibition of microglia overactivation restores neuronal survival in a mouse model of CDKL5 deficiency disorder. **J Neuroinflammation,** v. 18, n. 1, p. 155, Jul 08 2021. ISSN 1742-2094. Available at: < https://www.ncbi.nlm.nih.gov/pubmed/34238328 >.

GENNACCARO, L. et al. Age-Related Cognitive and Motor Decline in a Mouse Model of CDKL5 Deficiency Disorder is Associated with Increased Neuronal Senescence and Death. **Aging Dis,** v. 12, n. 3, p. 764-785, Jun 2021a. ISSN 2152-5250. Available at: < https://www.ncbi.nlm.nih.gov/pubmed/34094641 >.

GENNACCARO, L. et al.. A GABA$_B$ receptor antagonist rescue functional and structural impairments in the perirhinal cortex of a mouse model of CDKL5 deficiency disorder. **Neurobiol Dis,** v. 153, p. 105304, Jun 2021b. ISSN 1095-953X. Available at: < https://www.ncbi.nlm.nih.gov/pubmed/33621640 >.

GOLD, W. A. et al. Mitochondrial dysfunction in the skeletal muscle of a mouse model of Rett syndrome (RTT): implications for the disease phenotype. **Mitochondrion,** v. 15, p. 10-7, Mar 2014. ISSN 1872-8278. Available at: < https://www.ncbi.nlm.nih.gov/pubmed/24613463 >.

GOLDMAN, A. M. et al. Arrhythmia in heart and brain: KCNQ1 mutations link epilepsy and sudden unexplained death. **Sci Transl Med,** v. 1, n. 2, p. 2ra6, Oct 14 2009. ISSN 1946-6242. Available at: < https://www.ncbi.nlm.nih.gov/pubmed/20368164 >.

GRASER, S. et al. Cep164, a novel centriole appendage protein required for primary cilium formation. **J Cell Biol,** v. 179, n. 2, p. 321-30, Oct 22 2007. ISSN 0021-9525. Available at: < https://www.ncbi.nlm.nih.gov/pubmed/17954613 >.

GUERRINI, R.; PARRINI, E. Epilepsy in Rett syndrome, and CDKL5- and FOXG1-gene-related encephalopathies. **Epilepsia,** v. 53, n. 12, p. 2067-78, Dec 2012. ISSN 1528-1167. Available at: < https://www.ncbi.nlm.nih.gov/pubmed/22998673 >.

GUIDERI, F.; ACAMPA, M. Sudden death and cardiac arrhythmias in Rett syndrome. **Pediatr Cardiol,** v. 26, n. 1, p. 111, Jan-Feb 2005. ISSN 0172-0643 (Print)
0172-0643 (Linking). Available at: < https://www.ncbi.nlm.nih.gov/pubmed/15136902 >.

GUIDERI, F. et al. Progressive cardiac dysautonomia observed in patients affected by classic Rett syndrome and not in the preserved speech variant. **J Child Neurol,** v. 16, n. 5, p. 370-3, May 2001. ISSN 0883-0738 (Print)
0883-0738 (Linking). Available at: < https://www.ncbi.nlm.nih.gov/pubmed/11392524 >.

GURGONE, A. et al. mGluR5 PAMs rescue cortical and behavioural defects in a mouse model of CDKL5 deficiency disorder. **Neuropsychopharmacology,** v. 48, n. 6, p. 877-886, May 2023. ISSN 1740-634X. Available at: < https://www.ncbi.nlm.nih.gov/pubmed/35945276 >.

HAGBERG, B. et al. A progressive syndrome of autism, dementia, ataxia, and loss of purposeful hand use in girls: Rett's syndrome: report of 35 cases. **Ann Neurol,** v. 14, n. 4, p. 471-9, Oct 1983. ISSN 0364-5134. Available at: < https://www.ncbi.nlm.nih.gov/pubmed/6638958 >.

HAGEBEUK, E. E.; VAN DEN BOSSCHE, R. A.; DE WEERD, A. W. Respiratory and sleep disorders in female children with atypical Rett syndrome caused by mutations in the CDKL5 gene. **Dev Med Child Neurol,** v. 55, n. 5, p. 480-4, May 2013. ISSN 1469-8749. Available at: < https://www.ncbi.nlm.nih.gov/pubmed/23151060 >.

HAGEBEUK, E. E. O.; SMITS, A.; DE WEERD, A. Long time polysomnographic sleep and breathing evaluations in children with CDKL5 deficiency disorder. **Sleep Med,** v. 103, p. 173-179, Mar 2023. ISSN 1878-5506. Available at: < https://www.ncbi.nlm.nih.gov/pubmed/36812861 >.

HAO, S. et al. CDKL5 Deficiency Augments Inhibitory Input into the Dentate Gyrus That Can Be Reversed by Deep Brain Stimulation. **J Neurosci,** v. 41, n. 43, p. 9031-9046, Oct 27 2021. ISSN 1529-2401 (Electronic)
0270-6474 (Linking). Available at: < https://www.ncbi.nlm.nih.gov/pubmed/34544833 >.

HARA, M. et al. Disturbance of cardiac gene expression and cardiomyocyte structure predisposes Mecp2-null mice to arrhythmias. **Sci Rep,** v. 5, p. 11204, Jun 15 2015. ISSN 2045-2322 (Electronic)
2045-2322 (Linking). Available at: < https://www.ncbi.nlm.nih.gov/pubmed/26073556 >.

HAYFLICK, L. Biological aging is no longer an unsolved problem. **Ann N Y Acad Sci,** v. 1100, p. 1-13, Apr 2007. ISSN 0077-8923 (Print)
0077-8923 (Linking). Available at: < https://www.ncbi.nlm.nih.gov/pubmed/17460161 >.

HECTOR, R. D. et al. Characterisation of CDKL5 Transcript Isoforms in Human and Mouse. **PLoS One,** v. 11, n. 6, p. e0157758, 2016. ISSN 1932-6203. Available at: < https://www.ncbi.nlm.nih.gov/pubmed/27315173 >.

HECTOR, R. D. et al. variants: Improving our understanding of a rare neurologic disorder. **Neurol Genet,** v. 3, n. 6, p. e200, Dec 2017. ISSN 2376-7839. Available at: < https://www.ncbi.nlm.nih.gov/pubmed/29264392 >.

HUA, Y. et al. Chronic Akt activation accentuates aging-induced cardiac hypertrophy and myocardial contractile dysfunction: role of autophagy. **Basic Res Cardiol,** v. 106, n. 6, p. 1173-91, Nov 2011. ISSN 1435-1803. Available at: < https://www.ncbi.nlm.nih.gov/pubmed/21901288 >.

INDRIERI, A. et al. Mutations in COX7B cause microphthalmia with linear skin lesions, an unconventional mitochondrial disease. **Am J Hum Genet,** v. 91, n. 5, p. 942-9, Nov 02 2012. ISSN 1537-6605. Available at: < https://www.ncbi.nlm.nih.gov/pubmed/23122588 >.

JAGTAP, S. et al. Aberrant mitochondrial function in patient-derived neural cells from CDKL5 deficiency disorder and Rett syndrome. **Hum Mol Genet,** v. 28, n. 21, p. 3625-3636, Nov 01 2019. ISSN 1460-2083. Available at: < https://www.ncbi.nlm.nih.gov/pubmed/31518399 >.

JAKIMIEC, M.; PAPROCKA, J.; ŚMIGIEL, R. CDKL5 Deficiency Disorder-A Complex Epileptic Encephalopathy. **Brain Sci,** v. 10, n. 2, Feb 17 2020. ISSN 2076-3425. Available at: < https://www.ncbi.nlm.nih.gov/pubmed/32079229 >.

JEONG, E. M. et al. Metabolic stress, reactive oxygen species, and arrhythmia. **J Mol Cell Cardiol,** v. 52, n. 2, p. 454-63, Feb 2012. ISSN 1095-8584 (Electronic)
0022-2828 (Print)
0022-2828 (Linking). Available at: < https://www.ncbi.nlm.nih.gov/pubmed/21978629 >.

JHANG, C. L. et al. Mice lacking cyclin-dependent kinase-like 5 manifest autistic and ADHD-like behaviors. **Hum Mol Genet,** v. 26, n. 20, p. 3922-3934, Oct 15 2017. ISSN 1460-2083. Available at: < https://www.ncbi.nlm.nih.gov/pubmed/29016850 >.

JHANG, C. L. et al.. Dopaminergic loss of cyclin-dependent kinase-like 5 recapitulates methylphenidate-remediable hyperlocomotion in mouse model of CDKL5 deficiency disorder. **Hum Mol Genet,** v. 29, n. 14, p. 2408-2419, Aug 11 2020. ISSN 1460-2083. Available at: < https://www.ncbi.nlm.nih.gov/pubmed/32588892 >.

JONES, D. P. Determination of pyridine dinucleotides in cell extracts by high-performance liquid chromatography. **J Chromatogr,** v. 225, n. 2, p. 446-9, Oct 09 1981. Available at: < https://www.ncbi.nlm.nih.gov/pubmed/7298779 >.

JULU, P. O. et al. Characterisation of breathing and associated central autonomic dysfunction in the Rett disorder. **Arch Dis Child,** v. 85, n. 1, p. 29-37, Jul 2001. ISSN 1468-2044 (Electronic)
0003-9888 (Linking). Available at: < https://www.ncbi.nlm.nih.gov/pubmed/11420195 >.

KADAM, S. D. et al. Rett Syndrome and CDKL5 Deficiency Disorder: From Bench to Clinic. **Int J Mol Sci,** v. 20, n. 20, Oct 15 2019. ISSN 1422-0067. Available at: < https://www.ncbi.nlm.nih.gov/pubmed/31618813 >.

KALSCHEUER, V. M. et al. Disruption of the serine/threonine kinase 9 gene causes severe X-linked infantile spasms and mental retardation. **Am J Hum Genet,** v. 72, n. 6, p. 1401-11, Jun 2003. ISSN 0002-9297. Available at: < https://www.ncbi.nlm.nih.gov/pubmed/12736870 >.

KAMESHITA, I. et al. Cyclin-dependent kinase-like 5 binds and phosphorylates DNA methyltransferase 1. **Biochem Biophys Res Commun,** v. 377, n. 4, p. 1162-7, Dec 26 2008. ISSN 1090-2104. Available at: < https://www.ncbi.nlm.nih.gov/pubmed/18977197 >.

KAPITEIN, L. C.; HOOGENRAAD, C. C. Building the Neuronal Microtubule Cytoskeleton. **Neuron,** v. 87, n. 3, p. 492-506, Aug 05 2015. ISSN 1097-4199. Available at: < https://www.ncbi.nlm.nih.gov/pubmed/26247859 >.

KATAYAMA, S. et al. Cyclin-Dependent Kinase-Like 5 (CDKL5): Possible Cellular Signalling Targets and Involvement in CDKL5 Deficiency Disorder. **Neural Plast,** v. 2020, p. 6970190, 2020. ISSN 1687-5443. Available at: < https://www.ncbi.nlm.nih.gov/pubmed/32587608 >.

KATAYAMA, S.; SUEYOSHI, N.; KAMESHITA, I. Critical Determinants of Substrate Recognition by Cyclin-Dependent Kinase-like 5 (CDKL5). **Biochemistry,** v. 54, n. 19, p. 2975-87, May 19 2015. ISSN 1520-4995. Available at: < https://www.ncbi.nlm.nih.gov/pubmed/25905439 >.

KERR, A. M. et al. Rett syndrome: analysis of deaths in the British survey. **Eur Child Adolesc Psychiatry,** v. 6 Suppl 1, p. 71-4, 1997. ISSN 1018-8827. Available at: < https://www.ncbi.nlm.nih.gov/pubmed/9452925 >.

KILSTRUP-NIELSEN, C. et al. What we know and would like to know about CDKL5 and its involvement in epileptic encephalopathy. **Neural Plast,** v. 2012, p. 728267, 2012. ISSN 1687-5443. Available at: < https://www.ncbi.nlm.nih.gov/pubmed/22779007 >.

KISHK, N. A. et al. Interictal cardiac repolarization abnormalities in people with epilepsy. **Epilepsy Behav,** v. 79, p. 106-111, Feb 2018. ISSN 1525-5069. Available at: < https://www.ncbi.nlm.nih.gov/pubmed/29274604 >.

KOSCHKE, M. et al. Autonomy of autonomic dysfunction in major depression. **Psychosom Med,** v. 71, n. 8, p. 852-60, Oct 2009. ISSN 1534-7796 (Electronic)
0033-3174 (Linking). Available at: < https://www.ncbi.nlm.nih.gov/pubmed/19779146 >.

LA MONTANARA, P. et al. Cyclin-dependent-like kinase 5 is required for pain signaling in human sensory neurons and mouse models. **Sci Transl Med,** v. 12, n. 551, Jul 08 2020. ISSN 1946-6242. Available at: < https://www.ncbi.nlm.nih.gov/pubmed/32641489 >.

LAJINESS, J. D.; CONWAY, S. J. Origin, development, and differentiation of cardiac fibroblasts. **J Mol Cell Cardiol,** v. 70, p. 2-8, May 2014. ISSN 1095-8584 (Electronic)
0022-2828 (Linking). Available at: < https://www.ncbi.nlm.nih.gov/pubmed/24231799 >.

LAUDE, D.; BAUDRIE, V.; ELGHOZI, J. L. Effects of atropine on the time and frequency domain estimates of blood pressure and heart rate variability in mice. **Clin Exp Pharmacol Physiol,** v. 35, n. 4, p. 454-7, Apr 2008. ISSN 1440-1681. Available at: < https://www.ncbi.nlm.nih.gov/pubmed/18307740 >.

LEONCINI, S. et al. Cytokine Dysregulation in MECP2- and CDKL5-Related Rett Syndrome: Relationships with Aberrant Redox Homeostasis, Inflammation, and omega-3 PUFAs. **Oxid Med Cell Longev,** v. 2015, p. 421624, 2015. ISSN 1942-0994 (Electronic)
1942-0994 (Linking). Available at: < http://www.ncbi.nlm.nih.gov/pubmed/26236424 >.

LERNER, D. L. et al. Accelerated onset and increased incidence of ventricular arrhythmias induced by ischemia in Cx43-deficient mice. **Circulation,** v. 101, n. 5, p. 547-52, Feb 8 2000. ISSN 1524-4539 (Electronic)
0009-7322 (Linking). Available at: < https://www.ncbi.nlm.nih.gov/pubmed/10662753 >.

LI, M. C. H. et al. Acquired cardiac channelopathies in epilepsy: Evidence, mechanisms, and clinical significance. **Epilepsia,** v. 60, n. 9, p. 1753-1767, Sep 2019. ISSN 1528-1167. Available at: < https://www.ncbi.nlm.nih.gov/pubmed/31353444 >.

LI, W. et al. SCN5A Variants: Association With Cardiac Disorders. **Front Physiol,** v. 9, p. 1372, 2018. ISSN 1664-042X (Print)
1664-042X (Linking). Available at: < https://www.ncbi.nlm.nih.gov/pubmed/30364184 >.

LIANG, J. S. et al. Phenotypic manifestations between male and female children with CDKL5 mutations. **Brain Dev,** v. 41, n. 9, p. 783-789, Oct 2019. ISSN 1872-7131. Available at: < https://www.ncbi.nlm.nih.gov/pubmed/31122804 >.

LIGUORI, I. et al. Oxidative stress, aging, and diseases. **Clin Interv Aging,** v. 13, p. 757-772, 2018. ISSN 1178-1998 (Electronic)
1176-9092 (Linking). Available at: < https://www.ncbi.nlm.nih.gov/pubmed/29731617 >.

LIN, C.; FRANCO, B.; ROSNER, M. R. CDKL5/Stk9 kinase inactivation is associated with neuronal developmental disorders. **Hum Mol Genet,** v. 14, n. 24, p. 3775-86, Dec 15 2005. ISSN 0964-6906. Available at: < https://www.ncbi.nlm.nih.gov/pubmed/16330482 >.

LINDY, A. S. et al. Diagnostic outcomes for genetic testing of 70 genes in 8565 patients with epilepsy and neurodevelopmental disorders. **Epilepsia,** v. 59, n. 5, p. 1062-1071, May 2018. ISSN 1528-1167. Available at: < https://www.ncbi.nlm.nih.gov/pubmed/29655203 >.

LO MARTIRE, V. et al. CDKL5 deficiency entails sleep apneas in mice. **J Sleep Res,** v. 26, n. 4, p. 495-497, Aug 2017. ISSN 1365-2869. Available at: < https://www.ncbi.nlm.nih.gov/pubmed/28230307 >.

LOI, M. et al. Correction to: Increased DNA Damage and Apoptosis in CDKL5-Deficient Neurons. **Mol Neurobiol,** v. 57, n. 5, p. 2263-2264, May 2020. ISSN 1559-1182. Available at: < https://www.ncbi.nlm.nih.gov/pubmed/32064577 >.

LOPEZ-SANTIAGO, L. F. et al. Sodium channel Scn1b null mice exhibit prolonged QT and RR intervals. **J Mol Cell Cardiol,** v. 43, n. 5, p. 636-47, Nov 2007. ISSN 0022-2828 (Print)
0022-2828 (Linking). Available at: < https://www.ncbi.nlm.nih.gov/pubmed/17884088 >.

LOTUFO, P. A. et al. A systematic review and meta-analysis of heart rate variability in epilepsy and antiepileptic drugs. **Epilepsia,** v. 53, n. 2, p. 272-82, Feb 2012. ISSN 1528-1167. Available at: < https://www.ncbi.nlm.nih.gov/pubmed/22221253 >.

LOWRY, O. H. et al. Protein measurement with the Folin phenol reagent. **J Biol Chem,** v. 193, n. 1, p. 265-75, Nov 1951. ISSN 0021-9258. Available at: < https://www.ncbi.nlm.nih.gov/pubmed/14907713 >.

LUPORI, L. et al. Site-specific abnormalities in the visual system of a mouse model of CDKL5 deficiency disorder. **Hum Mol Genet,** v. 28, n. 17, p. 2851-2861, Sep 01 2019. ISSN 1460-2083. Available at: < https://www.ncbi.nlm.nih.gov/pubmed/31108505 >.

MA, Q. Role of nrf2 in oxidative stress and toxicity. **Annu Rev Pharmacol Toxicol,** v. 53, p. 401-26, 2013. ISSN 1545-4304 (Electronic)
0362-1642 (Linking). Available at: < https://www.ncbi.nlm.nih.gov/pubmed/23294312 >.

MACKAY, C. I. et al. Exploring genotype-phenotype relationships in the CDKL5 deficiency disorder using an international dataset. **Clin Genet,** v. 99, n. 1, p. 157-165, Jan 2021. ISSN 1399-0004. Available at: < https://www.ncbi.nlm.nih.gov/pubmed/33047306 >.

MANCUSO, C. et al. Mitochondrial dysfunction, free radical generation and cellular stress response in neurodegenerative disorders. **Front Biosci,** v. 12, p. 1107-23, Jan 1 2007. ISSN 1093-9946 (Print)
1093-4715 (Linking). Available at: < https://www.ncbi.nlm.nih.gov/pubmed/17127365 >.

MANGATT, M. et al. Prevalence and onset of comorbidities in the CDKL5 disorder differ from Rett syndrome. **Orphanet J Rare Dis,** v. 11, p. 39, Apr 14 2016. ISSN 1750-1172. Available at: < https://www.ncbi.nlm.nih.gov/pubmed/27080038 >.

MARI, F. et al. CDKL5 belongs to the same molecular pathway of MeCP2 and it is responsible for the early-onset seizure variant of Rett syndrome. **Hum Mol Genet,** v. 14, n. 14, p. 1935-46, Jul 15 2005. ISSN 0964-6906. Available at: < https://www.ncbi.nlm.nih.gov/pubmed/15917271 >.

MAZZIOTTI, R. et al. Searching for biomarkers of CDKL5 disorder: early-onset visual impairment in CDKL5 mutant mice. **Hum Mol Genet,** v. 26, n. 12, p. 2290-2298, Jun 15 2017. ISSN 1460-2083. Available at: < https://www.ncbi.nlm.nih.gov/pubmed/28369421 >.

MERTZ, J. et al. Sequential Elution Interactome Analysis of the Mind Bomb 1 Ubiquitin Ligase Reveals a Novel Role in Dendritic Spine Outgrowth. **Mol Cell Proteomics,** v. 14, n. 7, p. 1898-910, Jul 2015. ISSN 1535-9484. Available at: < https://www.ncbi.nlm.nih.gov/pubmed/25931508 >.

MING, X. et al. Reduced cardiac parasympathetic activity in children with autism. **Brain Dev,** v. 27, n. 7, p. 509-16, Oct 2005. ISSN 0387-7604 (Print)
0387-7604 (Linking). Available at: < https://www.ncbi.nlm.nih.gov/pubmed/16198209 >.

MIURA, T. et al. Electrocardiographic abnormalities in cerebrovascular accidents. **Jpn J Med,** v. 23, n. 1, p. 22-6, Feb 1984. ISSN 0021-5120 (Print)
0021-5120 (Linking). Available at: < https://www.ncbi.nlm.nih.gov/pubmed/6748347 >.

MOHANRAJ, R. et al. Mortality in adults with newly diagnosed and chronic epilepsy: a retrospective comparative study. **Lancet Neurol,** v. 5, n. 6, p. 481-7, Jun 2006. ISSN 1474-4422. Available at: < https://www.ncbi.nlm.nih.gov/pubmed/16713919 >.

MONTINI, E. et al. Identification and characterization of a novel serine-threonine kinase gene from the Xp22 region. **Genomics,** v. 51, n. 3, p. 427-33, Aug 01 1998. ISSN 0888-7543. Available at: < https://www.ncbi.nlm.nih.gov/pubmed/9721213 >.

MORITA, H.; WU, J.; ZIPES, D. P. The QT syndromes: long and short. **Lancet,** v. 372, n. 9640, p. 750-63, Aug 30 2008. ISSN 1474-547X. Available at: < https://www.ncbi.nlm.nih.gov/pubmed/18761222 >.

MORRISON-LEVY, N. et al. Early-Onset Developmental and Epileptic Encephalopathies of Infancy: An Overview of the Genetic Basis and Clinical Features. **Pediatr Neurol,** v. 116, p. 85-94, Mar 2021. ISSN 1873-5150. Available at: < https://www.ncbi.nlm.nih.gov/pubmed/33515866 >.

MULCAHEY, P. J. et al. Aged heterozygous Cdkl5 mutant mice exhibit spontaneous epileptic spasms. **Exp Neurol,** v. 332, p. 113388, Oct 2020. ISSN 1090-2430. Available at: < https://www.ncbi.nlm.nih.gov/pubmed/32585155 >.

MUÑOZ, I. M. et al. Phosphoproteomic screening identifies physiological substrates of the CDKL5 kinase. **EMBO J,** v. 37, n. 24, Dec 14 2018. ISSN 1460-2075. Available at: < https://www.ncbi.nlm.nih.gov/pubmed/30266825 >.

MYERS, K. A. et al. Heart rate variability in epilepsy: A potential biomarker of sudden unexpected death in epilepsy risk. **Epilepsia,** v. 59, n. 7, p. 1372-1380, Jul 2018. ISSN 1528-1167. Available at: < https://www.ncbi.nlm.nih.gov/pubmed/29873813 >.

NASHEF, L. Sudden unexpected death in epilepsy: terminology and definitions. **Epilepsia,** v. 38, n. 11 Suppl, p. S6-8, Nov 1997. ISSN 1528-1167. Available at: < https://www.ncbi.nlm.nih.gov/pubmed/19909329 >.

NASHEF, L. et al. Circumstances of death in sudden death in epilepsy: interviews of bereaved relatives. **J Neurol Neurosurg Psychiatry,** v. 64, n. 3, p. 349-52, Mar 1998. ISSN 0022-3050. Available at: < https://www.ncbi.nlm.nih.gov/pubmed/9527147 >.

NAWAZ, M. S. et al. CDKL5 and Shootin1 Interact and Concur in Regulating Neuronal Polarization. **PLoS One,** v. 11, n. 2, p. e0148634, 2016. ISSN 1932-6203. Available at: < https://www.ncbi.nlm.nih.gov/pubmed/26849555 >.

NEUL, J. L. et al. Specific mutations in methyl-CpG-binding protein 2 confer different severity in Rett syndrome. **Neurology,** v. 70, n. 16, p. 1313-21, Apr 15 2008. ISSN 1526-632X (Electronic) 0028-3878 (Linking). Available at: < http://www.ncbi.nlm.nih.gov/pubmed/18337588 >.

NGUYEN, T.; NIOI, P.; PICKETT, C. B. The Nrf2-antioxidant response element signaling pathway and its activation by oxidative stress. **J Biol Chem,** v. 284, n. 20, p. 13291-5, May 15 2009. ISSN 0021-9258 (Print) 0021-9258 (Linking). Available at: < https://www.ncbi.nlm.nih.gov/pubmed/19182219 >.

OI, A. et al. Subcellular distribution of cyclin-dependent kinase-like 5 (CDKL5) is regulated through phosphorylation by dual specificity tyrosine-phosphorylation-regulated kinase 1A (DYRK1A). **Biochem Biophys Res Commun,** v. 482, n. 2, p. 239-245, Jan 08 2017. ISSN 1090-2104. Available at: < https://www.ncbi.nlm.nih.gov/pubmed/27840050 >.

OKUDA, K. et al. CDKL5 controls postsynaptic localization of GluN2B-containing NMDA receptors in the hippocampus and regulates seizure susceptibility. **Neurobiol Dis,** v. 106, p. 158-170, Oct 2017. ISSN 1095-953X. Available at: < https://www.ncbi.nlm.nih.gov/pubmed/28688852 >.

OKUDA, K. et al. Comprehensive behavioral analysis of the Cdkl5 knockout mice revealed significant enhancement in anxiety- and fear-related behaviors and impairment in both acquisition and long-term retention of spatial reference memory. **PLoS One,** v. 13, n. 4, p. e0196587, 2018. ISSN 1932-6203. Available at: < https://www.ncbi.nlm.nih.gov/pubmed/29702698 >.

OLSON, H. E. et al. Cyclin-Dependent Kinase-Like 5 Deficiency Disorder: Clinical Review. **Pediatr Neurol,** v. 97, p. 18-25, Aug 2019. ISSN 1873-5150. Available at: < https://www.ncbi.nlm.nih.gov/pubmed/30928302 >.

PECORELLI, A. et al. Alteration of serum lipid profile, SRB1 loss, and impaired Nrf2 activation in CDKL5 disorder. **Free Radic Biol Med,** v. 86, p. 156-65, Sep 2015. ISSN 1873-4596 (Electronic) 0891-5849 (Linking). Available at: < https://www.ncbi.nlm.nih.gov/pubmed/26006105 >.

PECORELLI, A. et al. Increased levels of 4HNE-protein plasma adducts in Rett syndrome. **Clin Biochem,** v. 44, n. 5-6, p. 368-71, Apr 2011. ISSN 1873-2933 (Electronic) 0009-9120 (Linking). Available at: < https://www.ncbi.nlm.nih.gov/pubmed/21276437 >.

PHILIPPE, C. et al. Phenotypic variability in Rett syndrome associated with FOXG1 mutations in females. **J Med Genet,** v. 47, n. 1, p. 59-65, Jan 2010. ISSN 1468-6244. Available at: < https://www.ncbi.nlm.nih.gov/pubmed/19564653 >.

PIGNATELLI, P. et al. Oxidative stress and cardiovascular disease: new insights. **Kardiol Pol,** v. 76, n. 4, p. 713-722, 2018. ISSN 1897-4279 (Electronic)
0022-9032 (Linking). Available at: < https://www.ncbi.nlm.nih.gov/pubmed/29537483 >.

PINI, G. et al. Variant of Rett syndrome and CDKL5 gene: clinical and autonomic description of 10 cases. **Neuropediatrics,** v. 43, n. 1, p. 37-43, Feb 2012. ISSN 1439-1899. Available at: < https://www.ncbi.nlm.nih.gov/pubmed/22430159 >.

PIZZO, R. et al. Lack of Cdkl5 Disrupts the Organization of Excitatory and Inhibitory Synapses and Parvalbumin Interneurons in the Primary Visual Cortex. **Front Cell Neurosci,** v. 10, p. 261, 2016. ISSN 1662-5102. Available at: < https://www.ncbi.nlm.nih.gov/pubmed/27965538 >.

PIZZO, R. et al. Structural Bases of Atypical Whisker Responses in a Mouse Model of CDKL5 Deficiency Disorder. **Neuroscience,** v. 445, p. 130-143, Oct 01 2020. ISSN 1873-7544. Available at: < https://www.ncbi.nlm.nih.gov/pubmed/31472213 >.

POWELL, K. L. et al. HCN channelopathy and cardiac electrophysiologic dysfunction in genetic and acquired rat epilepsy models. **Epilepsia,** v. 55, n. 4, p. 609-20, Apr 2014. ISSN 1528-1167. Available at: < https://www.ncbi.nlm.nih.gov/pubmed/24592881 >.

RADEMACHER, S.; EICKHOLT, B. J. PTEN in Autism and Neurodevelopmental Disorders. **Cold Spring Harb Perspect Med,** v. 9, n. 11, Nov 01 2019. ISSN 2157-1422. Available at: < https://www.ncbi.nlm.nih.gov/pubmed/31427284 >.

RAVINDRAN, K. et al. The pathophysiology of cardiac dysfunction in epilepsy. **Epilepsy Res,** v. 127, p. 19-29, Nov 2016. ISSN 1872-6844. Available at: < https://www.ncbi.nlm.nih.gov/pubmed/27544485 >.

REILLY, C. A.; AUST, S. D. Measurement of lipid peroxidation. **Curr Protoc Toxicol,** v. Chapter 2, p. Unit 2.4, May 2001. ISSN 1934-9262. Available at: < https://www.ncbi.nlm.nih.gov/pubmed/23045044 >.

REN, E. et al. Functional and Structural Impairments in the Perirhinal Cortex of a Mouse Model of CDKL5 Deficiency Disorder Are Rescued by a TrkB Agonist. **Front Cell Neurosci,** v. 13, p. 169, 2019. ISSN 1662-5102. Available at: < https://www.ncbi.nlm.nih.gov/pubmed/31114483 >.

REZIN, G. T. et al. Mitochondrial dysfunction and psychiatric disorders. **Neurochem Res,** v. 34, n. 6, p. 1021-9, Jun 2009. ISSN 1573-6903. Available at: < https://www.ncbi.nlm.nih.gov/pubmed/18979198 >.

RICCIARDI, S. et al. CDKL5 influences RNA splicing activity by its association to the nuclear speckle molecular machinery. **Hum Mol Genet,** v. 18, n. 23, p. 4590-602, Dec 01 2009. ISSN 1460-2083. Available at: < https://www.ncbi.nlm.nih.gov/pubmed/19740913 >.

RICCIARDI, S. et al. CDKL5 ensures excitatory synapse stability by reinforcing NGL-1-PSD95 interaction in the postsynaptic compartment and is impaired in patient iPSC-derived neurons. **Nat Cell Biol,** v. 14, n. 9, p. 911-23, Sep 2012. ISSN 1476-4679. Available at: < https://www.ncbi.nlm.nih.gov/pubmed/22922712 >.

ROSENTHAL, N.; BROWN, S. The mouse ascending: perspectives for human-disease models. **Nat Cell Biol,** v. 9, n. 9, p. 993-9, Sep 2007. ISSN 1465-7392. Available at: < https://www.ncbi.nlm.nih.gov/pubmed/17762889 >.

RUSCONI, L.; KILSTRUP-NIELSEN, C.; LANDSBERGER, N. Extrasynaptic N-methyl-D-aspartate (NMDA) receptor stimulation induces cytoplasmic translocation of the CDKL5 kinase

and its proteasomal degradation. **J Biol Chem,** v. 286, n. 42, p. 36550-8, Oct 21 2011. ISSN 1083-351X. Available at: < https://www.ncbi.nlm.nih.gov/pubmed/21832092 >.

RUSCONI, L. et al. CDKL5 expression is modulated during neuronal development and its subcellular distribution is tightly regulated by the C-terminal tail. **J Biol Chem,** v. 283, n. 44, p. 30101-11, Oct 31 2008. ISSN 0021-9258. Available at: < https://www.ncbi.nlm.nih.gov/pubmed/18701457 >.

RUSSO, S. et al. Novel mutations in the CDKL5 gene, predicted effects and associated phenotypes. **Neurogenetics,** v. 10, n. 3, p. 241-50, Jul 2009. ISSN 1364-6753. Available at: < https://www.ncbi.nlm.nih.gov/pubmed/19241098 >.

SALCEDO-TELLO, P.; ORTIZ-MATAMOROS, A.; ARIAS, C. GSK3 Function in the Brain during Development, Neuronal Plasticity, and Neurodegeneration. **Int J Alzheimers Dis,** v. 2011, p. 189728, 2011. ISSN 2090-0252. Available at: < https://www.ncbi.nlm.nih.gov/pubmed/21660241 >.

SAXTON, R. A.; SABATINI, D. M. mTOR Signaling in Growth, Metabolism, and Disease. **Cell,** v. 169, n. 2, p. 361-371, Apr 06 2017. ISSN 1097-4172. Available at: < https://www.ncbi.nlm.nih.gov/pubmed/28388417 >.

SCALA, E. et al. CDKL5/STK9 is mutated in Rett syndrome variant with infantile spasms. **J Med Genet,** v. 42, n. 2, p. 103-7, Feb 2005. ISSN 1468-6244. Available at: < https://www.ncbi.nlm.nih.gov/pubmed/15689447 >.

SCHERZ-SHOUVAL, R. et al. Reactive oxygen species are essential for autophagy and specifically regulate the activity of Atg4. **EMBO J,** v. 38, n. 10, May 15 2019. ISSN 1460-2075 (Electronic)
0261-4189 (Linking). Available at: < https://www.ncbi.nlm.nih.gov/pubmed/31092559 >.

SCHROEDER, E. et al. Neuron-Type Specific Loss of CDKL5 Leads to Alterations in mTOR Signaling and Synaptic Markers. **Mol Neurobiol,** v. 56, n. 6, p. 4151-4162, Jun 2019. ISSN 1559-1182. Available at: < https://www.ncbi.nlm.nih.gov/pubmed/30288694 >.

SEKIGUCHI, M. et al. Identification of amphiphysin 1 as an endogenous substrate for CDKL5, a protein kinase associated with X-linked neurodevelopmental disorder. **Arch Biochem Biophys,** v. 535, n. 2, p. 257-67, Jul 15 2013. ISSN 1096-0384. Available at: < https://www.ncbi.nlm.nih.gov/pubmed/23651931 >.

SENONER, T.; DICHTL, W. Oxidative Stress in Cardiovascular Diseases: Still a Therapeutic Target? **Nutrients,** v. 11, n. 9, Sep 4 2019. ISSN 2072-6643 (Electronic)
2072-6643 (Linking). Available at: < https://www.ncbi.nlm.nih.gov/pubmed/31487802 >.

SEVERS, N. J. et al. Remodelling of gap junctions and connexin expression in diseased myocardium. **Cardiovasc Res,** v. 80, n. 1, p. 9-19, Oct 1 2008. ISSN 0008-6363 (Print)
0008-6363 (Linking). Available at: < https://www.ncbi.nlm.nih.gov/pubmed/18519446 >.

SHAFFER, F.; MCCRATY, R.; ZERR, C. L. A healthy heart is not a metronome: an integrative review of the heart's anatomy and heart rate variability. **Front Psychol,** v. 5, p. 1040, 2014. ISSN 1664-1078. Available at: < https://www.ncbi.nlm.nih.gov/pubmed/25324790 >.

SHAITO, A. et al. Oxidative Stress-Induced Endothelial Dysfunction in Cardiovascular Diseases. **Front Biosci (Landmark Ed),** v. 27, n. 3, p. 105, Mar 18 2022. ISSN 2768-6698 (Electronic)
2768-6698 (Linking). Available at: < https://www.ncbi.nlm.nih.gov/pubmed/35345337 >.

SILVANI, A. et al. Dysregulation of heart rhythm during sleep in leptin-deficient obese mice. **Sleep,** v. 33, n. 3, p. 355-61, Mar 2010. ISSN 0161-8105. Available at: < https://www.ncbi.nlm.nih.gov/pubmed/20337194 >.

SIVILIA, S. et al. CDKL5 knockout leads to altered inhibitory transmission in the cerebellum of adult mice. **Genes Brain Behav,** v. 15, n. 5, p. 491-502, Jun 2016. ISSN 1601-183X. Available at: < https://www.ncbi.nlm.nih.gov/pubmed/27108663 >.

SPINAZZI, M. et al. Assessment of mitochondrial respiratory chain enzymatic activities on tissues and cultured cells. **Nat Protoc,** v. 7, n. 6, p. 1235-46, May 31 2012. ISSN 1750-2799. Available at: < https://www.ncbi.nlm.nih.gov/pubmed/22653162 >.

STADHOUDERS, A. M. et al. Mitochondrial creatine kinase: a major constituent of pathological inclusions seen in mitochondrial myopathies. **Proc Natl Acad Sci U S A,** v. 91, n. 11, p. 5089-93, May 24 1994. ISSN 0027-8424 (Print)
1091-6490 (Electronic)
0027-8424 (Linking). Available at: < https://www.ncbi.nlm.nih.gov/pubmed/8197190 >.

STALPERS, X. L. et al. Clinical phenotype of 5 females with a CDKL5 mutation. **J Child Neurol,** v. 27, n. 1, p. 90-3, Jan 2012. ISSN 1708-8283. Available at: < https://www.ncbi.nlm.nih.gov/pubmed/21765152 >.

STANSAUK, J. et al. Analysis of electrocardiograms in individuals with CDKL5 deficiency disorder. **Am J Med Genet A,** v. 191, n. 1, p. 108-111, Jan 2023. ISSN 1552-4833. Available at: < https://www.ncbi.nlm.nih.gov/pubmed/36372969 >.

STAPLES, C. J. et al. The centriolar satellite protein Cep131 is important for genome stability. **J Cell Sci,** v. 125, n. Pt 20, p. 4770-9, Oct 15 2012. ISSN 1477-9137. Available at: < https://www.ncbi.nlm.nih.gov/pubmed/22797915 >.

SUGDEN, P. H.; CLERK, A. Oxidative stress and growth-regulating intracellular signaling pathways in cardiac myocytes. **Antioxid Redox Signal,** v. 8, n. 11-12, p. 2111-24, Nov-Dec 2006. ISSN 1523-0864 (Print)
1523-0864 (Linking). Available at: < https://www.ncbi.nlm.nih.gov/pubmed/17034354 >.

SYMONDS, J. D. et al. Incidence and phenotypes of childhood-onset genetic epilepsies: a prospective population-based national cohort. **Brain,** v. 142, n. 8, p. 2303-2318, Aug 01 2019. ISSN 1460-2156. Available at: < https://www.ncbi.nlm.nih.gov/pubmed/31302675 >.

SZAFRANSKI, P. et al. Neurodevelopmental and neurobehavioral characteristics in males and females with CDKL5 duplications. **Eur J Hum Genet,** v. 23, n. 7, p. 915-21, Jul 2015. ISSN 1476-5438. Available at: < https://www.ncbi.nlm.nih.gov/pubmed/25315662 >.

SZYLLER, J.; JAGIELSKI, D.; BIL-LULA, I. Antioxidants in Arrhythmia Treatment-Still a Controversy? A Review of Selected Clinical and Laboratory Research. **Antioxidants (Basel),** v. 11, n. 6, Jun 02 2022. ISSN 2076-3921. Available at: < https://www.ncbi.nlm.nih.gov/pubmed/35740006 >.

TANG, G. et al. Mitochondrial abnormalities in temporal lobe of autistic brain. **Neurobiol Dis,** v. 54, p. 349-61, Jun 2013. ISSN 1095-953X. Available at: < https://www.ncbi.nlm.nih.gov/pubmed/23333625 >.

TANG, S. et al. Altered NMDAR signaling underlies autistic-like features in mouse models of CDKL5 deficiency disorder. **Nat Commun,** v. 10, n. 1, p. 2655, Jun 14 2019. ISSN 2041-1723. Available at: < https://www.ncbi.nlm.nih.gov/pubmed/31201320 >.

TANG, S. et al. Loss of CDKL5 in Glutamatergic Neurons Disrupts Hippocampal Microcircuitry and Leads to Memory Impairment in Mice. **J Neurosci,** v. 37, n. 31, p. 7420-7437, Aug 02 2017. ISSN 1529-2401. Available at: < https://www.ncbi.nlm.nih.gov/pubmed/28674172 >.

TAO, J. et al. Mutations in the X-linked cyclin-dependent kinase-like 5 (CDKL5/STK9) gene are associated with severe neurodevelopmental retardation. **Am J Hum Genet,** v. 75, n. 6, p. 1149-54, Dec 2004. ISSN 0002-9297. Available at: < https://www.ncbi.nlm.nih.gov/pubmed/15499549 >.

TASSINARI, M. et al. Early-onset brain alterations during postnatal development in a mouse model of CDKL5 deficiency disorder. **Neurobiol Dis,** v. 182, p. 106146, May 08 2023. ISSN 1095-953X. Available at: < https://www.ncbi.nlm.nih.gov/pubmed/37164289 >.

TERZIC, B. et al. X-linked cellular mosaicism underlies age-dependent occurrence of seizure-like events in mouse models of CDKL5 deficiency disorder. **Neurobiol Dis,** v. 148, p. 105176, Jan 2021a. ISSN 1095-953X. Available at: < https://www.ncbi.nlm.nih.gov/pubmed/33197557 >.

TERZIC, B. et al. Temporal manipulation of Cdkl5 reveals essential postdevelopmental functions and reversible CDKL5 deficiency disorder-related deficits. **J Clin Invest,** v. 131, n. 20, Oct 15 2021b. ISSN 1558-8238. Available at: < https://www.ncbi.nlm.nih.gov/pubmed/34651584 >.

TOLEDO, M. A.; JUNQUEIRA, L. F., JR. Cardiac autonomic modulation and cognitive status in Alzheimer's disease. **Clin Auton Res,** v. 20, n. 1, p. 11-7, Feb 2010. ISSN 1619-1560 (Electronic) 0959-9851 (Linking). Available at: < https://www.ncbi.nlm.nih.gov/pubmed/19830511 >.

TOLLENAERE, M. A. X. et al. p38- and MK2-dependent signalling promotes stress-induced centriolar satellite remodelling via 14-3-3-dependent sequestration of CEP131/AZI1. **Nat Commun,** v. 6, p. 10075, Nov 30 2015. ISSN 2041-1723. Available at: < https://www.ncbi.nlm.nih.gov/pubmed/26616734 >.

TRAZZI, S. et al. HDAC4: a key factor underlying brain developmental alterations in CDKL5 disorder. **Hum Mol Genet,** v. 25, n. 18, p. 3887-3907, Sep 15 2016. ISSN 1460-2083. Available at: < https://www.ncbi.nlm.nih.gov/pubmed/27466189 >.

VAN BERGEN, N. J. et al. Abnormalities of mitochondrial dynamics and bioenergetics in neuronal cells from CDKL5 deficiency disorder. **Neurobiol Dis,** v. 155, p. 105370, Jul 2021. ISSN 1095-953X (Electronic)
0969-9961 (Linking). Available at: < https://www.ncbi.nlm.nih.gov/pubmed/33905871 >.

VAN NIEKERK, C.; VAN DEVENTER, B. S.; DU TOIT-PRINSLOO, L. Long QT syndrome and sudden unexpected infant death. **J Clin Pathol,** v. 70, n. 9, p. 808-813, Sep 2017. ISSN 1472-4146 (Electronic)
0021-9746 (Linking). Available at: < http://www.ncbi.nlm.nih.gov/pubmed/28663329 >.

VANOLI, E.; SCHWARTZ, P. J. Sympathetic--parasympathetic interaction and sudden death. **Basic Res Cardiol,** v. 85 Suppl 1, p. 305-21, 1990. ISSN 0300-8428 (Print)
0300-8428 (Linking). Available at: < https://www.ncbi.nlm.nih.gov/pubmed/2091609 >.

VIGLI, D. et al. Rescue of prepulse inhibition deficit and brain mitochondrial dysfunction by pharmacological stimulation of the central serotonin receptor 7 in a mouse model of CDKL5 Deficiency Disorder. **Neuropharmacology,** v. 144, p. 104-114, Jan 2019. ISSN 1873-7064 (Electronic)
0028-3908 (Linking). Available at: < https://www.ncbi.nlm.nih.gov/pubmed/30326240 >.

VIGLIONE, A. et al. Behavioral impulsivity is associated with pupillary alterations and hyperactivity in CDKL5 mutant mice. **Hum Mol Genet,** v. 31, n. 23, p. 4107-4120, Nov 28 2022. ISSN 1460-2083. Available at: < https://www.ncbi.nlm.nih.gov/pubmed/35861639 >.

VILLUMSEN, B. H. et al. A new cellular stress response that triggers centriolar satellite reorganization and ciliogenesis. **EMBO J,** v. 32, n. 23, p. 3029-40, Nov 27 2013. ISSN 1460-2075. Available at: < https://www.ncbi.nlm.nih.gov/pubmed/24121310 >.

VINCENT, A. E. et al. The Spectrum of Mitochondrial Ultrastructural Defects in Mitochondrial Myopathy. **Sci Rep,** v. 6, p. 30610, Aug 10 2016. ISSN 2045-2322 (Electronic)
2045-2322 (Linking). Available at: < https://www.ncbi.nlm.nih.gov/pubmed/27506553 >.

WALKER, A. et al. Nrf2 signaling and autophagy are complementary in protecting breast cancer cells during glucose deprivation. **Free Radic Biol Med,** v. 120, p. 407-413, May 20 2018. ISSN 1873-4596 (Electronic)
0891-5849 (Linking). Available at: < https://www.ncbi.nlm.nih.gov/pubmed/29649567 >.

WANG, C. et al. PARP1 promote autophagy in cardiomyocytes via modulating FoxO3a transcription. **Cell Death Dis,** v. 9, n. 11, p. 1047, Oct 15 2018. ISSN 2041-4889 (Electronic). Available at: < https://www.ncbi.nlm.nih.gov/pubmed/30323296 >.

WANG, H. T. et al. CDKL5 deficiency in forebrain glutamatergic neurons results in recurrent spontaneous seizures. **Epilepsia,** v. 62, n. 2, p. 517-528, Feb 2021. ISSN 1528-1167. Available at: < https://www.ncbi.nlm.nih.gov/pubmed/33400301 >.

WANG, I. T. et al. Loss of CDKL5 disrupts kinome profile and event-related potentials leading to autistic-like phenotypes in mice. **Proc Natl Acad Sci U S A,** v. 109, n. 52, p. 21516-21, Dec 26 2012. ISSN 1091-6490. Available at: < https://www.ncbi.nlm.nih.gov/pubmed/23236174 >.

WANG, Y.; LUO, W. PARP-1 and its associated nucleases in DNA damage response. **DNA Repair (Amst),** v. 81, p. 102651, Sep 2019. ISSN 1568-7856. Available at: < https://www.ncbi.nlm.nih.gov/pubmed/31302005 >.

WEAVING, L. S. et al. Mutations of CDKL5 cause a severe neurodevelopmental disorder with infantile spasms and mental retardation. **Am J Hum Genet,** v. 75, n. 6, p. 1079-93, Dec 2004. ISSN 0002-9297. Available at: < https://www.ncbi.nlm.nih.gov/pubmed/15492925 >.

WEAVING, L. S. et al. Rett syndrome: clinical review and genetic update. **J Med Genet,** v. 42, n. 1, p. 1-7, Jan 2005. ISSN 1468-6244. Available at: < https://www.ncbi.nlm.nih.gov/pubmed/15635068 >.

WILLIAMSON, S. L. et al. A novel transcript of cyclin-dependent kinase-like 5 (CDKL5) has an alternative C-terminus and is the predominant transcript in brain. **Hum Genet,** v. 131, n. 2, p. 187-200, Feb 2012. ISSN 1432-1203. Available at: < https://www.ncbi.nlm.nih.gov/pubmed/21748340 >.

XIONG, L.; LEUNG, T. W. H. Autonomic dysfunction in neurological disorders. **Aging (Albany NY),** v. 11, n. 7, p. 1903-1904, Apr 9 2019. ISSN 1945-4589 (Electronic)
1945-4589 (Linking). Available at: < https://www.ncbi.nlm.nih.gov/pubmed/30969941 >.

ZHANG, Y. et al. Capping of the N-terminus of PSD-95 by calmodulin triggers its postsynaptic release. **EMBO J,** v. 33, n. 12, p. 1341-53, Jun 17 2014. ISSN 1460-2075. Available at: < https://www.ncbi.nlm.nih.gov/pubmed/24705785 >.

ZHOU, A.; HAN, S.; ZHOU, Z. J. Molecular and genetic insights into an infantile epileptic encephalopathy - CDKL5 disorder. **Front Biol (Beijing),** v. 12, n. 1, p. 1-6, Feb 2017. ISSN 1674-7984. Available at: < https://www.ncbi.nlm.nih.gov/pubmed/28580010 >.

ZHU, Y. C. et al. Palmitoylation-dependent CDKL5-PSD-95 interaction regulates synaptic targeting of CDKL5 and dendritic spine development. **Proc Natl Acad Sci U S A,** v. 110, n. 22, p. 9118-23, May 28 2013. ISSN 1091-6490. Available at: < https://www.ncbi.nlm.nih.gov/pubmed/23671101 >.

ZHU, Y. C.; XIONG, Z. Q. Molecular and Synaptic Bases of CDKL5 Disorder. **Dev Neurobiol,** v. 79, n. 1, p. 8-19, Jan 2019. ISSN 1932-846X. Available at: < https://www.ncbi.nlm.nih.gov/pubmed/30246934 >.